Title
Carbonyl Sulfide Exchange Between Soils and the Atmosphere: Observations and Modeling

Author
Sun, Wu

Publication Date
2017

Peer reviewed|Thesis/dissertation

UNIVERSITY OF CALIFORNIA
Los Angeles

Carbonyl Sulfide Exchange Between Soils and the Atmosphere: Observations and Modeling

A dissertation submitted in partial satisfaction
of the requirements for the degree
Doctor of Philosophy in Atmospheric and Oceanic Sciences

by

Wu Sun

2017

Abstract of the Dissertation

Carbonyl Sulfide Exchange Between Soils and the Atmosphere: Observations and Modeling

by

Wu Sun

Doctor of Philosophy in Atmospheric and Oceanic Sciences

University of California, Los Angeles, 2017

Professor Ulrike Seibt, Chair

Carbonyl sulfide (COS) is a trace gas participating in key processes of the terrestrial carbon cycle. Despite its low mixing ratio in the troposphere (400–550 pmol mol^{-1}), the amplitude of seasonal variability of COS greatly exceeds that of CO_2 and is in phase with the gross photosynthesis of the terrestrial biosphere. Over the recent decade, COS has emerged as a promising tracer for quantifying terrestrial gross primary productivity (GPP) independently from respiration across the ecosystem to the global scales, because of the parallel uptake of COS and CO_2 through leaf stomata. While leaf uptake of COS dominates surface COS flux on land in the absence of industrial and biomass burning emissions, soil COS flux is another smaller but significant component. Neglecting the soil component in ecosystem COS budget may bias GPP estimates derived from COS measurements. Soil may also vary from a sink to a source of COS depending on temperature and microbial sulfur metabolism. Due to the presence of potential interference from soil COS activities, using COS as a photosynthetic tracer requires soil COS flux to be separated from the net ecosystem COS exchange. This dissertation is dedicated to the mechanistic understanding of the soil–atmosphere exchange of COS using process-oriented modeling and field observations.

A reactive transport model for soil COS processes is constructed to simulate soil–atmosphere COS flux from environmental variables. This model takes into account the dual-phase diffusive transport and the microbial sources and sinks of COS in the soil column. COS uptake and production rates are parameterized with enzyme kinetics and thermodynamics, consistent with lab incuba-

tion data. Leaf litter layer is explicitly resolved to account for litter COS uptake, whenever a litter layer is present. The model is evaluated against published field data of COS flux and demonstrates good skill in predicting both soil uptake and emission of COS. Model simulations further confirm that COS flux dependence on soil moisture is a result of two rivaling controls—the diffusive limitation on COS supply and the water limitation on microbial activity.

Field observations on soil COS exchange have been conducted at an oak woodland in southern California and a boreal pine forest in southern Finland using automated soil chambers and mid-infrared quantum cascade laser spectrometer. Soils at both sites show consistent uptake behavior related to soil moisture and respiration. At the semi-arid oak woodland in California, microbial COS uptake is strongly limited by water availability in the dry season. The intact leaf litter layer contributes a significant portion to the overall soil COS uptake. Litter COS uptake increases with moisture content and shows a strong pulse immediately after the rain event, indicating a rapid reactivation of litter microbial activity following alleviated water stress. In the Finnish pine forest, soil COS uptake is limited by the diffusional supply of COS to soil microbes, according to the negative correlation with soil moisture. The contrasting responses of soil COS uptake to moisture in semi-arid and humid ecosystems reflect the coupling of diffusion and microbial uptake controls on COS flux. At both sites, soil COS uptake correlates well with respiration and the COS : CO_2 flux ratio varies with temperature. The temperature dependence of COS : CO_2 flux ratio may be a common feature of soils and indicate underlying shifts in active microbial groups.

This dissertation advances knowledge of the physical and biological drivers of soil–atmosphere exchange of COS. Anticipated applications of the findings will be to better constrain global soil COS flux and derive COS-based estimates of GPP, which will be useful in understanding the responses of photosynthesis to climate variability.

The dissertation of Wu Sun is approved.

Aradhna E. Tripati

Alexander D. Hall

Daniela F. Cusack

Ulrike Seibt, Committee Chair

University of California, Los Angeles

2017

OBSERVO ERGO EST VNIVERSVM

Table of Contents

List of Figures

List of Tables

Acknowledgments

First, I am most grateful to my advisor Ulli Seibt for her guidance and support throughout my years as a graduate student. I am also very appreciative of the assistances and valuable feedbacks from my committee members, Alex Hall, Aradhna Tripati, and Daniela Cusack.

Many thanks to the good fellas in my graduate program who have enriched my life, enlightened my thoughts, and provided me with great help: Daniel Dauhajre, Kathleen Schiro, Baird Langenbrunner, Yi-Hung Kuo, and Julia Hazel. You guys are awesome.

I owe great thanks to my coauthors and colleagues on the other side of the Atlantic, Kadmiel Maseyk, Céline Lett, Linda Kooijmans, Huilin Chen, Kukka-Maaria Erkkilä, Ivan Mammarella, and Timo Vesala, without whom the work presented here would not be possible. I would also like to thank a bunch of wonderful people I met on my journey of carbonyl sulfide research: Mary Whelan, Ian Baker, Laura Meredith, Elliott Campbell, and Tim Hilton, who have always been sources of inspiration to me.

Chapter 2 is a version of *Sun et al.* [2015], which was supported by the European Research Council (ERC) Starting Grant (202835) to my advisor Ulli Seibt.

Chapter 3 is a version of *Sun et al.* [2016], which was supported by the ERC Starting Grant (202835) to Ulli Seibt and the University of California Institute for the Study of Ecological and Evolutionary Climate Impacts (ISEECI) fellowship. I would like to thank Phil Rundel for help and support during our field campaign, and the support at the Stunt Ranch Natural Reserve. I would also like to thank Mary Whelan for data sharing and valuable discussions. This work has been published on the *Journal of Geophysical Research: Biogeosciences*, ©2016 American Geophysical Union (AGU). Permission to reproduce this work in full in this dissertation has been granted by the John Wiley and Sons and the Copyright Clearance Center (license no. 4127791160326).

Chapter 4 is a version of *Sun et al.* [2017]. This study received support from the European Commission's Seventh Framework Programme (FP7/2007–2013) in the InGOS project (284274), the Academy of Finland projects Centre of Excellence (118780), Academy Professor (284701 and 282842) and CARB-ARC (286190), ICOS-Finland (281255), and the NOAA contract NA13OAR4310082. I would like to thank the staff at the SMEAR (Station for Measuring Forest Ecosystem–Atmosphere Relations) II Hyytiälä field station, Finland for their gracious help and support during the field campaign.

I would like to acknowledge a scholarship awarded by the China Scholarship Council to support my doctoral study through 2012–2014 at UCLA, and a fellowship from the University of California Institute for the Study of Ecological and Evolutionary Climate Impacts (ISEECI) in 2015.

Finally, I would like to thank my parents for their support to the path I have chosen.

Wu Sun

Los Angeles, California, USA
August 2017

Vita

2014	M.Sc. Atmospheric and Oceanic Sciences, UCLA
2012	B.Sc. Geology, Nanjing University
2013–2017	Graduate Student Researcher Department of Atmospheric and Oceanic Sciences, UCLA
2014–2015 & Fall 2016	Teaching Assistant Department of Atmospheric and Oceanic Sciences, UCLA

Publications

Sun, W., Kooijmans, L. M. J., Maseyk, K., Chen, H., Mammarella, I., Vesala, T., Levula, J., Keskinen, H. & Seibt, U. Soil fluxes of carbonyl sulfide (COS), carbon monoxide, and carbon dioxide in a boreal forest in southern Finland. *Atmos. Chem. Phys. Discuss.*, in review, doi:10.5194/acp-2017-180 (2017).

Kooijmans, L. M. J., Maseyk, K., Seibt, U., Sun, W., Vesala, T., Mammarella, I., Kolari, P., Aalto, J., Franchin, A., Vecchi, R., Valli, G., and Chen, H. Canopy uptake dominates nighttime carbonyl sulfide fluxes in a boreal forest. *Atmos. Chem. Phys. Discuss.*, in press, doi:10.5194/acp-2017-407 (2017).

Sun, W., Maseyk, K., Lett, C. & Seibt, U. Litter dominates surface fluxes of carbonyl sulfide in a Californian oak woodland. *J. Geophys. Res. Biogeosci.* **121**, 438–450, doi:10.1002/2015JG003149 (2016).

Sun, W., Maseyk, K., Lett, C. & Seibt, U. A soil diffusion–reaction model for surface COS flux: COSSM v1. *Geosci. Model Dev.* **8**, 3055–3070, doi:10.5194/gmd-8-3055-2015 (2015).

CHAPTER 1

Introduction

Carbonyl sulfide (COS) is a trace gas with the concentration 400–550 pmol mol^{-1} in the free troposphere. Due much to its chemical similarity to CO_2, COS is taken up in the leaf chloroplast by carbonic anhydrase and other enzymes that routinely catalyze CO_2 hydration. COS hydrolysis in the leaf interior creates a concentration gradient that drives the deposition of COS through stomata, which parallels the leaf uptake of CO_2. The coupling of leaf COS and CO_2 uptake enables us to use COS as a quantitative proxy for leaf CO_2 assimilation. Thus, canopy gross primary productivity may be inferred from daytime measurements of COS uptake alone, bypassing the nighttime uncertainty in eddy covariance methods that have long plagued ecosystem flux measurements. Because soil can act as a COS sink or source, inferring canopy photosynthesis from COS measurements requires soil contribution to the ecosystem COS exchange to be separated. This problem is what motivates the research in my dissertation.

This chapter serves as a general introduction to our current understanding of the biogeochemical cycle of COS in the earth system. The main theme of this dissertation, soil COS exchange, should not only be viewed within the soil compartment but also in the broad framework of the global COS cycle to better appraise its significance.

1.1 Chemical properties and reactions of COS

1.1.1 Chemical properties

COS is a linear molecule with the structure O=C=S. As COS and CO_2 are structurally similar and have the same number of valence electrons, they share some similarities in chemical properties and reactions. The boiling point of COS is $-50°C$ at 1 atm [*Ferm*, 1957], and hence, COS exists in gas phase at the earth's surface. COS is soluble in water, though having a smaller solubility than CO_2 [*Wilhelm et al.*, 1977]. Due to the difference between electronegativities of oxygen and sulfur, the C=S bond length is significantly larger than the C=O bond length in COS (1.56 Å vs. 1.16 Å) [*Ferm*, 1957]. Thus, unlike CO_2, COS is a polar molecule (dipole moment 0.715 D) [*Muenter*, 1968]. Its hydrolysis in water differ from CO_2 hydrolysis (see section 1.1.2). The asymmetry of COS molecule gives rise to a more complicated rotational and vibrational spectrum than that of CO_2 [*Coblentz Society, Inc.*, 2015].

1.1.2 Uncatalyzed hydrolysis of COS

In aqueous solutions, COS undergoes hydrolysis to yield H_2S and CO_2 [*Thompson et al.*, 1935; *Elliott et al.*, 1989]. Unlike CO_2, COS hydrolysis is unidirectional because the reverse reaction is unfavorable [*Notni et al.*, 2007]. In acidic and in alkaline conditions, the hydrolysis of COS can be represented respectively with

$$\mathrm{COS} + \mathrm{H_2O} \longrightarrow \mathrm{H_2S} + \mathrm{CO_2} \quad \text{(acidic or neutral)} \tag{1.1a}$$

$$\mathrm{COS} + \mathrm{OH^-} \longrightarrow \mathrm{HS^-} + \mathrm{CO_2} \quad \text{(alkaline)} \tag{1.1b}$$

The two reactions differ in the order of the overall reaction and their rate-limiting steps.

Hydration of COS forms monothiocarbonate species as intermediates [*Elliott et al.*, 1989]:

$$\mathrm{COS} + \mathrm{H_2O} \longrightarrow \mathrm{H_2CO_2S} \tag{1.2a}$$

$$\mathrm{COS} + \mathrm{OH^-} \longrightarrow \mathrm{HCO_2S^-} \tag{1.2b}$$

Kinetics calculations show that the hydration steps are rate-limiting steps of the overall reaction. In acidic conditions with low [$\mathrm{OH^-}$], reaction (1.2a) is the dominant pathway of monothiocarbonate formation, and the overall hydrolysis rate follows the first-order kinetics with [COS]. However, in alkaline conditions with high [$\mathrm{OH^-}$], both reactions are important in monothiocarbonate formation, and the hydrolysis rate increases nonlinearly with pH.

The subsequent dissociation of monothiocarbonate species into $\mathrm{CO_2}$ and $\mathrm{HS^-}$ (or $\mathrm{H_2S}$) is faster than the hydration steps. The estimated characteristic timescale is 0.05 s for the dissociation of $\mathrm{HCO_2S^-}$ in intermediate pH conditions (4–12) [*Elliott et al.*, 1989], about 10^6 faster than the hydration step. The overall first-order rate constant of COS hydrolysis, as a function of pH, can be fitted as [*Elliott et al.*, 1989; *Ogée et al.*, 2016],

$$k = 2.15 \times 10^{-5} \exp\left[-10450\left(\frac{1}{T} - \frac{1}{298}\right)\right] + 12.7 \times 10^{-\mathrm{p}K_\mathrm{w}+\mathrm{pH}} \exp\left[-6040\left(\frac{1}{T} - \frac{1}{298}\right)\right] \tag{1.3}$$

1.1.3 Enzyme-mediated hydrolysis of COS

In most natural conditions, uncatalyzed hydrolysis of COS is very slow and unable to account for the observed large uptake rates of COS in leaves and soils. In contrast, enzymatic reactions are able to accelerate COS hydrolysis by a factor of 10^4 to 10^7. Carbonic anhydrases, a family of enzymes that catalyze $\mathrm{CO_2}$ hydrolysis to bicarbonate, have been found to also catalyze the hydrolysis of COS. Despite different carbonic anhydrase types associated with the phylogenic tree, many types have been demonstrated with COS catalyzing activity, such as those in cows and rats [*Chengelis and Neal*, 1979, 1980], in vascular plants [*Protoschill-Krebs and Kesselmeier*, 1992; *Protoschill-Krebs et al.*, 1996], in freshwater algae [*Protoschill-Krebs et al.*, 1995], and in cyanobacteria [*Miller et al.*, 1989; *Badger and Price*, 1990]. The ability to catalyze COS hydrolysis seems to be a

general feature of carbonic anhydrase enzymes.

Other enzymes have also been reported to show COS hydrolysis activity. The CS_2 hydrolase isolated from an hyperthermophilic archaea (*Acidianus* strain) exhibits a typical β-carbonic anhydrase structure but catalyzes only the hydrolysis of COS and CS_2, not CO_2 [*Smeulders et al.*, 2011]. Similarly, COS hydrolase, an enzyme isolated from a *Thiobacillus thioparus* strain that structurally resembles β-carbonic anhydrase, shows dominant COS reaction specificity over CO_2 [*Ogawa et al.*, 2013]. Enzymes that are unrelated to carbonic anhydrases may also show COS catalyzing activity, for example, RuBisCO [*Lorimer and Pierce*, 1989], nitrogenase [*Seefeldt et al.*, 1995], and carbon monoxide dehydrogenase [*Ensign*, 1995].

The mechanisms of enzymatic COS hydrolysis have been investigated with density functional theory simulations. Carbonic anhydrase has a zinc complex as the active site for CO_2 or COS hydrolysis. This active site can be mimicked with the simple analog $[(H_3N)_3ZnOH]^+$, where NH_3 imitates amino acid ligands [*Schenk et al.*, 2004]. First, the Zn-complex performs a nucleophilic addition onto the double $C=S$ bond to form a carboxylic acid complex $[(H_3N)_3ZnSCOOH]^+$. This intermediate undergoes configuration changes and forms a cyclic structure following water addition. Then after proton transfer from the water (solvent) to the sulfur atom, the Zn-complex casts out the CO_2 molecule and forms a hydrosulfide analog to the active site, $[(H_3N)_3ZnSH]^+$. This hydrosulfide analog can be converted back to its original moiety through protonation and dissociation of H_2S [*Notni et al.*, 2007]. Due to the low concentration of H_2S in the ambient, the dissociation of H_2S is practically irreversible. Thus, the overall hydrolysis reaction of COS is irreversible. The rate-limiting step in the enzymatic hydrolysis of COS is the nucleophilic attack of carbonic anhydrase enzyme on COS, with an activation energy higher but comparable to the same reaction on CO_2 [*Schenk et al.*, 2004]. Compared with the uncatalyzed hydrolysis, the enzymatic reaction has a much lower activation energy and hence proceeds more readily.

1.1.4 Oxidation of COS in the atmosphere

COS participates in photochemical and radical reactions and is ultimately oxidized to sulfate in the atmosphere. In the troposphere, oxidation via OH and O radicals is a more dominant pathway of COS loss than photolysis.

$$COS + O(^3P) \longrightarrow CO + SO \tag{1.4a}$$

$$COS + OH \longrightarrow CO_2 + HS \tag{1.4b}$$

The HS radical is then oxidized to SO radical by common oxidants in the troposphere [*Friedl et al.*, 1985],

$$HS + O_2 \longrightarrow SO + OH \tag{1.5a}$$

$$HS + NO_2 \longrightarrow HSO + NO \tag{1.5b}$$

$$HS + O_3 \longrightarrow HSO + O_2 \tag{1.5c}$$

$$HSO + O_2 \longrightarrow SO + HO_2 \tag{1.5d}$$

$$HSO + HO_2 \longrightarrow SO + H_2O_2 \tag{1.5e}$$

The SO radical continues to be oxidized to SO_2, and further, to H_2SO_4 to form sulfate aerosols [*Seinfeld and Pandis*, 2006].

In the stratosphere, COS is photolyzed by UV light [*Crutzen*, 1976],

$$COS + h\nu \longrightarrow CO + S(^1D) \text{ or } S(^3P) \tag{1.6}$$

The molecular S is then oxidized to form SO radical.

$$S(^1D) \text{ or } S(^3P) + O_2 \longrightarrow SO + O \tag{1.7}$$

The SO radical undergoes the same oxidation processes as in the troposphere to ultimately form sulfate aerosols.

1.1.5 Formation of COS

In natural environments excepting anthropogenic activities, COS is mainly produced from two types of reactions, degradation of organosulfur compounds and photolysis or oxidation of reduced sulfur gases. The production of COS may happen in the atmosphere, in the surface ocean, and in soils.

In the atmosphere, COS may be produced from the reaction between CS_2 and the OH radical [*Kurylo*, 1978; *Sze and Ko*, 1979]:

$$CS_2 + OH \longrightarrow \left[\begin{array}{l} S \\ | \\ C - OH \\ | \\ S \end{array} \right]^{\ddagger} \longrightarrow COS + HS \tag{1.8}$$

In addition, the reactions between dimethylsulfide (DMS) and oxidative agents may also produce COS [*Barnes et al.*, 1994]:

$$H_3CSCH_3 \xrightarrow{O_2,NO} CH_3S \xrightarrow{HO_2,O_2} H_2CS \xrightarrow[h\nu]{OH} COS \tag{1.9}$$

In raindrops and cloud water, COS are produced from photochemical reactions [*Belviso et al.*, 1987; *Mu et al.*, 2004]. However, the precursors of COS and the reactions in atmospheric water remain poorly understood.

In the surface layer of the ocean, COS can be produced from chromophoric dissolved organic matter through both photolysis [*Ferek and Andreae*, 1984; *Zepp and Andreae*, 1994; *Ulshöfer and Andreae*, 1998] and dark reactions [*Ulshöfer et al.*, 1996; *Von Hobe et al.*, 2001].

In soils, COS may be produced from abiotic processes and microbial sulfur metabolism. It has been shown that abiotic production of COS can be driven by temperature [*Maseyk et al.*, 2014] or by solar radiation [*Whelan and Rhew*, 2015; *Kitz et al.*, 2017]. The details of reaction mechanisms remain unclear, though. Sulfur-containing amino acids (methionine and cysteine) has been hypothesized as plausible sources of COS in abiotic production [*Maseyk et al.*, 2014; *Rennenberg*, 1991],

but direct evidence is absent. For microbial COS production, a well-studied pathway is the hydrolysis of thiocyanate in acidic conditions [*Katayama et al.*, 1992, 1993; *Kim and Katayama*, 2000],

$$SCN^- + H_3O^+ \longrightarrow COS + NH_3 \tag{1.10}$$

The reaction is mediated by thiocyanate hydrolase, an enzyme present in sulfur utilizing chemoautotrophs. How the relative importance of abiotic vs. biotic production of COS varies among soils is unclear.

1.2 The biogeochemical cycle of COS

As a reactive trace gas, COS is continuously cycled through the compartments of the earth system. COS is produced in the surface ocean and from industrial activities and biomass burning, while consumed in the terrestrial biosphere and to a lesser extent in the atmosphere.

1.2.1 COS in the atmosphere

The global annual mean concentration of COS has been relatively stable during the past decade, ranging from 485 to 500 pmol mol^{-1} according to flask sampling data [*Campbell et al.*, 2017; *Montzka et al.*, 2007]. In the recent past, instrumental record (since 1977) has witnessed a peak global mean concentration in the mid 1980s around 570 pmol mol^{-1} and a decline ever since, indicating significant changes in the global budget of COS [*Campbell et al.*, 2017]. Tracing back to the early Holocene from the ice core record, the COS concentration has been increasing steadily since 5000 years ago, from 250 pmol mol^{-1} to 320 pmol mol^{-1} before the industrial revolution [*Aydin et al.*, 2014]. An abrupt increase of COS took place following the industrial revolution as a result of the rapidly growing anthropogenic emissions [*Campbell et al.*, 2015, 2017].

There is pronounced seasonality in the tropospheric concentration of COS. Seasonal variations in

COS concentration have been observed from sites across different latitudes in both hemispheres [*Montzka et al.*, 2007]. Across the northern hemisphere, COS seasonal variations are in phase with variations of CO_2, showing a spring maximum and a fall minimum. This correspondence in COS and CO_2 seasonal variations suggests a predominant control of vegetative uptake (section 1.2.2) on the seasonality of COS in the northern hemisphere. The relative seasonal amplitude of COS, however, greatly exceeds that of CO_2, and increases toward higher latitude. In the southern hemisphere, COS seasonal variations are not in phase with terrestrial photosynthesis and seem to be influenced mostly by oceanic processes (section 1.2.3).

The atmosphere is an active chemical reactor rather than a static pool of COS, responsible for a small fraction of global COS budget. CS_2 and DMS emitted from the ocean and from industrial activities are oxidized to COS in the troposphere, and the resultant COS is then destroyed by oxidation and photolysis to ultimately form sulfate aerosols (section 1.1.4). In the stratosphere, the sulfate aerosol layer formed from COS has an important climate effect—to reduce the radiative forcing by reflecting and scattering the solar radiation. The total atmospheric sink of COS is estimated to be around 101 Gg S yr^{-1} (Gg: *giga*-gram, 10^9 g) [*Kettle et al.*, 2002; *Berry et al.*, 2013; *Launois et al.*, 2015a], about 8–10% of the total global budget [*Launois et al.*, 2015a].

1.2.2 Terrestrial ecosystem exchange of COS

The terrestrial biosphere is the largest sink of COS. Uptake by vegetation through leaf stomata is the dominant component of terrestrial uptake (65–77%), whereas soil uptake or emission is of secondary importance [*Kettle et al.*, 2002; *Berry et al.*, 2013; *Launois et al.*, 2015a]. Due to the enzyme-mediated hydrolysis of COS (section 1.1.3), the leaf interior—chloroplast or mesophyll—is depleted of COS with respect to the ambient environment. Thus the concentration gradient drives the inward diffusion of COS whenever the stomata are open. The hydrolysis of COS is a one-way reaction and no apparent emission of COS has been detected from live and healthy leaves. These facts suggest that leaf COS uptake is a direct indicator of stomatal conductance.

The coupling between stomatal conductance and photosynthesis [*Ball*, 1988; *Collatz et al.*, 1991] further links leaf COS uptake with CO_2 uptake [*Sandoval-Soto et al.*, 2005; *Stimler et al.*, 2010a], hinting the possibility of using COS uptake to infer gross primary productivity (GPP) of terrestrial ecosystems. The concentration normalized ratio of COS to CO_2 leaf uptake, dubbed as the *leaf relative uptake* (LRU) ratio, is a relatively well constrained parameter for describing the relationship between COS and CO_2 fluxes [*Seibt et al.*, 2010; *Wohlfahrt et al.*, 2012]. The LRU ratio has been found to be a function of light, temperature, possibly relative humidity [*Stimler et al.*, 2010a; *Maseyk et al.*, 2014], plant species [*Sandoval-Soto et al.*, 2005], and leaf intrinsic physiological parameters [*Seibt et al.*, 2010]. Using the calculated LRU and other related variables, it is possible to infer ecosystem GPP from COS flux measurements alone, without incurring any CO_2 flux partitioning that is known to be compromised by systematic uncertainty associated with the eddy covariance method during the nighttime [*Goulden et al.*, 1996].

The link between COS and CO_2 uptake by the vegetation is observable beyond the canopy scale. At the regional scale, the pattern of boundary layer COS drawdown over the continental interior is mainly controlled by ecosystem uptake [*Campbell et al.*, 2008; *Berry et al.*, 2013]. With coupled simulations using atmospheric transport model and terrestrial biosphere model, it is possible to use the information in COS and CO_2 drawdown to constrain regional scale GPP [*Hilton et al.*, 2015]. Globally, the signal of terrestrial ecosystem uptake is also evident in seasonal variations of northern hemisphere COS concentration [*Montzka et al.*, 2007].

Soil represents a minor sink in the terrestrial ecosystem. Since carbonic anhydrases are ancient enzymes and are ubiquitous among life forms, soil microbes that typically contain carbonic anhydrases are capable of consuming COS [*Conrad*, 1996; *Kesselmeier et al.*, 1999]. Indeed, field measurements and laboratory incubations have shown that most soils behave as COS sink [*Castro and Galloway*, 1991; *Simmons et al.*, 1999; *Steinbacher et al.*, 2004; *Yi et al.*, 2007; *Kesselmeier et al.*, 1999; *Van Diest and Kesselmeier*, 2008; *Whelan et al.*, 2016], except soils under anoxic [e.g., *Whelan et al.*, 2013] or high temperature or radiation conditions [*Maseyk et al.*, 2014; *Kitz et al.*, 2017]. Soil COS uptake rates are typically within the order of 1 to 10 pmol m^{-2} s^{-1}. Environmental variables that

may control the uptake rates of COS include soil porosity, water content [*Van Diest and Kesselmeier*, 2008], temperature [*Kesselmeier et al.*, 1999], and microbial activity [*Yi et al.*, 2007].

When soils act as COS sources, the production rates vary greatly and may reach up to the order of 100 pmol m^{-2} s^{-1} [*Whelan et al.*, 2013; *DeLaune et al.*, 2002]. In wetland soils, the dominant environmental controls on COS production rate seem to be redox potential (a measure of the extent of anoxia) and salinity [*Devai and DeLaune*, 1995; *DeLaune et al.*, 2002]. Saline wetlands generally have stronger COS production than freshwater wetlands, possibly because of enhanced sulfur metabolism with more dissolved sulfates. In oxic upland soils, the observed cases with significant COS emissions are associated with either high temperature conditions, for example, a wheatfield in the Southern Great Plains (Billings, Oklahoma, USA) [*Maseyk et al.*, 2014], or high radiation conditions, e.g., a hay meadow in the Central Alps (Neustift, Austria) [*Kitz et al.*, 2017]. Laboratory incubations have confirmed the existence of thermal [*Whelan et al.*, 2016] and photochemical [*Whelan and Rhew*, 2015] pathways of COS production in soils. Thus, as multiple COS consumption and production activities exist in the soil, the response of net COS exchange to environmental variables is a net result of the diverging responses of multiple COS processes.

Recent estimates of the global COS budget of the terrestrial biosphere (vegetation + soil) range from 1093 to 1229 Gg S yr^{-1}, with vegetation uptake 663–772 Gg S yr^{-1}, and net soil uptake 233–457 Gg S yr^{-1} [*Berry et al.*, 2013; *Launois et al.*, 2015a]. The uncertainty in vegetation uptake of COS may come from inadequate knowledge of stomatal conductance and leaf-level and ecosystem-level COS : CO_2 relative uptake ratios. The estimate of global net soil COS uptake is much more uncertain with a nearly twofold range. This is probably because that soil COS fluxes are parameterized empirically with an indirect relationship between COS flux and the flux of a related trace gas (CO_2 in *Berry et al.* [2013] or H_2 in *Launois et al.* [2015a]), without a physical representation of soil COS processes. The key to improving the estimates of terrestrial biosphere COS budget probably lies in the refinement of the process-level understanding and associated model representations of COS processes, for example, microbial COS uptake and abiotic COS production.

1.2.3 Ocean COS emissions

The ocean is the largest source of COS. COS and its precursors, typically CS_2 and DMS, are produced in the surface water of the ocean. The precursors of COS are quickly oxidized to COS after admission into the atmosphere, and are considered as part of the indirect emission of COS from the ocean [*Kettle et al.*, 2002; *Suntharalingam et al.*, 2008]. The flux of COS into the atmosphere is mainly controlled by production and air–sea exchange processes. COS and its precursors can be produced from photochemical reactions [*Ferek and Andreae*, 1984; *Ulshöfer and Andreae*, 1998] and dark reactions [*Von Hobe et al.*, 2001]. The production rate is considered to be proportional to the concentration of the chromophoric dissolved organic matter (CDOM) [*Launois et al.*, 2015b]. The air–sea exchange acts to transport COS but neither create nor destroy COS. The process is governed by wind speed and the concentration gradient at the air–sea interface. In the ocean water, COS is also expected to undergo hydrolysis. The loss of COS through hydrolysis is often calculated from the uncatalyzed hydrolysis kinetics only (section 1.1.2). It is unclear whether there is significant uptake of COS by marine phytoplankton through catalyzed hydrolysis (section 1.1.3).

Current knowledge of ocean COS sources remains largely uncertain. Estimates of the ocean source strength from field measurements based studies are between 41 and 320 Gg S yr^{-1} [*Rasmussen et al.*, 1982; *Ferek and Andreae*, 1984; *Johnson and Harrison*, 1986; *Mihalopoulos et al.*, 1992; *Chin and Davis*, 1993; *Ulshöfer and Andreae*, 1998; *Watts*, 2000; *Xu et al.*, 2001]. The global simulation by *Kettle et al.* [2002] suggests on average a small ocean source with a large uncertainty range, −110 to 190 Gg S yr^{-1}. Recently, because the vegetation sink of COS has been revised upward by threefold, to maintain a balanced global COS budget, the ocean source strength is considered to have been greatly underestimated [*Berry et al.*, 2013]. A recent modeling study has estimated the ocean source strength to be 813 Gg S yr^{-1}, with most of the emissions in the tropics [*Launois et al.*, 2015b]. Top-down estimates of tropical ocean COS fluxes from satellite observations of surface COS concentration (Aura Tropospheric Emission Spectrometer) also show that the tropical ocean is a significant source of COS. However, a very recent field study in the tropical Atlantic ocean gives a much smaller estimate of the ocean source strength, 345 Gg S yr^{-1}, because of widespread under-

saturation of COS in the tropical ocean [*Lennartz et al.*, 2017]. Arguably, a one-time cruise along a longitudinal section has limited spatial and temporal coverage and cannot fully capture the variability of COS in the surface ocean, but it does show that there are great unknowns in the distribution and seasonality of ocean COS sources. More extensive field measurements are needed to better constrain the ocean COS sources.

1.2.4 COS emissions from anthropogenic activities and biomass burning

Anthropogenic emissions of COS are the second largest source of COS in total. The largest anthropogenic source term is rayon production, which emits CS_2 that is rapidly converted to COS after entering the atmosphere [*Campbell et al.*, 2015]. Smaller anthropogenic source terms include coal burning, aluminum smelting, and biomass burning. From industrial activity record, it is estimated that the current global industrial source of COS is 257 ± 107 Gg S yr^{-1}, accounting for rayon, coal, and aluminum industries. The biomass burning source is estimated as 116 ± 52 Gg S yr^{-1} [*Campbell et al.*, 2015].

Anthropogenic sources of COS have shown large variability since the industrial revolution. An abrupt increase of industrial emission of CS_2 was seen in the 1930s following the expansion of rayon industry [*Campbell et al.*, 2015]. Other sources have increased gradually. However, there is a decline in the COS emission from coal burning since 1990. This may be related to shifts in technologies or energy consumption patterns. The simulated record of anthropogenic COS source is useful in interpreting the historical COS trend [*Campbell et al.*, 2017].

1.2.5 Volcanic COS emissions

Volcanic emissions of COS have often been neglected from the global budget of COS. Because globally significant volcanic eruptions happen only sporadically, it has been assumed that vol-

canic COS input into the troposphere, when amortized over time, is a small fraction. However, a recent estimate of global annual volcanic COS flux has cast doubt upon this assumption. From the COS/SO_2 ratio in volcanic gases, the mean annual volcanic COS flux during 1972–2000 has been estimated as 0.094–320 Gg S yr^{-1} [*Halmer et al.*, 2002]. The enormous uncertainty range associated with this estimate comes from the lack of COS measurements in volcanic emissions and the large variability in the COS/SO_2 ratio (6.1×10^{-8} to 7.9×10^{-4} for subduction zone related volcanoes, and 3.4×10^{-5} to 7.9×10^{-2} for other volcanoes). Volcanic flux of COS needs to be better constrained with field observations and modeling studies.

1.3 Chemical analysis and instrumentation

1.3.1 Gas chromatography based methods

Before the advent of high precision and sensitivity spectroscopy techniques, analysis of COS in air samples were routinely done with gas chromatography (GC) based methods. First, COS and other reduced sulfur gases are caught in a cryogenic trap [*Kesselmeier et al.*, 1999; *Hofmann et al.*, 1992]. The trapped sample is then regenerated and diluted to desired levels before sent to the GC. Different species of reduced sulfur gases are separated in the GC and then analyzed using a flame photometric detector (FPD). The FPD detects the intensity of the spectral lines (usually at 394 nm) emitted from sulfur-containing compounds. An alternative method uses mass spectrometer to obtain sulfur gas concentrations, but still involves cryo-trap and GC for gas separation [*Montzka et al.*, 2007; *Blake et al.*, 2008; *Whelan et al.*, 2013]. Both GC-FPD and GC-MS methods require lengthy calibration and sample preparation steps. Measurements of COS with GC based methods are time and labor intensive and cannot be operated in realtime or with high time resolution. Thus, eddy covariance measurements of ecosystem COS exchange is not possible with GC based methods..

1.3.2 Spectroscopy

Laser spectroscopic methods have recently become available to offer high sensitivity and fast response in-situ measurements of COS mixing ratio without pretreatment. Commercially available spectrometers are now able to perform 10 Hz sampling that suits eddy covariance measurements of ecosystem fluxes [e.g., *Aerodyne Research*, 2017; *Los Gatos Research*, 2017]. The spectroscopy based sampling system can be fully controlled by computers and once set up, may work continuously on its own with relatively little human intervention. Recent studies on ecosystem COS exchange have mostly adopted spectroscopic methods for COS measurements.

Because the ambient concentration of COS is very low, around one millionth of CO_2 concentration, traditional spectrometer design falls short of achieving required signal-to-noise ratio and sensitivity. Several advanced spectroscopic techniques are employed in commercially available COS analyzers to tackle these challenges. For example, the COS analyzer from Aerodyne Research (Billerica, MA, USA) uses a continuous-wave quantum cascade tunable diode laser[1] with high sensitivity and an astigmatic Herriott style multi-pass absorption cell with an effective path length of 76 m [*McManus et al.*, 2010]. The precision at 1 Hz sampling rate is around 5 pmol mol^{-1} according to the manufacturer. Measurements on precalibrated cylinders suggest that the overall uncertainty of this type of analyzer is 7.5 pmol mol^{-1} at 1 Hz [*Kooijmans et al.*, 2016]. Another commonly used COS analyzer model, from Los Gatos Research (San Jose, CA, USA), employs the cavity ring-down spectroscopy (CRDS) technique to increase the absorption signal. In the sample cell, the laser signal is trapped within a cavity bounded by mirrors and the concentration of a gas species is determined from the time of decay of the laser signal intensity within the cavity. The manufacturer also claims 5 pmol mol^{-1} precision for COS measurements at 1 Hz.

Deployment of the COS sampling system requires at the minimum a vacuum pump to maintain the pressure level of the sample cell in the analyzer (e.g., 40 Torr or 53.3 hPa for the Aerodyne

[1] "Tunable" means the wavelength of the laser can be tuned using some technique to focus in a narrow region of absorption bands. Quantum cascade laser is tunable in a wide range because the semiconductor crystal in the laser is a specially designed superlattice material that provides continuous one-dimensional multiple quantum wells.

analyzer), a cooling system to keep the laser unit at its working temperature, and cylinders to provide zero-gas (usually ultrapure dry N_2) for background calibration [*Stimler et al.*, 2010b]. When used for eddy covariance measurements, the vacuum pump and tubing specifications must be chosen such that flow rate in the sampling line is enough to sustain turbulent flow. Because the spectral curve fitting may drift over time, regular background spectra calibration is needed to ensure reliable measurements. The Aerodyne COS analyzer, as an example, allows periodically scheduled auto-calibration of background spectra. The instrument has a solenoid valve system that can switch between different sampling lines and a zero-gas line. It has been suggested that in field operations, background calibration should be performed at least every six hours to prevent significant drift in concentration measurements [*Kooijmans et al.*, 2016].

1.4 Motivation and organization of this dissertation

In the recent decade, COS has gained much attention for its capability as a tracer of terrestrial carbon cycle processes [*Montzka et al.*, 2007; *Berry et al.*, 2013]. Measurements of leaf or ecosystem COS exchange have the potential to offer a variety of value-added applications in carbon cycle studies:

- elucidating leaf-scale physiological mechanisms such as internal conductance [*Stimler et al.*, 2010a] and nighttime stomatal conductance [*Kooijmans et al.*, 2017]
- deriving COS-based estimates of ecosystem GPP [*Blonquist et al.*, 2011; *Asaf et al.*, 2013; *Commane et al.*, 2015] and canopy conductance [*Wehr et al.*, 2017]
- inferring regional scale GPP pattern from surface COS drawdown [*Campbell et al.*, 2008; *Berry et al.*, 2013; *Hilton et al.*, 2015]
- deciphering long-term global GPP trends from COS concentration record [*Campbell et al.*, 2017]
- diagnosing uncertainty sources in carbon cycle models

Ideally, surface COS exchange in the terrestrial ecosystem is dominated by leaf uptake of COS. However, the occurrence of strong soil COS emissions that exceed canopy COS uptake [*Maseyk et al.*, 2014; *Billesbach et al.*, 2014] challenges this assumption. Even if the soil behaves unsurprisingly as a small, consistent sink of COS (as in temperate forests), neglecting such component in the ecosystem COS budget would impose a bias about the order of 20% in COS-derived GPP estimates. Such bias could void the potential gain in the accuracy of GPP estimates from additional COS measurements, compared with the conventional, CO_2 flux partitioned GPP. Using COS measurements to infer ecosystem GPP requires an accurate account of sources and sinks of COS in the ecosystem, especially those in the soils.

This dissertation advances the understanding of soil–atmosphere exchange of COS with process-oriented modeling and field observations. We have developed the first mechanistic model for soil COS flux that accounts properly the diffusive transport, microbial uptake, and thermal production of COS (Chapter 2). We have conducted field measurements using automated soil chambers in an oak woodland in southern California and used the model to explore what environmental factors may control the soil flux (Chapter 3). Another field campaign was conducted in a boreal forest in southern Finland to measure soil COS flux and examine its seasonal pattern and the implication for COS-based GPP inference (Chapter 4). Finally, I summarize the results and what they mean to the ecosystem COS exchange and establish priorities for future research (Chapter 5).

CHAPTER 2

Soil reactive transport model for surface COS flux

2.1 Chapter introduction

Carbonyl sulfide (COS) is an atmospheric trace gas, with average concentration around 480 pmol mol^{-1} [*Montzka et al.*, 2007]. COS uptake in leaves is coupled with CO_2 uptake through stomatal diffusion and hydrolysis mediated by carbonic anhydrase (CA) [*Sandoval-Soto et al.*, 2005; *Stimler et al.*, 2010a; *Seibt et al.*, 2010]. Therefore plant COS flux measurements can be used to partition net carbon exchange into gross primary productivity (GPP) and respiration using the quantitative relationship between leaf COS and CO_2 uptake [*Campbell et al.*, 2008; *Asaf et al.*, 2013]. Since the COS flux observed at ecosystem level and above is the sum of plant and soil fluxes, soil COS fluxes must be well quantified for COS-based flux partitioning. For many biomes where soils have active COS reactions, neglecting soil COS flux would result in significant biases of estimated GPP [*Whelan et al.*, 2016]. To enable COS-based flux partitioning, particularly at larger scales, a soil diffusion-reaction model is needed to generate estimates of soil COS exchange from soil parameters and environmental variables.

Laboratory studies have shown that soil COS uptake is a function of soil temperature and moisture, microbial CA enzyme activity, and ambient COS concentration [*Kesselmeier et al.*, 1999; *Van Diest and Kesselmeier*, 2008]. These empirical relationships were used by *Kettle et al.* [2002] to model global soil COS flux from climatological soil data. Recently, *Berry et al.* [2013] simulated global soil

COS flux in the Simple Biosphere Model (SiB3) with the assumption that soil COS flux is a function of heterotrophic respiration and soil water-filled pore space fraction (WFPS). Here the effect of WFPS on diffusion was represented with an empirical function. Diffusion is not explicitly resolved in any existing model. The effect of a litter layer is also not considered. A litter layer may either act as a barrier for COS diffusion to the soil, or participate in COS exchange. Plant litter has been found to contribute to the surface COS flux in forests [*Kesselmeier and Hubert*, 2002], with magnitudes comparable to that of soil uptake [*Berkelhammer et al.*, 2014].

Existing models have also not considered the possibility of COS production in oxic, upland soils, based on the assumption that they usually behave as a COS sink [e.g. *Kesselmeier et al.*, 1999; *Yi et al.*, 2007; *Van Diest and Kesselmeier*, 2008; *Liu et al.*, 2010a]. However, soil COS fluxes varied between uptake and strong emissions in a wheat field depending on soil environmental variables [*Maseyk et al.*, 2014]. The presence of a compensation point for COS uptake also indicates that uptake and production can co-exist in soils [*Kesselmeier et al.*, 1999; *Conrad and Meuser*, 2000; *Liu et al.*, 2010a].

Here we develop a diffusion-reaction model for soil COS flux, with four major advantages compared to previous empirical approaches:

1. Diffusion is explicitly resolved, providing a more realistic concentration-dependent uptake in the soil column.
2. The model accounts for flux activity in surface litter layers.
3. The model includes COS production terms.
4. Litter and soil COS uptake and production terms can be constrained or optimized using field data.

We evaluate the model using field data from a wheat field in the Southern Great Plains (Billings, OK, USA) and an oak woodland in the Santa Monica Mountains in southern California (Stunt Ranch Reserve, CA, USA).

2.2 Model description

2.2.1 The diffusion equation with source–sink terms

We construct a two-phase 1D diffusion model with microbial COS source–sink terms in soil and litter layers to calculate surface COS fluxes. Diffusion of COS in the soil and litter is described by Fick's law in porous media,

$$\frac{\partial}{\partial t}\left[\left(k_{\mathrm{H}}\theta_{\mathrm{w}}+\theta_{\mathrm{a}}\right)C\right]=\frac{\partial}{\partial z}\left(D\frac{\partial C}{\partial z}\right)+S \tag{2.1}$$

where θ_{w} and θ_{a} ($\mathrm{m^3\ m^{-3}}$ soil) are water-filled and air-filled porosities, C (mol $\mathrm{m^{-3}}$) is the gas concentration of COS, k_{H} (dimensionless) is the Henry's law constant, D ($\mathrm{m^2\ s^{-1}}$) is the effective COS diffusivity in soil. The source–sink terms, S (mol $\mathrm{m^{-3}\ s^{-1}}$), are COS uptake and production in litter and soil. The boundary conditions are (1) concentration at the top boundary equals atmospheric concentration and (2) no flux at the bottom boundary.

For computational efficiency, diffusion in the aqueous phase is not prognostically evaluated but forced by the solubility equilibrium. By invoking Henry's law, the above equation assumes that the aqueous concentration is always in equilibrium with the gaseous concentration, ensuring mass balance. Approximating aqueous diffusive flux with this assumption does not significant bias the surface flux (see Chapter Appendix), since aqueous diffusivity of COS is several orders of magnitude smaller than the gas-phase diffusivity [*Ulshöfer et al.*, 1996].

Advective transport is not considered since the evaluation datasets were not affected by advection. However, advection effects on surface COS flux may not be negligible when there is strong wind pumping causing pressure fluctuations [*Massman et al.*, 1997]. Advective transport, and prognostic aqueous processes (diffusion, dissolution and possibly ebullition) will be considered in future development once relevant data are collected.

2.2.2 Numerical implementation

2.2.2.1 Vertical grid

We use a face-centered finite-volume grid for discretizing the soil column, with 26 computational nodes down to 1 m depth. The vertical grid is constructed using an equation similar to that in the Community Land Model 4.5 [*Oleson et al.*, 2013], which is more densely spaced at the upper boundary. This has advantages of resolving litter layers at the surface, and reducing the computational demand. The depths of the computational nodes are defined with,

$$z_i = \exp(0.2i - 5), \quad i = 0, \ldots, N \tag{2.2}$$

where $N = 25$. The thicknesses of control volumes are,

$$\Delta z_i = \begin{cases} \dfrac{z_0 + z_1}{2}, & i = 0 \\ \dfrac{z_{i+1} - z_{i-1}}{2}, & i = 1, \ldots, N-1 \\ z_N - z_{N-1}, & i = N \end{cases} \tag{2.3}$$

The depths of the layer interfaces are defined with,

$$z_{i+1/2} = \begin{cases} \dfrac{z_i + z_{i+1}}{2}, & i = 0, \ldots, N-1 \\ z_N + \dfrac{z_N - z_{N-1}}{2}, & i = N \end{cases} \tag{2.4}$$

The use of face-centered rather than node-centered control volumes generally gives better evaluation of diffusive fluxes across interfaces.

2.2.2.2 Discretization

We use the Crank–Nicolson method to discretize the diffusion–reaction equation, which ensures numerical stability when using large time steps [*Crank and Nicolson*, 1947]. The method is im-

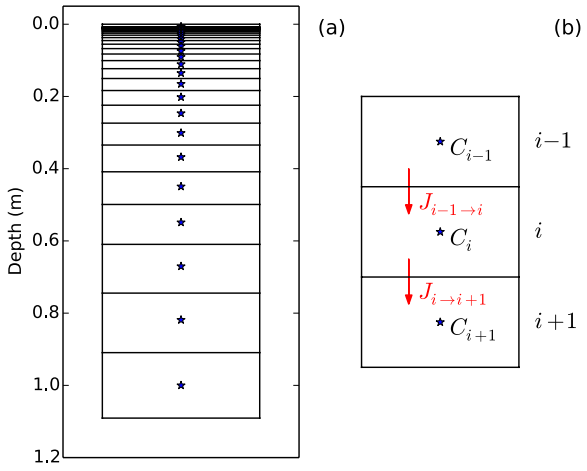

Figure 2.1: (a) The vertical finite-volume boxes and computational nodes (asterisk). (b) A schematic figure showing the diffusive fluxes (J) across boxes, which relate to concentration changes through mass balance.

plemented with second order accuracy in space and in time. The discretized finite difference equations are a sparse linear system that can be easily solved.

We first discretize spatially Eq. (2.1) on the defined grid by integrating in each control volume [*Durran*, 2010; *Tang and Riley*, 2014],

$$\eta_i \Delta z_i \frac{\mathrm{d}C_i}{\mathrm{d}t} = \begin{cases} J_{a\to 0} - J_{0\to 1} + S_0 \Delta z_0, & i = 0 \\ J_{i-1\to i} - J_{i\to i+1} + S_i \Delta z_i, & 1 \le i \le N-1 \\ J_{N-1\to N} + S_N \Delta z_N, & i = N \end{cases} \tag{2.5}$$

where $\eta_i = (k_\mathrm{H}\theta_\mathrm{w} + \theta_\mathrm{a})$ at $z = z_i$ is a simplifying notation, $J_{a\to 0}$ represents diffusive flux from the atmosphere to soil layer 0, and $J_{i-1\to i}$ represents diffusive flux from layer $i-1$ to layer i. The flux term J can be evaluated with a central difference scheme,

$$J_{i-1\to i} = J_{i-1/2} = \left(-D\frac{\partial C}{\partial z}\right)_{i-1/2} = -D_{i-1/2}\frac{C_i - C_{i-1}}{z_i - z_{i-1}} \tag{2.6}$$

The diffusivity at the interface, $D_{i-1/2}$ can be interpolated linearly, $D_{i-1/2} = (D_i + D_{i-1})/2$, since the interface locates at the center of two computational nodes. For the ease of denotation, we define $G_{i-1/2} = D_{i-1/2}/(z_i - z_{i-1})$ as the conductance at the interface.

The flux at the topmost layer is thus,

$$J_{a\to 0} = -D_{a\to 0}\frac{C_0 - C_a}{z_0 - 0} = -G_{a\to 0}(C_0 - C_a) \tag{2.7}$$

Again, $D_{a\to 0}$ is the diffusivity at the soil–atmosphere boundary, and $G_{a\to 0}$ is the conductance. We use the harmonic mean of soil diffusivity D_0 and air diffusivity D_a for $D_{a\to 0}$, following the conductance model in *Tang and Riley* [2013],

$$D_{a\to 0} = \frac{2}{\dfrac{1}{D_0} + \dfrac{1}{D_a}} \tag{2.8}$$

By rewriting Eq. (2.5) in a matrix form, we obtain an ordinary differential equation (ODE) system for time,

$$\mathbf{A}\frac{\mathrm{d}}{\mathrm{d}t}\mathbf{C} = \mathbf{B}\mathbf{C} + \mathbf{S} \tag{2.9}$$

where

$$\mathbf{C} = (C_0, C_1, \ldots, C_N)^{\mathbf{T}}$$

$$\mathbf{A} = \text{diag}\ (\eta_0\Delta z_0, \eta_1\Delta z_1, \ldots, \eta_N\Delta z_N)$$

$$\mathbf{B} = \begin{pmatrix} -G_{a\to 0} - G_{1/2} & G_{1/2} & 0 & \cdots & 0 & 0 & 0 \\ G_{1/2} & -G_{1/2} - G_{3/2} & G_{3/2} & \cdots & 0 & 0 & 0 \\ \vdots & \vdots & \vdots & \ddots & \vdots & \vdots & \vdots \\ 0 & 0 & 0 & \cdots & G_{N-3/2} & -G_{N-3/2} - G_{N-1/2} & G_{N-1/2} \\ 0 & 0 & 0 & \cdots & 0 & G_{N-1/2} & -G_{N-1/2} \end{pmatrix} \tag{2.10}$$

$$\mathbf{S} = \left(S_0\Delta z_0 + \frac{D_{a\to 0}}{z_0}C_a, S_1\Delta z_1, \ldots, S_N\Delta z_N\right)^{\mathbf{T}}$$

The above linear ODE system is then discretized at time step $t = (n + 1/2)\Delta t$,

$$\mathbf{A}\frac{\mathbf{C}_{n+1} - \mathbf{C}_n}{\Delta t} = \mathbf{B}\frac{\mathbf{C}_{n+1} + \mathbf{C}_n}{2} + \mathbf{S} \tag{2.11}$$

Therefore the evolution in time is,

$$\mathbf{C}_{n+1} = (2\mathbf{A} - \Delta t\mathbf{B})^{-1}\left[(2\mathbf{A} + \Delta t\mathbf{B})\mathbf{C}_n + 2\Delta t\mathbf{S}\right] \tag{2.12}$$

At each time step, the concentration profile is evolved to the next time step with the diffusion–reaction operator. Thus the model can simulate transient conditions in real time.

2.2.3 Parameterization

2.2.3.1 Diffusivities

The diffusivity of COS in soil media (D, $m^2\ s^{-1}$) is calculated following *Moldrup et al.* [2003],

$$\frac{D}{D_m} = \theta_a^2 \left(\frac{\theta_a}{\theta_{sat}}\right)^{3/b} \left(\frac{T}{T_{ref}}\right)^n \tag{2.13}$$

where θ_{sat} ($m^3\ m^{-3}$) is the soil total porosity ($\theta_{sat} = \theta_a + \theta_w$), D_m ($m^2\ s^{-1}$) is the COS–air diffusivity at $T_{ref} = 25°C$ and 1 atm, $n = 1.5$ [*Bird et al.*, 2002], and b is parameterized with water retention function [*Wingate et al.*, 2008; *Clapp and Hornberger*, 1978]. We assume that the same function holds for litter layer diffusivity since litter is also a porous medium like the soil.

For COS, D_m is calculated as $1.337 \times 10^{-5}\ m^2\ s^{-1}$ at 25°C and 1 atm, based on the theoretical CO_2/COS diffusivity ratio of 1.21 derived in *Seibt et al.* [2010] from the Chapman-Enskog kinetic theory, and the molecular diffusivity of CO_2 ($1.618 \times 10^{-5}\ m^2\ s^{-1}$, 25°C and 1 atm) is calculated from *Massman* [1998].

2.2.3.2 COS solubility function

In solubility equilibrium, the chemical potentials of COS in gas phase (μ_g) and in aqueous solution (μ_{aq}) are equal,

$$\mu_g = \mu_g^{\ominus}(T) + RT \ln \frac{p}{p^{\ominus}} + RT \ln \phi = \mu_{aq}^{*}(T, p) + RT \ln x + RT \ln \gamma = \mu_{aq} \tag{2.14}$$

where p is the partial pressure in gas phase, x is the molar fraction in aqueous phase, ϕ is the fugacity coefficient, γ is the activity coefficient, and $p^{\ominus}$ is the standard pressure. Here, $\mu_g^{\ominus}$ and μ_{aq}^{*} are both chemical potentials under chosen standard conditions. Note that $\mu_g^{\ominus}$ depends only on temperature, whereas μ_{aq}^{*} depends on both temperature and pressure.

Table 2.1: COS solubility functions in the literature and in this study.

Reference	Model	Unit	Parameters
Wilhelm et al. [1977]	$\ln k_{\mathrm{H},xp} = \frac{A}{R} + \frac{B}{RT} + \frac{C}{R}\ln\frac{T}{\mathrm{K}}$	atm^{-1}	$A = -1839\ \mathrm{J\ K^{-1}\ mol^{-1}}$ $B = 99981\ \mathrm{J\ mol^{-1}}$ $C = 252\ \mathrm{J\ K^{-1}\ mol^{-1}}$
De Bruyn et al. [1995]	$\ln k_{\mathrm{H},xp} = \frac{A}{R} + \frac{B}{RT}$	atm^{-1}	$A = -124\ \mathrm{J\ K^{-1}\ mol^{-1}}$ $B = 17552\ \mathrm{J\ mol^{-1}}$
This study with data from *Elliott et al.* [1989]	$k_{\mathrm{H},cc} = (T/\mathrm{K})\exp\left(\alpha + \frac{\beta}{T/\mathrm{K}}\right)$	$\mathrm{mol\ mol^{-1}}$	$\alpha = -20.00$ $\beta = 4050$

For a dilute solution, as $x \longrightarrow 0$ and $p/p^{\ominus} \longrightarrow 0$, we have $\phi \longrightarrow 1$ and $\gamma \longrightarrow 1$. This is valid for COS in natural environments because its molar fraction is only $\sim 10^{-10}$ in the atmosphere [*Montzka et al.*, 2007] and $\sim 10^{-12}$ in seawater [*Ulshöfer et al.*, 1996; *Von Hobe et al.*, 1999]. Therefore,

$$\mu^{*}_{\mathrm{aq}} - \mu^{\ominus}_{\mathrm{g}} = -RT\ln\frac{x}{p/p^{\ominus}} \equiv -RT\ln k_{\mathrm{H},xp} \tag{2.15}$$

where $k_{\mathrm{H},xp}$ is the Henry's law constant defined as the ratio of aqueous phase molar fraction to gas phase partial pressure. According to van 't Hoff equation,

$$\frac{\partial \ln k_{\mathrm{H},xp}}{\partial T} = \frac{\Delta_{\mathrm{sol}}H^{\ominus}_{\mathrm{m}}}{RT^2} \tag{2.16}$$

where $\Delta_{\mathrm{sol}}H^{\ominus}_{\mathrm{m}}$ is the standard partial molar enthalpy of dissolution. We assume that it is constant within the temperature range of ambient conditions. With respect to a reference state T_0, integrating yields,

$$\ln k_{\mathrm{H},xp} = -\frac{\Delta_{\mathrm{sol}}H^{\ominus}_{\mathrm{m}}}{R}\left(\frac{1}{T} - \frac{1}{T_0}\right) \tag{2.17}$$

Temperature dependence of $k_{\mathrm{H},xp}$ can thus be described by the following function, with A and B constants,

$$k_{\mathrm{H},xp} = \exp\left(\frac{A}{R} + \frac{B}{RT}\right) \tag{2.18}$$

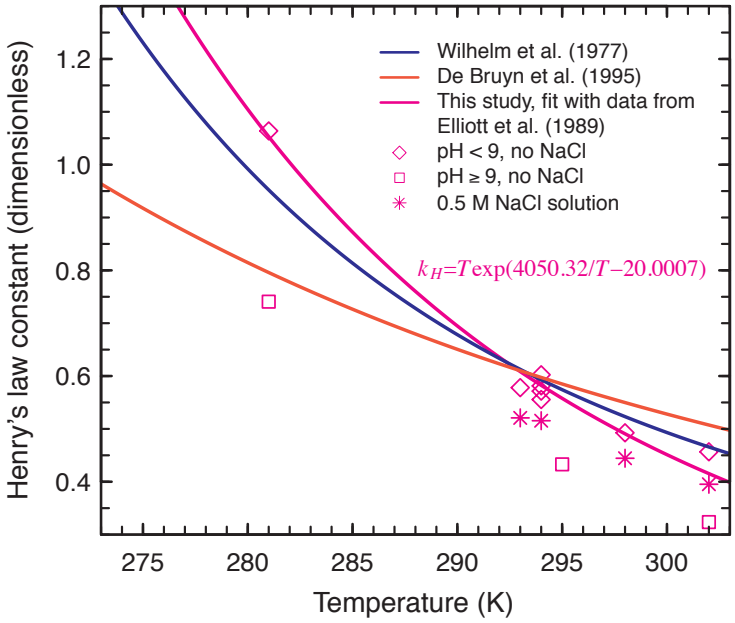

Figure 2.2: COS solubility function used in this study (pink), obtained from regression with *Elliott et al.* [1989] data (pink). Solubility data measured under pH < 9, non-saline conditions (pink diamonds) were used for the regression. Also plotted are the COS solubility functions from *Wilhelm et al.* [1977] and *De Bruyn et al.* [1995].

The dimensionless Henry's law constant, $k_{\mathrm{H},cc}$, is defined as the ratio of aqueous molar concentration to gaseous molar concentration.

$$k_{\mathrm{H},cc} \equiv \frac{c_{\mathrm{aq}}}{c_{\mathrm{g}}} = \frac{\rho_{\mathrm{w}} x / M_{\mathrm{w}}}{p/(RT)} = \frac{\rho_{\mathrm{w}} RT}{M_{\mathrm{w}} p^{\ominus}} \cdot \frac{x}{p/p^{\ominus}} = \frac{\rho_{\mathrm{w}} RT}{M_{\mathrm{w}} p^{\ominus}} k_{\mathrm{H},xp} = T \exp\left(\frac{A}{R} + \ln \frac{\rho_{\mathrm{w}} R}{M_{\mathrm{w}} p^{\ominus}} + \frac{B}{RT}\right) \quad (2.19)$$

Thus, we can build a nonlinear regression model for temperature dependence of the dimensionless Henry's law constant,

$$k_{\mathrm{H},cc}(T) = (T/\mathrm{K}) \exp\left(\alpha + \frac{\beta}{T/\mathrm{K}}\right) \quad (2.20)$$

Using *Elliott et al.* [1989] data for the regression (Figure 2.2), we obtained that $\alpha = -20.00^{+1.48}_{-1.46}$, and $\beta = 4050^{+424}_{-430}$ (95% confidence interval).

2.2.3.3 Soil fluxes

Because both COS uptake and production activities exist in soils, and the net COS flux exhibits a linear response to COS concentration [*Kesselmeier et al.*, 1999; *Conrad and Meuser*, 2000], we assume that uptake and production are separable terms.

Soil COS uptake (U) is formulated based on Michaelis–Menten kinetics, with dependence on soil temperature and moisture:

$$U = -V_{\mathrm{SU,max}} \cdot \frac{k_{\mathrm{H}} C}{K_{\mathrm{m}} + k_{\mathrm{H}} C} \cdot f(T) \cdot g(w) \tag{2.21}$$

where $K_{\mathrm{m}} = 1.9$ mol m^{-3} is the Michaelis constant for COS hydrolysis by CA [*Ogawa et al.*, 2013], $V_{\mathrm{SU,max}}$ (mol m^{-3} s^{-1}) is the soil COS uptake capacity, and $f(T)$ and $g(w)$ are temperature and moisture limitation functions.

We assume that the temperature limitation function for soil COS uptake reflects the temperature dependence of enzyme activity, which is described as [*Peterson et al.*, 2004; *Daniel et al.*, 2010],

$$f(T) = A_T \frac{T \exp\left(-\dfrac{\Delta^{\ddagger} G_{\mathrm{cat}}}{RT}\right)}{1 + \exp\left[-\dfrac{\Delta H_{\mathrm{eq}}}{R}\left(\dfrac{1}{T} - \dfrac{1}{T_{\mathrm{eq}}}\right)\right]} \tag{2.22}$$

where $\Delta^{\ddagger} G_{\mathrm{cat}}$ (J mol^{-1}) is the activation free energy of the transition state of CA enzyme in terms of COS reactions, ΔH_{eq} (J mol^{-1}) is the enthalpy change during conversion from activated to inactivated form of the enzyme, T_{eq} (K) is the temperature at which the concentrations of the activated enzyme and the inactivated enzyme are equal, A_T is the pre-exponential factor to normalize the equation so that $\max f(T) = 1$. The function has a temperature optimum, T_{opt}, defined at which the function reaches its maximum value. This temperature optimum is close to the parameter T_{eq}, and always smaller than it [*Peterson et al.*, 2004]. Other enzymes in soil microbes may also contribute to COS uptake, for example, COSase, nitrogenase and CS_2 hydrolase [*Ogawa et al.*, 2013]. These enzymes are not considered here due to lack of information on their kinetics and distribution in the microbial community. They are also unlikely to be as ubiquitous as CA.

Typical fit values of $\Delta^{\ddagger}G_{cat}$ for a range of enzymes are between 51 and 88 kJ mol^{-1}, whereas ΔH_{eq} varies from 86 to 826 kJ mol^{-1} [*Daniel et al.*, 2010]. We assume that $\Delta^{\ddagger}G_{cat}$ = 84.10 kJ mol^{-1} (20.1 kcal mol^{-1}) for CA-catalyzed COS hydrolysis, based on calculations of CA–COS nucleophilic attack, the rate-determining step of COS hydrolysis, which used $[(H_3N)_3Zn(OH)]^+$ as a structural analog of the active site of CA [*Schenk et al.*, 2004].

The temperature dependence (Eq. 2.22) has a similar mathematical form as that in *Kesselmeier et al.* [1999], but the temperature limitation of COS uptake is now linked to enzyme kinetics that can be determined in the laboratory. Using $\Delta^{\ddagger}G_{cat}$ = 84.10 kJ mol^{-1}, ΔH_{eq} = 358.9 kJ mol^{-1}, and T_{eq} = 293.14 K, we can approximate the temperature function $\varphi(T)$ in *Kesselmeier et al.* [1999] (Figure 2.3a). In this study, T_{eq} will be an adjustable parameter to fit temperature dependence for different soils (see section 2.2.4.2 and Table 2.2).

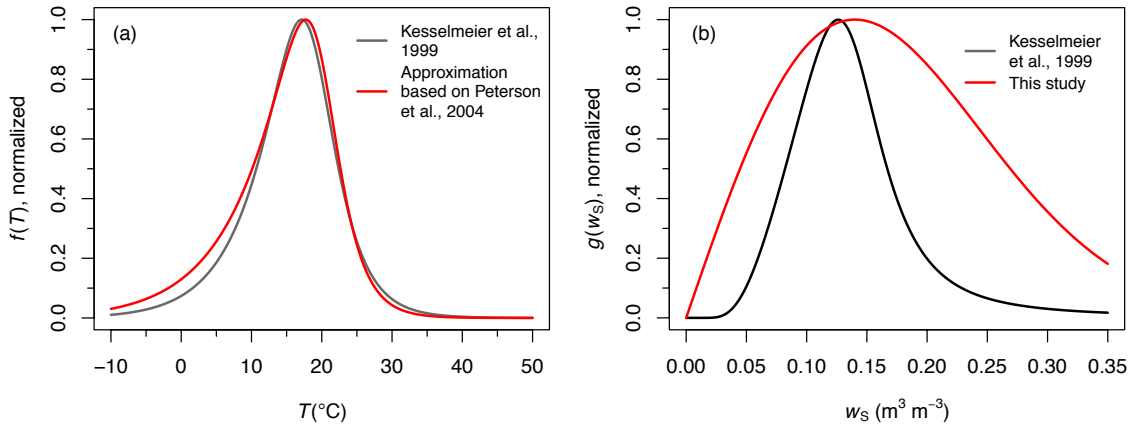

Figure 2.3: (a) Temperature dependence function of soil COS uptake (Eq. 2.22) with ΔH_{eq} = 358.9 kJ mol^{-1} and T_{eq} = 20°C. (b) Moisture dependence function of soil COS uptake (Eq. 2.23) with w_{opt} = 0.14 m^3 m^{-3}. Also plotted are the temperature and moisture dependence functions of *Kesselmeier et al.* [1999].

For the parameterization of moisture dependence, we use a simple bell-shaped function, de-

scribed by the form of Rayleigh distribution function,

$$g(w) = A_w \cdot \frac{w}{w_{\text{opt}}^2} \cdot \exp\left(-\frac{w^2}{2w_{\text{opt}}^2}\right) \tag{2.23}$$

where w_{opt} ($\text{m}^3\ \text{m}^{-3}$) is the optimal water content for COS uptake, and A_W is the normalization factor such that $\max g(w) = 1$. The parameter w_{opt} can be adjusted to fit observed data (see section 2.2.4.2 and Table 2.2). The function has a wider range than that in *Kesselmeier et al.* [1999] (Figure 2.3b), and does not approach zero at high soil moisture. It represents the dependence of microbial uptake per se instead of a combination of diffusion and microbial uptake, because diffusion has already been accounted for. We found no empirical reason to assume that microbial uptake of COS to be zero at high soil water content, if it is not diffusion-limited.

Soil COS production is represented as an exponential function of temperature,

$$P = V_{\text{SP,max}} \cdot \exp\left[k_T(T - T_{\text{ref}})\right] \tag{2.24}$$

where $V_{\text{SP,max}}$ ($\text{mol}\ \text{m}^{-3}\ \text{s}^{-1}$) is the soil COS production capacity, k_T (K^{-1}) is the temperature dependence factor that is equivalent to $Q_{10} = 1.9$, and $T_{\text{ref}} = 25°\text{C}$. The Q_{10} value here is set as the average value of the Q_{10} associated with the two regression lines of COS flux vs. temperature in *Maseyk et al.* [2014]. Lab incubation of various soils has found that soil COS emissions generally exhibit exponential responses with temperature [*Whelan et al.*, 2016]. Although COS may be produced by both soil microbes and roots [*Maseyk et al.*, 2014], we use a single production term in Eq. (2.24) due to a lack of data on the individual temperature responses of the different components.

2.2.3.4 Litter fluxes and litter properties

Litter was present at one of the model evaluation sites (Stunt Ranch). We obtained an equation for litter COS fluxes based on an incubation experiment with litter at the Stunt Ranch site [*Sun*

et al., 2016],

$$F_{\mathrm{SL}} = -V_{\mathrm{LU,max}} \cdot \frac{k_{\mathrm{H}} C}{K_{\mathrm{m}} + k_{\mathrm{H}} C} \cdot \sinh\left(k_{\mathrm{L}} w_{\mathrm{L}}\right) + V_{\mathrm{LP,max}} \cdot \exp\left[k_T (T - T_{\mathrm{ref}})\right] \tag{2.25}$$

where $V_{\mathrm{LU,max}}$ (mol m^{-3} s^{-1}) and $V_{\mathrm{LP,max}}$ (mol m^{-3} s^{-1}) are the litter COS uptake and production capacities, k_T (K^{-1}) is the temperature dependence factor for COS production equivalent to $Q_{10} = 1.9$, and k_L (dimensionless) is the moisture limitation factor for COS uptake. The hyperbolic sine function is chosen to describe the exponential dependence on litter water content.

Litter porosity is usually much larger than that of soils. In the model, the porosity at the grid point near the litter–soil interface is interpolated so as to prevent numerical instability caused by discontinuity (Figure 2.4).

Temperatures of the litter layers were interpolated between soil and chamber air temperature by assuming a logarithmic temperature profile in the surface layer, according to mixing length theory [*Prandtl*, 1925]. The roughness length was assumed to be 0.01 m [*Stull*, 1988].

2.2.4 Field datasets for model evaluation

2.2.4.1 Field sites

Southern Great Plains, OK (SGP): Soil COS fluxes were measured from 1 April to 31 May 2012 in a wheat field at the ARM Southern Great Plains Central Facility (36.61°N, 97.49°W) near Billings, OK. The soils are mainly silt loam to clay loam, with 33% sand, 22% silt, and 45% clay [*Fischer et al.*, 2007]. Further details on the site and data are provided in *Maseyk et al.* [2014].

Stunt Ranch, CA (SR): Surface COS fluxes were measured from 1 April to 15 April 2013 in a Mediterranean oak woodland at the University of California Stunt Ranch Santa Monica Mountains Reserve (34°05′38″N, 118°39′26″W) in southern California. The soil is a gravelly sandy loam,

covered with 2 cm of leaf litter from a coast live oak tree (*Quercus agrifolia*). The site received 2 mm precipitation the day before the measurements started. The experimental setup was largely identical to that used at SGP [see *Maseyk et al.*, 2014]. Further details on the site and data are provided in *Sun et al.* [2016].

2.2.4.2 Site-specific parameters

Table 2.2: Site-specific parameters (SR: Stunt Ranch, CA; SGP: Southern Great Plains, OK).

Site	θ_{sat} ($m^3\ m^{-3}$)	θ_{FC} ($m^3\ m^{-3}$)	z_T (m)	T_{eq} (°C)	w_{opt} ($m^3\ m^{-3}$)	θ_{lit} ($m^3\ m^{-3}$)	d_{lit} (cm)
SGP	0.50 (0.60 in the top 2 cm)	N/A	0.11	10	0.20	N/A	N/A
SR	0.35	0.20	0.14	15	0.14	0.94	2

Site-specific parameters are summarized in Table 2.2. We used site-specific values for soil porosity that were constant with depth except in the top few centimeters when there is loose topsoil. Soil porosity is estimated as 0.50 $m^3\ m^{-3}$ at the SGP site from the maximum observed soil moisture [*Fischer et al.*, 2007; *Maseyk et al.*, 2014], but that in the top 2 cm is assumed to be 0.60 $m^3\ m^{-3}$ as the topsoil is looser due to agricultural activity. At the SR site, soil porosity was measured as 0.35 $m^3\ m^{-3}$. We assume the field capacity (θ_{FC}) is 0.20 $m^3\ m^{-3}$ at the SR site based on soil textures [*Or and Wraith*, 2002]. For the parameter b in Eq. (2.13), we use 4.9 for SR (sandy loam) and 5.3 for SGP (silt loam) based on *Clapp and Hornberger* [1978].

Soil temperature profiles are modeled with the observations at 5 cm depth. The temperature signals are considered as a superposition of fast varying diurnal signals (T_F) and slowly varying synoptic scale signals (T_S) [*Van Wijk and de Vries*, 1963],

$$T(z,t) = T_S + T_F \cdot \exp(-z/z_T)\sin(\omega t + \psi - z/z_T) \tag{2.26}$$

where z_T is the damping depth for diurnal temperature waves, $\omega = 2\pi$ day^{-1} is the angular

frequency, ψ is the phase constant. z_T is determined from,

$$z_T = \sqrt{2\alpha_T/\omega} \tag{2.27}$$

where α_T ($m^2\ s^{-1}$) is the soil thermal diffusivity, calculated from soil mineral composition and water content using empirical formulae in *Peters-Lidard et al.* [1998] and *Johansen* [1975]. Soil thermal diffusivities are $2.5–5.0 \times 10^{-7}\ m^2\ s^{-1}$ at the SGP site, and $6.8–8.1 \times 10^{-7}\ m^2\ s^{-1}$ at the SR site, assuming typical mineral compositions. The thermal diffusivities are translated to average damping depths of 0.11 m (SGP) and 0.14 m (SR), respectively.

For the SR data, we observed that the temperature optimum for COS uptake is $T_{opt} \approx 13°C$ [*Sun et al.*, 2016]. This is reproduced by setting T_{eq} at 15°C in Eq. (2.22). For the SGP soil, because COS flux did not show a temperature optimum for uptake during the observed temperature range (7–47°C) in *Maseyk et al.* [2014], we set $T_{eq} = 10°C$ (equivalent to $T_{opt} \approx 7°C$) to get a monotonic relationship with temperature.

Soil moisture was measured at 5 cm depth at both sites, and additionally at 30 cm at SGP. We generate soil moisture profiles for the SGP site by interpolating between the 5 and 30 cm data, and assuming constant soil moisture below 30 cm (cf. 1D simulations with gravity drainage boundary condition in *Walker*, 1999). For the SR site, we assume soil moisture at 1 m depth is at field capacity (θ_{FC}, $m^3\ m^{-3}$), and interpolated smoothly between the values at the surface and 1 m depth (Figure 2.4). The conditions below 10 cm do not significantly affect surface COS flux according to Figure 2.11 (see also section 2.4.2). The optimum water content for soil COS uptake, w_{opt}, is assumed to be $0.20\ m^3\ m^{-3}$ for SGP soils, corresponding to a threshold for the COS flux-temperature response [*Maseyk et al.*, 2014]. For SR soils, we set $w_{opt} = 0.14\ m^3\ m^{-3}$, estimated from lab incubation data of the same soils [*Whelan et al.*, 2016].

Since litter was present at the SR site, litter layers are included in model simulations when validating the model with the SR dataset. The 2 cm thick litter layer is represented in the top 6 grid points. Litter porosity was measured to be $0.94\ m^3\ m^{-3}$. Litter water content (LWC) is an important variable controlling litter COS fluxes. Since LWC was not measured at SR, we test two

scenarios: (1) fast decreasing LWC, and (2) slowly decreasing LWC following the precipitation event on the day before the measurements started. We also evaluate the surface COS flux in the absence of litter fluxes.

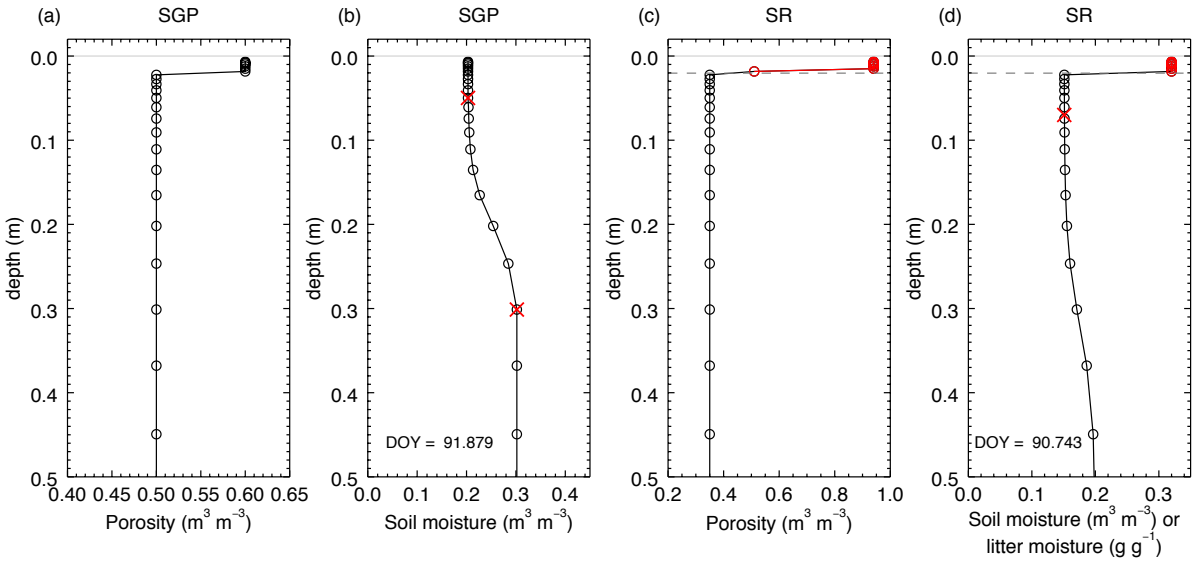

Figure 2.4: Soil porosity and moisture profiles at the SGP site (a, c) and the SR site (c, d) in the top 50 cm. Note that in (c) and (d), the profiles also show the porosity in the litter layers and litter water content (g g^{-1}) in red. The dashed lines denote litter-soil interfaces, and the light gray lines represent air-litter interfaces (same for Figure 2.7). One computational node near litter-soil interface is interpolated for porosity in order to prevent numerical instability. Measured data of soil moisture at 5 and 30 cm for SGP, and 5 cm for SR, are shown as red crosses.

2.3 Evaluation results

In the evaluation, soil COS uptake and production capacities ($V_{SU,max}$ and $V_{SP,max}$) are chosen to fit the general trend of observed data. The aim here is to demonstrate that the model can reproduce the data with the proper settings, and thus has the potential to be applied at large scales. Model performance in the evaluation tests is summarized in Table 2.3.

Table 2.3: Summary of model evaluation results.

Site	$V_{SU,max}$ (mol m^{-3} s^{-1})	$V_{SP,max}$ (mol m^{-3} s^{-1})	Mean flux, observed (pmol m^{-2} s^{-1})	Mean flux, modeled (pmol m^{-2} s^{-1})	RMSE	r^2
SGP	1.2×10^{-1}	1×10^{-10} [a], 3.3×10^{-11} [b]	1.0	0.7	2.3	0.688
SR	1×10^{-2}	2×10^{-11}	−1.5	−1.6	0.5	0.869

[a] For the growing season (before DOY 130). [b] For the post-senescence stage (after DOY 134).

2.3.1 Evaluation against data from the wheat field soil (SGP)

The simulated COS fluxes at the SGP site are generally in good agreement with the observations (Figure 2.5), especially the diurnal variations and the transition from uptake to emissions. Model results and the data lie on a 1:1 line, albeit with large scatter at high emission fluxes (Figure 2.5c). As shown in the distribution of model residuals with respect to surface soil temperature and moisture (Figure 2.5d), the model tends to underestimate the high emissions at high temperatures. In the growing season (before DOY 130), the model captures the high uptake instances, but tends to underestimate high emission instances at mid-day. This is mainly because some high emissions are not associated with high soil temperature. During the senescence and post-harvest period (after DOY 134), the model reproduces the strong diurnal variations, except that the mid-day peak emissions are underestimated. Examples for COS profiles during overall soil COS uptake and emissions show exponential decrease and increase of the COS concentration in soil air with depth, respectively (Figure 2.7a).

From the incubation experiments, *Maseyk et al.* [2014] shows that the root-free soil exhibited uptake at −0.21 pmol kgDW^{-1} s^{-1} (−0.4 pgS gDW^{-1} min^{-1}) in the peak growing season, but emissions at 0.10 pmol kgDW^{-1} s^{-1} (0.2 pgS gDW^{-1} min^{-1}) during late growing season and senescence. When translated to the V_{max} parameters as in Eq. (2.21) and (2.24), the incubation data correspond to estimates of $V_{SU,max}$ at 2.6×10^{-2} mol m^{-3} s^{-1} in April, and $V_{SP,max}$ at 1.3×10^{-10} mol m^{-3} s^{-1} in

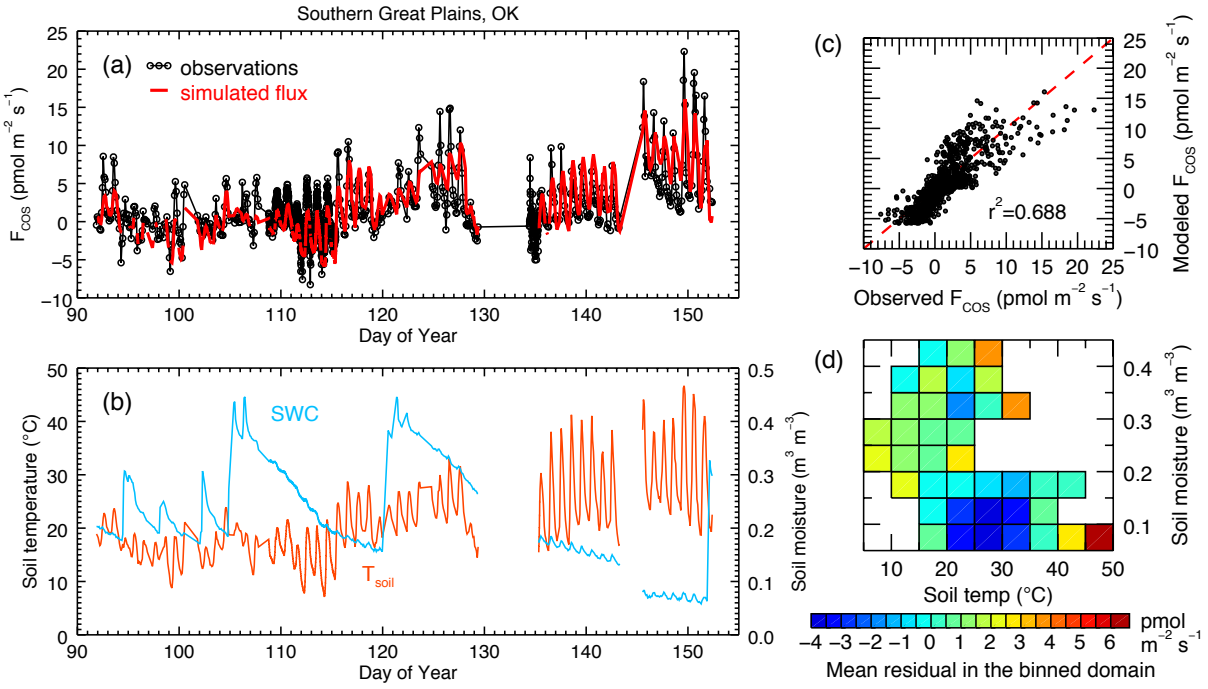

Figure 2.5: (a) Observed COS fluxes (black) and modeled COS fluxes (red) at the Southern Great Plains site. (b) Surface soil temperature and moisture at the site during the same period. (c) Model vs. data for COS fluxes. (d) Mean residuals (observed – modeled) binned by 5°C soil temperature and 0.05 m^3 m^{-3} soil moisture steps.

May, assuming ambient COS concentration at 2.04×10^{-8} mol m^{-3} (500 pptv, 1 atm, 25°C), $k_H \sim 1$, and soil dry density 1.33×10^3 kg m^{-3} estimated from porosity (0.50). These estimates from incubation data are reasonably similar to the model parameters needed to fit the data (Table 2.3) given that there were only a few incubation experiments.

The observed COS emissions were higher in the senescence and post-harvest stages (after DOY 134) than during the growing season. However, when the temperature dependence is considered, the COS production capacity in the growing season (before DOY 130) must be higher than after harvest to account for the high fluxes under relatively low soil temperatures ($<$ 20°C) in this period (Figure 2.5a and Table 2.3). We hypothesize that root production of COS may have peaked during the late growing season following increased root sulfate uptake during seed ripening [*Zhao et al.*, 1999], and then decreased during the following senescence stage.

Surprisingly, to simulate the strong diurnal variability of COS emissions in the senescence and post-harvesting stages, the high emissions need to be counteracted by continuing COS uptake, with the same uptake capacity as during the growing season. Without uptake activity, COS would accumulate in the soil column from high production in the daytime, and still exhibit high emissions at night. An additional contribution to daytime emissions could have come from photochemical production of COS, as observed for SGP soil in lab incubations [*Whelan and Rhew*, 2015]. However, this would only be a minor component since the maximum photochemical production rate translated to a per area basis was around 2 pmol m^{-2} s^{-1}, less than 10% of the observed diurnal variability. In addition, photochemical production would not have affected the fluxes measured inside the chamber because it was opaque. However, it may have affected the fluxes measured at the ecosystem scale [*Billesbach et al.*, 2014; *Maseyk et al.*, 2014]. Hence, photochemical production will be included in a future model version.

2.3.2 Evaluation against data from the oak woodland soil (SR)

The observation period at SR started with a rain event, and thus at high LWC. We set the starting LWC to 0.32 g g^{-1} to fit the observed high uptake fluxes, and simulated a rapid water loss (Figure 2.8b) due to strong evaporation at typically warm and sunny conditions. The LWC was assumed to decrease to 0.06 g g^{-1} following an exponential decay function. This assumption fits well with the observed fluxes, both for the diurnal variations and the overall trend (Figure 2.6). As an alternative, we used a scenario with slowly decreasing LWC (Figure 2.8b), or assuming no litter flux at all. In the first case, the uptake during the dry period was overestimated, whereas the no-litter flux scenario did not reproduce the general trend, even after soil uptake capacity was increased by 10-fold to compensate for the missing litter uptake (Figure 2.8a). The soil moisture change in this period was not strong enough to drive the overall trend from strong uptake to weak uptake.

The simulated COS profiles show that the presence of litter layers on top of the soil reduces the COS supply available to the soil, especially when there is strong uptake in the litter layers, thus

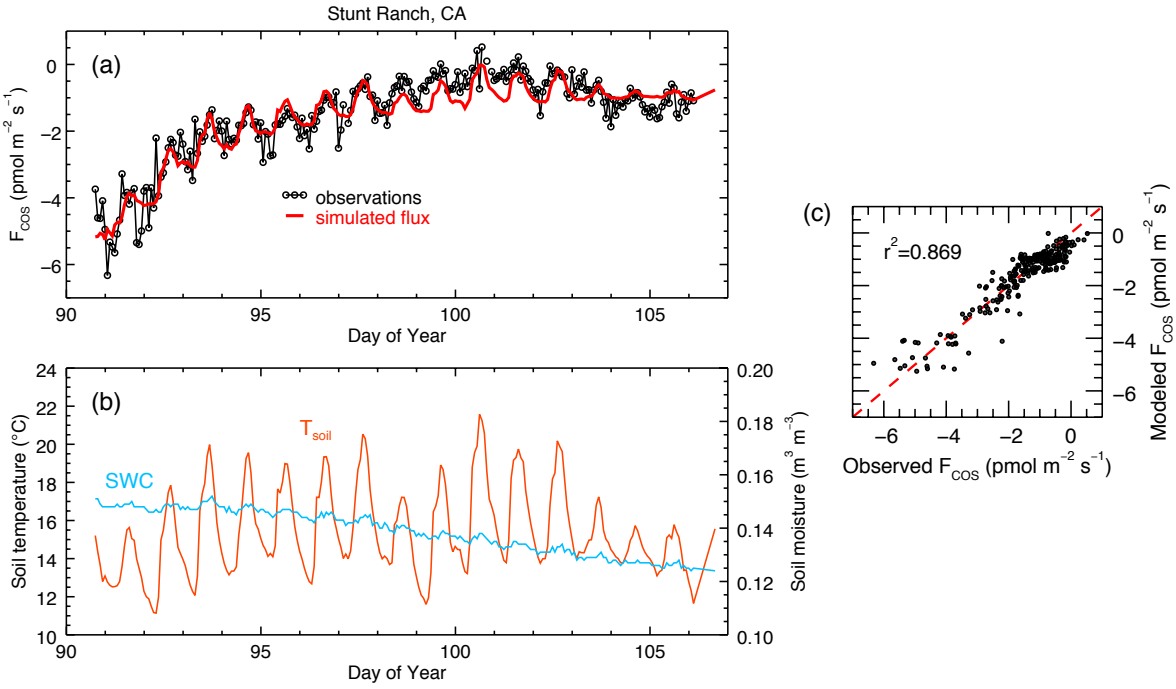

Figure 2.6: (a) Observed COS fluxes (black) and modeled COS fluxes (red) at the Stunt Ranch site. (b) Surface soil temperature and moisture at the site during the same period. (c) Model vs. data for COS fluxes.

limiting the contribution of soil uptake to the overall surface uptake (Figure 2.7b). When LWC is low and litter uptake is weak, this limiting effect is not significant.

2.4 Discussion

2.4.1 Sensitivity tests: diffusion-controlled uptake

Laboratory studies have found that soil COS uptake has an optimum at 19–30% water-filled pore space fraction (WFPS) and approaches zero as WFPS becomes higher [*Kesselmeier et al.*, 1999; *Van Diest and Kesselmeier*, 2008]. We conducted a set of idealized simulations to find what factors control such dependence. Based on model results, the shape of the surface flux vs. soil moisture curve

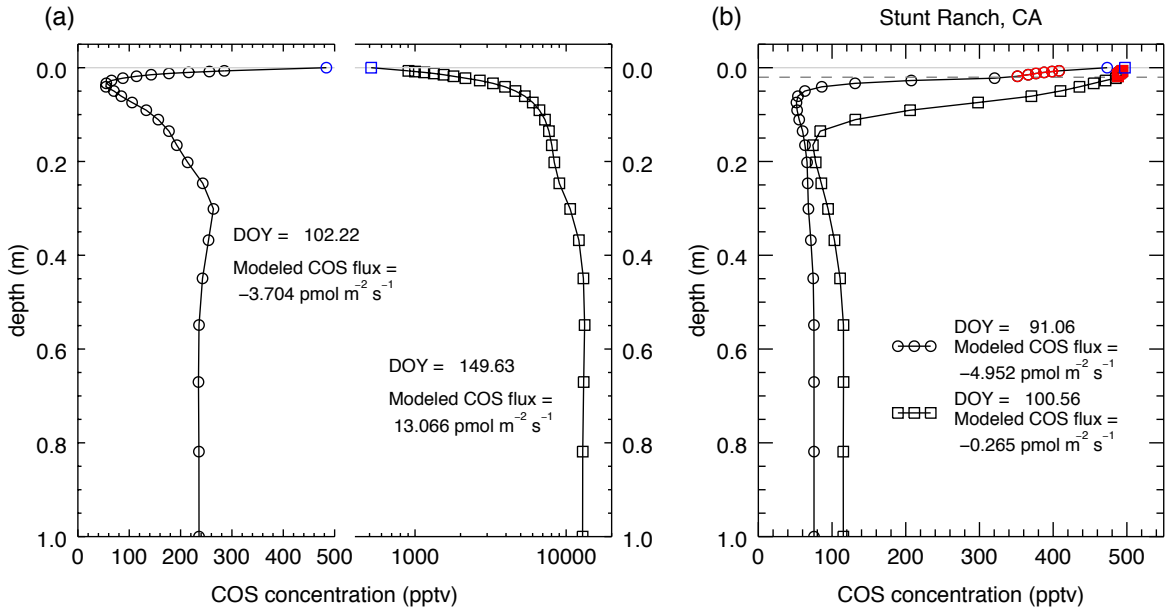

Figure 2.7: Typical simulated profiles of COS concentration. (a) COS profiles of a strong uptake case (circles) and a strong emission case (squares) at SGP. The right side of the x-axis is on logarithmic scale. (b) COS profiles during the wet period (circles) and the dry period (squares). Blue color is used for the atmospheric concentrations, and red for the concentrations in the litter layers in (b).

is the net result of two competing effects: with increasing soil moisture, the higher microbial activity is counteracted by stronger diffusion limitation. The resultant surface COS uptake has an optimum value of 20% WFPS, much lower than the optimum value of microbial uptake per se (Figure 2.9). The shape of the microbial activity curve is not important at high soil water content where the diffusion limitation is dominant.

We also show that for diffusion-controlled, concentration-dependent uptake, the surface flux does not increase linearly with soil COS uptake capacity ($V_{\mathrm{SU,max}}$), but follows a logarithmic relationship (Figure 2.10). Hence, if we can constrain the range of soil COS uptake capacity from laboratory experiments, the uncertainty in fluxes arising from this parameter would not be dominant. The non-linear increase also shows that empirical methods that assume a linear response

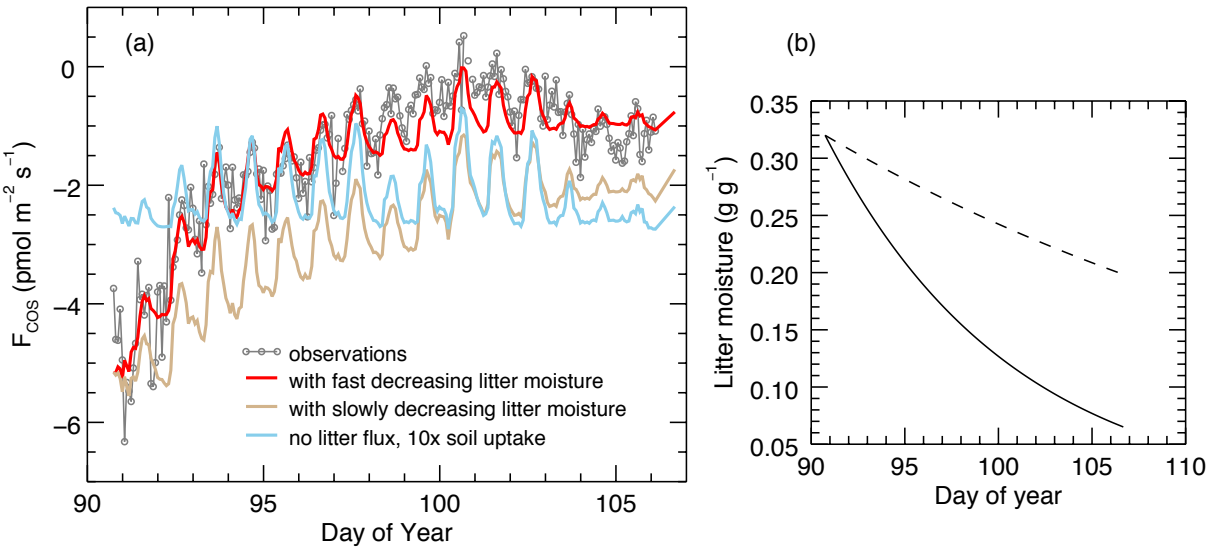

Figure 2.8: (a) Simulated COS fluxes at the Stunt Ranch site for three scenarios, compared with the observations: fast decreasing litter moisture (red), slowly decreasing litter moisture (light brown), and no litter flux but 10x soil uptake (light blue). (b) Changes in litter water content for the fast loss (solid) and slow loss (dashed) scenarios.

of fluxes to soil COS uptake capacity would not give accurate results.

2.4.2 Advantages of a depth-resolved model

One of the main advantages of using a depth-resolved model is that it enables the analysis of changes in uptake and production capacities over time, or between sites. For example, an unexpected finding was that the production capacity parameter at SGP needed to be decreased after the senescence stage (from 1×10^{-10} to 3.3×10^{-11} mol m^{-3} s^{-1}, Table 2.3). Surface COS emissions strongly increased after senescence, but were associated with much higher temperatures. The post-senescence decrease in production capacity indicates that soil COS production may be related to plant activity. We also found that during the period of strong surface COS emissions after the harvest at SGP, the pronounced diurnal variations required the same soil COS uptake

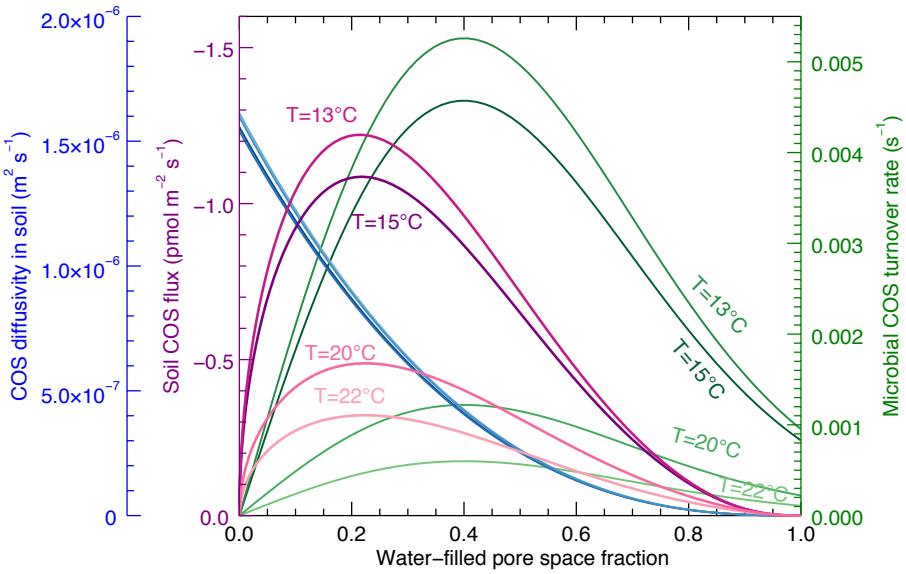

Figure 2.9: Modeled sensitivity of surface soil COS uptake to water-filled pore space fraction (purple) at soil temperatures of 13°C, 15°C, 20°C and 22°C, ambient COS mixing ratio of 500 pmol mol^{-1}, and $V_{\mathrm{SU,max}} = 10^{-2}$ mol m^{-3} s^{-1} as in Eq. (2.21). Soil porosity is set at 0.35 m^3 m^{-3}, and T_{opt} is about 13°C. Only soil COS uptake activity is included in these simulations. Also shown are the two model variables that dominate the simulated flux response, the effective soil COS diffusivities (blue) and microbial COS uptake turnover rates (green) at the same soil temperatures. Note the y-axis of soil COS flux is reversed to show the uptake.

capacity as during the growing season, indicating that soil COS uptake does not directly depend on plant activity. Soil COS uptake could be partly abiotic [*Liu et al.*, 2008, 2010b] or largely due to microbial activity [*Kesselmeier et al.*, 1999], but even in the latter case may not respond quickly to changes in plant cover.

The uptake and production parameters that best fit at each site and during distinct phenological periods can be obtained by optimization procedures used with a particular soil dataset, another significant advantage of a depth-resolved model. Given reasonable initial guesses of the uptake and production parameters, the optimization runs iteratively over the data with the gradient descent or Newton's method until the minimal sum of square errors is attained. An example of

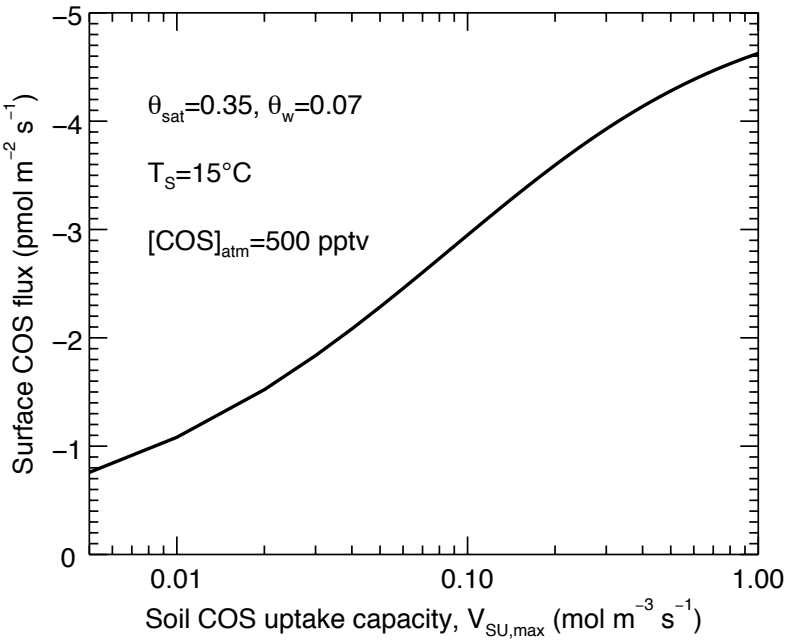

Figure 2.10: An idealized numerical experiment to test the sensitivity of COS flux to soil COS uptake capacity, with $\theta_{sat} = 0.35$ m^3 m^{-3}, $\theta_w = 0.07$ m^3 m^{-3}, soil temperature at 15°C, and ambient COS concentration at 500 pmol mol^{-1}. Note that the x-axis is in logarithmic scale and the y-axis is reversed for showing COS uptake.

data optimization applied to the SR dataset is in *Sun et al.* [2016].

We found that soil COS uptake is largely determined by activity in the top 10 cm of the soil. For each layer, we calculated how much the surface uptake would increase as a result of increasing the COS uptake capacity ($V_{SU,max}$) in that layer by a factor of 10 (Figure 2.11). Surface uptake is sensitive to $V_{SU,max}$ changes in the top 10 cm, even though the layer sizes are the smallest, but not sensitive to changes below 10 cm. Thus, physical parameters in the top layers of the soil are most important for soil COS fluxes. On the other hand, it also means that information on sources and sinks of COS in the deeper soil cannot be obtained from surface flux measurements.

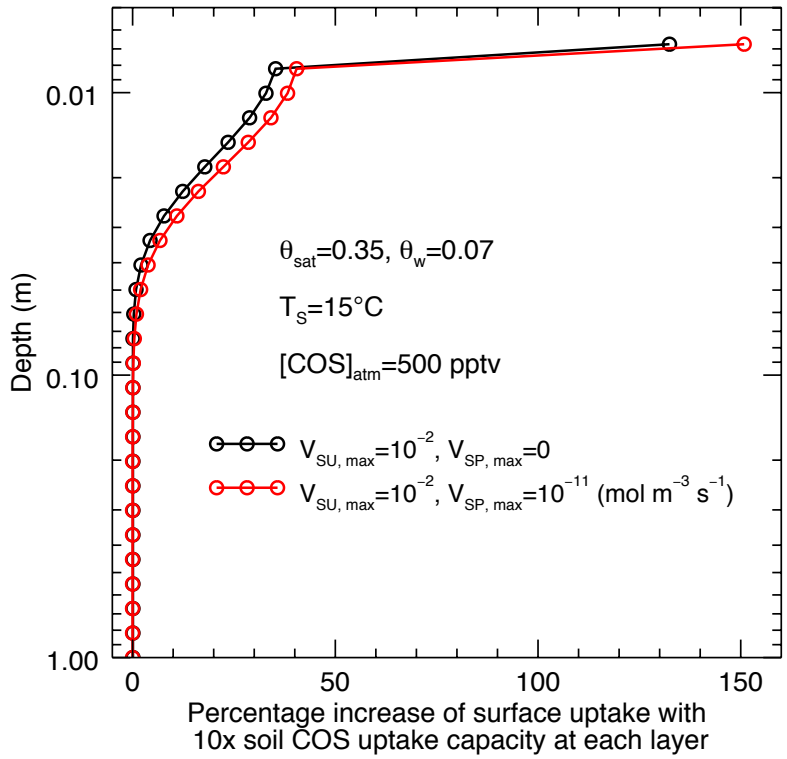

Figure 2.11: Increase of surface COS uptake (in percentage) from 10-fold changes of $V_{SU,max}$ at each depth. The black line shows the changes for an uptake-only case ($V_{SU,max} = 10^{-2}$ mol m^{-3} s^{-1}), while the red line shows the changes when both uptake and source activities are included ($V_{SU,max} = 10^{-2}$ mol m^{-3} s^{-1}, $V_{SP,max} = 10^{-11}$ mol m^{-3} s^{-1}, but the soil is still a sink). Soil conditions are the same as for Figure 2.10.

2.4.3 Which biome-specific parameters are needed for a global simulation?

The COS flux model can be integrated into more comprehensive land surface models (e.g. CLM4.5 and SiB3) to simulate global fluxes. Soil temperature and moisture are usually generated from prognostic equations in these models. Litter layers would need to be added as they are often not represented separately but embedded in soil layers as soil organic carbon (e.g. in CLM4.5). Several parameters may be biome-specific: (1) the uptake and production capacities of COS ($V_{SU,max}$, $V_{SP,max}$); (2) the optimum temperature and moisture of soil COS uptake (T_{opt}, w_{opt}); (3) the Q_{10} parameter of COS production from microbial, root, or abiotic sources; and (4) the function form

of litter COS uptake.

The V_{max} parameters should be controlled by microbial biomass and enzyme content in the soil, which in turn are related to soil physical state and organic carbon content. These parameters can be estimated by optimizing model results against field data. The T_{opt} and w_{opt} parameters can be determined from laboratory experiments, and extended to soils in similar environments, considering that they are likely related to local climate regimes and soil hydrology. Root COS production as a function of temperature needs to be determined from laboratory experiments. More studies are also needed to constrain litter COS fluxes, and how they change with litter type, level of litter degradation, and litter moisture content and temperature. With more field observations and lab incubations, we expect a database of these parameters in different biomes will be constructed for regional and global simulations of soil COS fluxes.

2.5 Chapter conclusion

This study presents a mechanistic diffusion-reaction model coupling physics and biogeochemistry to simulate soil COS flux, as well as its evaluation with field data. The model explicitly accounts for diffusion in the soil column, COS production, and COS exchange in the litter layer. The model reproduced well the observed fluxes at two sites, and has enabled us to gain novel (and unexpected) insights such as the higher COS production capacity at SGP during the growing season despite lower soil COS emissions, and the continuing COS uptake capacity required to partly counteract the large COS emissions at SGP after harvest. We also demonstrate that diffusion must be considered to accurately simulate surface COS fluxes. Diffusion control on surface uptake is evident in its sensitivity to soil water content, and the sub-linear response of uptake flux to soil COS uptake capacity. For large-scale simulations of soil COS fluxes, further lab and field studies are needed to establish a database of soil and litter COS uptake and production capacities and parameters for typical soil types across key biomes.

2.6 Supplement

2.6.1 List of variables and parameters

Table 2.4: List of variables and parameters.

	Value and unit	Description	Reference
Physical and biological constants			
D_m	1.337×10^{-5} m^2 s^{-1}	COS-air mass diffusivity at 25°C	*Massman* [1998]; *Seibt et al.* [2010]
T_{ref}	298.15 K	Reference temperature	
R	8.3145 J K^{-1} mol^{-1}	Universal gas constant	
$k_H(T)$	mol mol^{-1}	Henry's law constant of COS	This study, data from *Elliott et al.* [1989]
K_m	1.9 mol m^{-3}	Michaelis-Menten constant for COS hydrolysis by carbonic anhydrase	*Ogawa et al.* [2013]
Soil and litter properties			
θ_a	m^3 m^{-3}	Volumetric air content	
θ_w or w	m^3 m^{-3}	Volumetric water content	
θ_{sat}	m^3 m^{-3}	Soil porosity	
θ_{lit}	0.94 m^3 m^{-3}	Litter porosity	

continued on the next page

continued from the previous page

	Value and unit	Description	Reference
θ_{FC}	$m^3\ m^{-3}$	Field capacity	*Or and Wraith* [2002]
T	K	Soil or litter temperature	
T_S	K	Slowly varying component of soil temperature	
T_F	K	Fast varying component of soil temperature	
T_L	K	Litter temperature	
w_L	$g\ g^{-1}$	Litter water content	
D	$m^2\ s^{-1}$	COS diffusivity in soil	*Moldrup et al.* [2003]
z_T	m	Damping depth for diurnal temperature waves	
α_T	$m^2\ s^{-1}$	Soil thermal diffusivity	*Peters-Lidard et al.* [1998]; *Johansen* [1975]
COS solubility model			
μ_g	$J\ mol^{-1}$	Chemical potential of COS in gas phase	
μ_{aq}	$J\ mol^{-1}$	Chemical potential of COS in aqueous phase	
$\mu_g^{\ominus}$	$J\ mol^{-1}$	Chemical potential of COS in gas phase under a chosen standard condition	

continued on the next page

continued from the previous page

	Value and unit	Description	Reference
μ^*_{aq}	J mol^{-1}	Chemical potential of COS in aqueous phase under a chosen standard condition	
c_g	mol m^{-3}	Gaseous concentration of COS	
c_{aq}	mol m^{-3}	Aqueous concentration of COS	
ϕ	dimensionless	Fugacity coefficient	
γ	dimensionless	Activity coefficient	
p	atm	Partial pressure of COS	
$p^\ominus$	1 atm	Standard pressure	
T_0	273.15 K	Standard temperature	
x	dimensionless	Molar fraction of COS in aqueous phase	
ρ_w	1×10^3 kg m^{-3}	Density of water	
M_w	18.016 g mol^{-1}	Molar mass of water	
$k_{H,xp}$	atm^{-1}	Henry's law constant of COS	
$k_{H,cc}$	mol mol^{-1}	Henry's law constant of COS (dimensionless)	
$\Delta_{sol}H_m$	J mol^{-1}	Standard partial molar enthalpy of COS dissolution	
α	dimensionless	Fitting parameter	

continued on the next page

continued from the previous page

	Value and unit	Description	Reference
β	dimensionless	Fitting parameter	
Fluxes and model parameters			
F_{SL}	pmol s^{-1} kg^{-1} dry weight	COS fluxes from litter incubation	
U	mol m^{-3} s^{-1}	Soil COS uptake term	
P	mol m^{-3} s^{-1}	Soil COS production term	
C	mol m^{-3}	COS gaseous concentration profile	
k_L	11.56	Factor for moisture dependence of litter COS uptake	*Sun et al.* [2016]
$V_{LU,max}$	1.68×10^{-3} mol m^{-3} s^{-1}	Litter COS uptake capacity	*Sun et al.* [2016]
$V_{LP,max}$	1.33×10^{-11} mol m^{-3} s^{-1}	Litter COS production capacity	*Sun et al.* [2016]
$V_{SU,max}$	mol m^{-3} s^{-1}	Soil COS uptake capacity	
$V_{SP,max}$	mol m^{-3} s^{-1}	Soil COS production capacity	

2.6.2 The effect of aqueous diffusion

To demonstrate quantitatively that aqueous diffusive flux is small compared to gaseous diffusive flux, we assume a soil column of vertically uniform profiles of porosity, temperature and mois-

ture,

$$\theta_{\text{sat}} = 0.50\ \text{m}^3\ \text{m}^{-3}$$

$$T = 25^{\circ}\text{C}$$

$$\theta_{\text{w}} = 0.25\ \text{m}^3\ \text{m}^{-3}$$

The factor b in Eq. (2.13) in the main text is set to 5.3 here, without losing generality. The soil gaseous diffusivity for COS calculated based on Eq. (2.13) in the main text is, $D_{\text{g}} = 5.64 \times 10^{-7}\ \text{m}^2\ \text{s}^{-1}$. The molecular aqueous diffusivity for COS calculated from *Ulshöfer et al.* [1996] is $D_{\text{m,aq}} = 1.94 \times 10^{-9}\ \text{m}^2\ \text{s}^{-1}$. Then by counting the tortuosity effect using Eq. (2.3) in *Moldrup et al.* [2003], we obtain the actual soil aqueous diffusivity for COS, $D_{\text{aq}} = 7.13 \times 10^{-11}\ \text{m}^2\ \text{s}^{-1}$.

We consider the steady-state COS flux of the soil (i.e. $\partial C/\partial t$=0) with a sink proportional to the concentration and no production term. We obtain the equation,

$$D\frac{\text{d}^2C}{\text{d}z^2} = -S = kC \tag{2.28}$$

with the boundary condition $C(z = 0) = C_{\text{atm}}$. We obtain the general solution,

$$C(z) = C_{\text{atm}} \exp(-\sqrt{k/D} \cdot z) \tag{2.29}$$

The surface flux is thus

$$F = -D\frac{\text{d}C}{\text{d}z}\Big|_{z=0} = \sqrt{kD}C_{\text{atm}} \tag{2.30}$$

which is proportional to $\sqrt{D}$. We can then calculate the ratio of aqueous diffusive flux (F_{aq}) to gaseous diffusive flux (F_{g}),

$$\frac{F_{\text{aq}}}{F_{\text{g}}} = \sqrt{\frac{D_{\text{aq}}}{D_{\text{g}}}} = 0.0112 \tag{2.31}$$

Under most conditions, the aqueous diffusive flux is a small fraction of the total flux (Figure 2.12). Hence, any errors from neglecting aqueous diffusion are usually small (< 10% at water filled pore space below 83%), except at high soil moisture when the overall flux also tends to be small (see Figure 2.9).

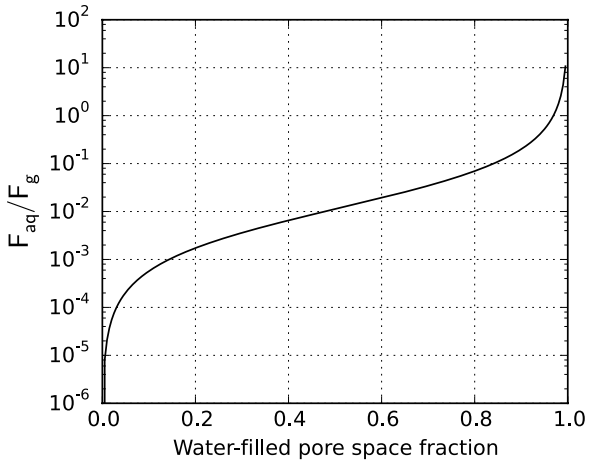

Figure 2.12: The ratio of aqueous flux to gaseous flux for an ideal case with soil porosity 0.50 m^3 m^{-3}. COS uptake velocity is assumed constant.

CHAPTER 3

Litter uptake dominates soil–atmosphere exchange of COS in a Southern Californian oak woodland

3.1 Chapter introduction

Carbonyl sulfide (COS), a trace gas in the atmosphere (~484 pmol mol^{-1}), has been recently recognized as a promising indicator of gross photosynthetic carbon flux in terrestrial ecosystems due to its close coupling with CO_2 during leaf uptake [*Montzka et al.*, 2007; *Campbell et al.*, 2008; *Asaf et al.*, 2013; *Berry et al.*, 2013]. This coupling is a result of co-diffusion of CO_2 and COS into leaf stomata [*Sandoval-Soto et al.*, 2005; *Seibt et al.*, 2010; *Stimler et al.*, 2010a], and subsequent hydrolysis mediated by carbonic anhydrase (CA) enzymes [*Protoschill-Krebs and Kesselmeier*, 1992; *Protoschill-Krebs et al.*, 1996; *Schenk et al.*, 2004; *Notni et al.*, 2007]: $COS + H_2O \longrightarrow H_2S + CO_2$. This hydrolytic reaction can also happen in soils, complicating the link between ecosystem COS and CO_2 uptake.

The global biogeochemical cycle of COS is predominantly driven by vegetation and soil microbial uptake, and production from ocean biogenic activities and photochemical reactions [*Kettle et al.*, 2002; *Berry et al.*, 2013]. Other known significant COS sources include anthropogenic emissions [*Campbell et al.*, 2015] and biomass burning [*Campbell et al.*, 2015; *Blake et al.*, 2004; *Montzka et al.*, 2007], both of which are much smaller than the vegetation sink. The seasonal amplitudes of atmospheric COS and CO_2 concentrations in the northern hemisphere are highly correlated [*Montzka et al.*, 2007]. Regional atmospheric drawdown and ecosystem and leaf-level fluxes of COS

and CO_2 also exhibit strong covariation [*Campbell et al.*, 2008; *Asaf et al.*, 2013; *Stimler et al.*, 2010a]. The COS-based GPP tracer approach is promising because COS plant uptake appears to dominate the continental COS budget. However, other continental sources and sinks, in particular those in soils, need to be better understood to develop a robust tracer approach.

The catalytic reaction between COS and CA enzymes in soils is indicated by the reduced COS uptake after treatment with CA inhibitor [*Kesselmeier et al.*, 1999], and by the oxygen isotope signatures of soil CO_2 efflux [*Seibt et al.*, 2006; *Wingate et al.*, 2009]. Soil COS uptake is a function of temperature, soil porosity and water content, with different optimum temperatures and water contents identified for a range of soils in laboratory experiments [*Kesselmeier et al.*, 1999; *Van Diest and Kesselmeier*, 2008; *Whelan et al.*, 2016]. In field studies, soil COS uptake has been observed in a handful of ecosystems. Soil uptake rates of COS measured in the field are mostly in the order of 1–10 pmol m^{-2} s^{-1} [*Castro and Galloway*, 1991; *Simmons et al.*, 1999; *Yi et al.*, 2007; *Berkelhammer et al.*, 2014; *Maseyk et al.*, 2014]. Larger soil uptake rates have been observed in an oak woodland in northern California but were likely biased by pressure-driven advection [*Kuhn et al.*, 1999]. Leaf litter also acted as a COS sink [*Kesselmeier and Hubert*, 2002; *Berkelhammer et al.*, 2014], contributing a significant fraction of surface fluxes in a subtropical forest [*Yi et al.*, 2007]. Although the majority of observations have shown that soils generally behave as COS sinks, the presence of a compensation point [*Kesselmeier et al.*, 1999; *Conrad and Meuser*, 2000; *Liu et al.*, 2010a] indicates that COS may also be produced in the soil. Net emissions of COS have been observed in a wheat field soil at high temperature [*Maseyk et al.*, 2014] and samples from a range of other oxic soils [*Whelan et al.*, 2016], and in anoxic soils such as peatlands, salt marshes and flooded paddy fields [*de Mello and Hines*, 1994; *Li et al.*, 2006; *Yi et al.*, 2008, 2013; *Whelan et al.*, 2013].

However, most of the field studies were conducted using sparse sampling, limiting our ability to link COS fluxes to environmental and biological factors. Therefore, soil COS fluxes have been either assumed to be negligible [*Asaf et al.*, 2013], or empirically parameterized from soil respiration and moisture [*Berry et al.*, 2013] or H_2 fluxes [*Launois et al.*, 2015a]. Litter fluxes have rarely been quantified separately in the field [*Berkelhammer et al.*, 2014], and not included yet in any budget

or modeling studies.

Here we analyze the response of soil and litter COS fluxes to environmental conditions during a 40-day field campaign in an oak woodland in southern California in spring 2013. We quantify the contributions of litter uptake to the net surface fluxes of both COS and CO_2 using a depth-resolved diffusion-reaction model that includes an interactive litter layer [*Sun et al.*, 2015]. Our study addresses a crucial gap in closing ecosystem COS budgets, an important step towards a COS-based carbon flux partitioning approach.

3.2 Methods and materials

3.2.1 Field site

We conducted measurements from 1 April to 11 May 2013 (DOY 91–131) at the Stunt Ranch UC Reserve (34°05′38″ N, 118°39′26″ W, 397 m above sea level) in the Santa Monica Mountains, California. The study site was in a mediterranean oak woodland dominated by coast live oak (*Quercus agrifolia*). The soil is a gravelly loam [*USDA Natural Resources Conservation Service*, 2014], covered by a 2–6 cm thick layer of leaf litter. Annual rainfall was about 180 mm in 2012–2013, mostly received during the winter, and average annual temperature is 19°C (July: 24°C, January: 14°C). The site has large interannual variability in precipitation. Rainfall was observed on 31 March (DOY 90, 2 mm) and 5–6 May (DOY 125–126, 13.5 mm, see Figure 3.7, Supplement).

3.2.2 Experimental setup

A mid-infrared quantum cascade laser (QCL) spectrometer (Aerodyne Research Inc., Billerica, MA) was used to measure COS, CO_2 and H_2O concentrations. The RMS noise (1 σ) at 1 Hz was 3–5

pptv for COS. Flow through the instrument was maintained by a TriScroll 600 pump (Agilent Technologies) connected to the analyzer by a 1″ vacuum line. The analyzer was housed in a small shed that was ventilated but not temperature controlled. To account for instrument drift due to temperature changes, we implemented frequent background calibrations (every 15 minutes) with dry N_2 as the zero gas, and corrected the drift linearly in all calculations (section 3.6.2). A solenoid valve at the analyzer inlet was actuated to switch from the sampling line to the background/zero gas. Due to insufficient background correction, the measured gas concentrations were affected by instrument drift on 1–2 April (DOY 91–92). The calculated chamber fluxes were not affected because they are based on relative concentration changes.

We deployed two chambers for soil flux observations. The chambers were modified versions of LI-8100 long-term soil chambers (LI-COR Biosciences Inc., Lincoln, NE), with custom-made stainless steel chamber bowls and collars. A third, identical chamber was used as a blank control chamber by sealing the bottom with FEP Teflon film (see SI for details on uncertainty estimates). Soil chamber 1 (SC1) was placed 4.5 m away from a coast live oak tree, SC2 was 0.5 m away from the tree, and underneath the tree canopy. The litter layer was 2 cm thick in SC1, and 6 cm thick in SC2. We kept the litter in the chambers intact as much as possible. The soil chambers were connected to the COS analyzer via 1/4″ sampling lines (Synflex tubing). Teflon filters (1 µm Millipore Millex) were placed at each chamber sampling line and at the analyzer inlet to prevent particle contamination. To keep all sampling lines flushed at all times, a second dry scroll pump (IDP3, Agilent) was used to provide bypass flow for the lines not directed into the QCL. The bypass flow was directed via 1/4″ Dekabon tubing back into the chambers to provide the incoming air for the chamber measurements. The flow rate of the incoming air was adjusted with needle valves to provide slightly more flow (0.1 to 0.2 slm) into the chamber than pulled through the outlet. The open vent on top of the chamber provided sufficient release for the small additional incoming flow to maintain ambient pressure inside the chamber.

Flow rates in the sampling lines were monitored with flowmeters (Honeywell AWM5104VN). We also measured atmospheric temperature and humidity (Vaisala HMP 45 AC probes), chamber air

temperatures (type T thermocouples, PFA coated), and soil temperatures and volumetric soil water content (SWC) in the upper 5 cm (Stevens Hydra Probe II, Stevens Water Monitoring Systems Inc., Portland, OR). A datalogger (CR1000, Campbell Scientific Inc., Logan, UT) was used to control the opening and closing of chambers, and switching of solenoid valves to select sampling lines, and record sensor data. Chambers were sampled in 15-minute intervals, with zero offset correction at the start of each interval. Chambers were closed for 8 min, with the transient changes in chamber air concentrations monitored by the QCL. Before and after chamber closure, the air in the open chamber was measured for 2 min each. Chamber fluxes were calculated from the difference between the transient changes and the incoming air concentrations interpolated from the two open chamber measurements (see Figure 3.8, Supplement). Each soil chamber was sampled once per 90-minute period (before DOY 116) or per 120-minute period (after DOY 116).

3.2.3 Litter incubation experiments

To constrain the litter fluxes, we conducted two litter incubation experiments from 7–9 and 9–11 May (DOY 127–129, 129–131). Litter samples were collected from the area between the two soil chambers and from a similar footprint to the chambers, placed in SC3, and measured as part of the sampling sequence. The samples as well as in-situ litter content of the soil chambers were then collected for laboratory analysis of litter wet and dry weight (Table 3.2, Supplement).

Litter fluxes of COS (F_{SL}, pmol kg^{-1} s^{-1}) and CO_2 (F_{CL}, µmol kg^{-1} s^{-1}, both per unit litter dry weight) were assumed to be functions of litter temperature (T_L, K, approximated by the air temperature in the incubation chamber) and litter water content (w_L, g water g^{-1} litter). Changes in water content of the litter samples were calculated by integrating litter water fluxes over time. We formulated nonlinear regression models for litter COS and CO_2 fluxes (see section 3.6.3):

$$F_{SL}(w_L, T_L, C_{S,a}) = V_{SLU,max} \cdot \sinh(k_{SL} w_L) \cdot k_{H,S}(T_L) \cdot C_{S,a} + V_{SLP,max} \cdot \exp[k_T(T_L - T_{ref})] \quad (3.1)$$

$$F_{CL}(w_L, T_L) = V_{CLP,max} \cdot \sinh(k_{CL} w_L) \cdot \exp\left[-\frac{E_{RL}}{R}\left(\frac{1}{T_L} - \frac{1}{T_{ref}}\right)\right] \quad (3.2)$$

where $V_{\mathrm{SLU,max}}$ ($\mathrm{m^3\ kg^{-1}\ s^{-1}}$) and $V_{\mathrm{SLP,max}}$ ($\mathrm{pmol\ kg^{-1}\ s^{-1}}$) are the baseline rates of litter COS uptake and production (i.e. uptake/production capacity), $V_{\mathrm{CLP,max}}$ ($\mathrm{\mu mol\ kg^{-1}\ s^{-1}}$) is the baseline rate of litter respiration (i.e. CO_2 production capacity), k_T ($\mathrm{K^{-1}}$) is the temperature dependence factor for COS production which is equivalent to $Q_{10} = 1.9$ (see section 3.6.3), $T_{\mathrm{ref}} = 25°\mathrm{C}$ is a reference temperature, k_{SL} and k_{CL} (both dimensionless) are moisture limitation factors for COS uptake and CO_2 production, E_{RL} ($\mathrm{J\ mol^{-1}}$) is the activation energy of litter respiration, and $k_{\mathrm{H,S}}$ (dimensionless) is the Henry's law constant for COS. We obtained a new equation for $k_{\mathrm{H,S}}(T)$ from a fit to empirical data [*Elliott et al.*, 1989]:

$$k_{\mathrm{H,S}}(T) = (T/\mathrm{K}) \exp\left(\alpha + \frac{\beta}{T/\mathrm{K}}\right) \tag{3.3}$$

with parameters $\alpha = -20.00$, $\beta = 4050$ [*Sun et al.*, 2015]. The term $k_{\mathrm{H,S}}(T)$ is applied to the ambient concentration, $C_{\mathrm{S,a}}$ ($\mathrm{pmol\ m^{-3}}$), to get the aqueous concentration of COS, since COS hydrolysis typically occurs in the aqueous phase. Hyperbolic functions are chosen for moisture dependence so that fluxes approach zero in completely dry conditions. Outliers were excluded from the regression of litter fluxes by using Cook's distance statistic [*Cook*, 1977]. The fit parameters from Eqs. (3.1) and (3.2) were then used to parameterize litter fluxes in the soil–litter flux model described below.

3.2.4 Litter and soil environmental variables

Litter porosity was estimated to be 0.94 (section 3.6.4). The litter water content was calculated by integrating litter water fluxes from multiple regressions of litter incubation data (Figure 3.12 and 3.13, Supplement). Due to the lack of direct field data, the initial litter moisture and that after the second rain (DOY 126) was set to about half of the observed litter water content at saturation (Table 3.6) to fit the observed COS fluxes and the litter water content measured prior to the litter incubations.

Soil porosity was measured as 0.35 $\mathrm{m^3\ m^{-3}}$. At the soil–litter interface, porosity values were in-

terpolated to prevent numerical instability caused by discontinuity. Soil temperature and moisture profiles were parameterized from the values measured at 5 cm depth. We assume that the temperature variations are a superposition of fast varying diurnal sine waves and slowly varying background signals [*Van Wijk and de Vries*, 1963]. Temperatures of deeper soil that are not measured are constructed by superposing the background signals with depth-damped, phase-lagged diurnal variations (section 3.6.5 and Figure 3.15, Supplement). We assumed that soil water content is 0.20 m^3 m^{-3} at 1 m depth, corresponding to typical field capacity of loamy soils [*Or and Wraith*, 2002]. Soil water content profiles were constructed from data collected at 5 cm depth assuming a smooth increase with depth (Figure 3.14 and Table 3.7, Supplement).

3.2.5 Modeling surface (soil + litter) fluxes

We use a depth-resolved diffusion–reaction model to simulate surface COS and CO_2 fluxes from soil parameters and environmental variables, with flux activity in the litter included. A detailed description and evaluation of the COS model is presented in *Sun et al.* [2015]. Briefly, the model evaluates COS profiles accounting for vertical diffusion and local sources and sinks. The source and sink terms are related to temperature and moisture in each soil/litter layer. Here we incorporate a CO_2 model with the same structure as the COS model but its own production terms.

Briefly, the soil COS sink term is parameterized as the soil COS uptake capacity ($V_{SSU,max}$, mol m^{-3} s^{-1}) multiplied by temperature and moisture limitation functions [*Sun et al.*, 2015]. The soil COS production term is the COS production capacity ($V_{SSP,max}$, mol m^{-3} s^{-1}) modified by an exponential temperature function with $Q_{10} = 1.9$ [*Sun et al.*, 2015; *Maseyk et al.*, 2014].

For CO_2 fluxes, the soil CO_2 source term is,

$$P_C(T, w_S, z) = V_{CSP,max} \cdot f_C(T) \cdot w_S/w_0 \cdot \exp(-z/z_D) \tag{3.4}$$

where $V_{CSP,max}$ (mol m^{-3} s^{-1}) is the CO_2 production capacity, $f_C(T)$ is the temperature limitation

function, w_S/w_0 is the linear moisture dependence function with $w_0 = 0.10$, and $z_D = 0.2$ m is assumed for the exponential decay depth for the CO_2 production profile. The temperature dependence $f_C(T)$ was adapted from the widely used modified Arrhenius equation [*Lloyd and Taylor*, 1994], but was normalized so that $f_C(T_{ref} = 25°C) = 1$. The V_{max} parameters ($V_{SSU,max}$, $V_{SSP,max}$ and $V_{CSP,max}$) are optimized by minimizing the sum of square errors (SSE) cost function (model result vs. observations) with the gradient descent or Newton's method.

Litter source and sink terms of COS and CO_2 are described in Eqs. (3.1) and (3.2). For model implementation, the litter COS uptake and production capacities ($V_{SLU,max}$ and $V_{SLP,max}$) and CO_2 production capacity ($V_{CLP,max}$) were converted from per unit litter dry weight to per unit volume of litter (mol m^{-3} s^{-1}) using the litter dry bulk density (31.3 kg m^{-3}, see section 3.6.4).

3.3 Results

3.3.1 Surface (soil + litter) fluxes

During the campaign, both observed surface areas behaved primarily as net COS sinks, with fluxes from −6.3 to +3.0 and from −7.9 to +2.5 pmol m^{-2} s^{-1} in chambers 1 and 2, respectively, and an overall mean flux of −1 pmol m^{-2} s^{-1} (Table 3.1 and Figure 3.1a). Net emissions were observed in 15% of measurements, mostly associated with soil temperatures above 15°C (Figure 3.17a, Supplement). Larger emissions (> +1 pmol m^{-2} s^{-1}) were only observed in 1% of cases.

The overall trends of surface COS fluxes in the two chambers were very similar, and generally followed changes in soil moisture (Figure 3.1). COS uptake was strongest after rain events, peaking at −6 to −8 pmol m^{-2} s^{-1}, and gradually decreasing to about −1 pmol m^{-2} s^{-1} within 10 days after the rain. The peak COS fluxes in both chambers lagged the rain event on DOY 126 by approximately 1 day. The diurnal variations of COS fluxes resembled those in soil temperature

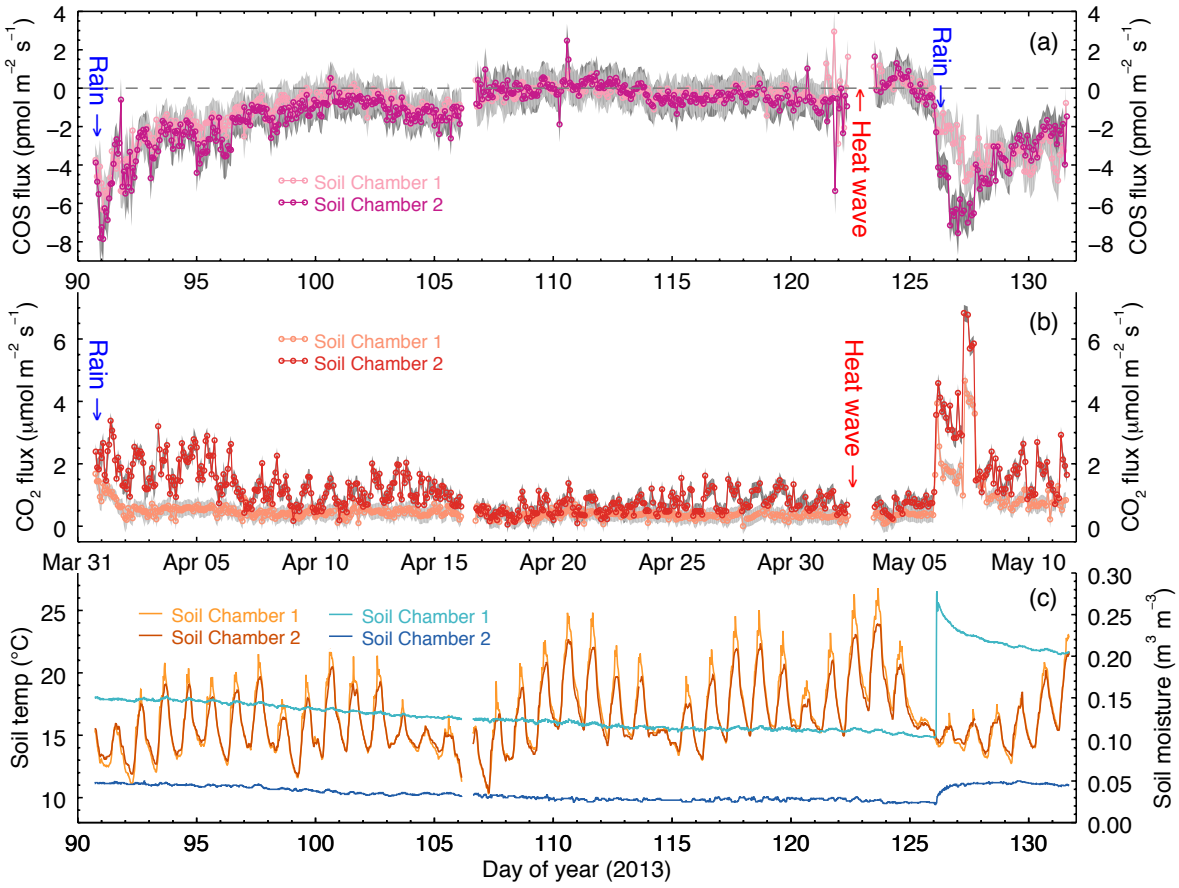

Figure 3.1: Observed surface fluxes of COS (a) and CO_2 (b) measured in two soil chambers at an oak woodland in southern California in spring 2013 (1 April to 11 May, DOY 91–131), with soil temperatures and volumetric soil water content (c). Shaded areas are 95% confidence intervals of fluxes, including uncertainty estimates from blank chamber measurements (see SI). Arrows indicate two rain events and a heat wave. Note that SC1 had much less litter and was farther from the tree than SC2.

(Figure 3.2c), and were small compared to the long-term variations. Diurnal amplitudes of COS fluxes were smallest during the dry period. CO_2 fluxes showed broadly similar temporal patterns as COS fluxes (Figure 3.1b). In contrast to the COS fluxes, however, the CO_2 fluxes were very different between the two chambers, probably due to root respiration as SC2 was located next to a tree.

For both chambers, net COS uptake increased exponentially with soil water content (SWC), with a similar shape of the SWC response (Figure 3.2a). Surprisingly, the two curves appear shifted along the SWC axis, indicating that changes in the surface COS flux are related to soil moisture variations but soil moisture is not the main driver of the COS fluxes at our site (see discussion). Net COS and CO_2 fluxes were negatively correlated in both chambers (Figure 3.2b), consistent with previous observations [*Yi et al.*, 2007; *Berkelhammer et al.*, 2014].

3.3.2 Litter fluxes

In both incubation experiments, the leaf litter of coast live oak was mostly a net COS sink, with fluxes ranging from -4.3 to $+1.3$ pmol s^{-1} kg^{-1} dry weight (Figure 3.3a), and a source of CO_2 (Figure 3.3b). Litter COS uptake and CO_2 production decreased as the litter was drying over time (fluxes in Figure 3.3 are plotted vs. litter moisture). Based on nonlinear fits (Eqs. 3.1 and 3.2), we found a strong relationship between COS and CO_2 fluxes and litter moisture, but only a weak correlation with temperature. Deviations from the fit were observed below 15°C at night (Figure 3.3) and associated with high relative humidity, probably due to dew formation on the litter surface. Dew formation would result in increased litter moisture not detected by our water flux measurements. COS uptake and CO_2 production were well correlated (Figure 3.10, Supplement), with stronger correlation when chamber air temperature was below 15°C ($r = -0.77$). At higher temperature, the correlation between the fluxes was weaker ($r = -0.65$) as litter CO_2 fluxes had a stronger temperature response than COS fluxes.

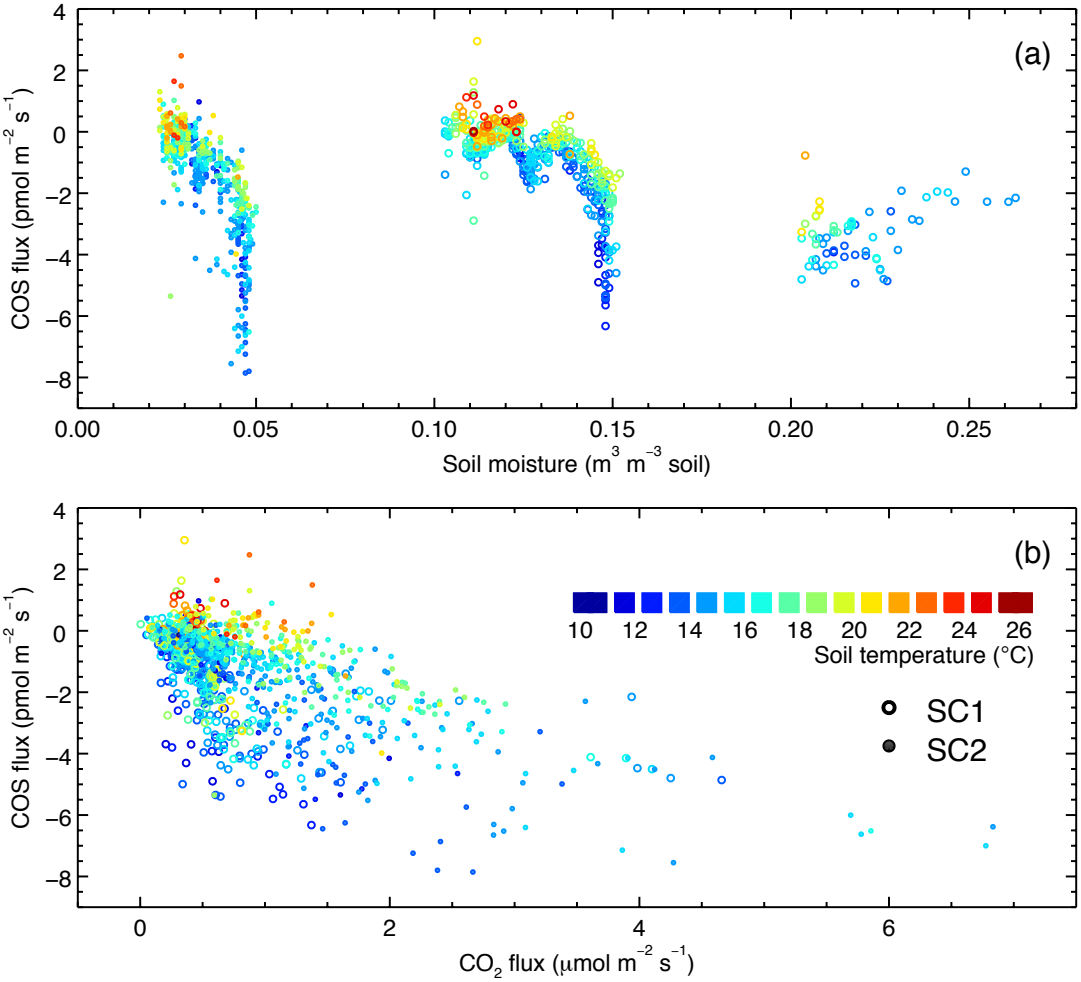

Figure 3.2: The observed surface COS fluxes appear to have different relationships with soil water content (a) for the two soil chambers, although the overall shape of the SWC response is similar for both chambers. Surface COS uptake is positively correlated with CO_2 efflux in both chambers (b). Data points are colored for soil temperatures.

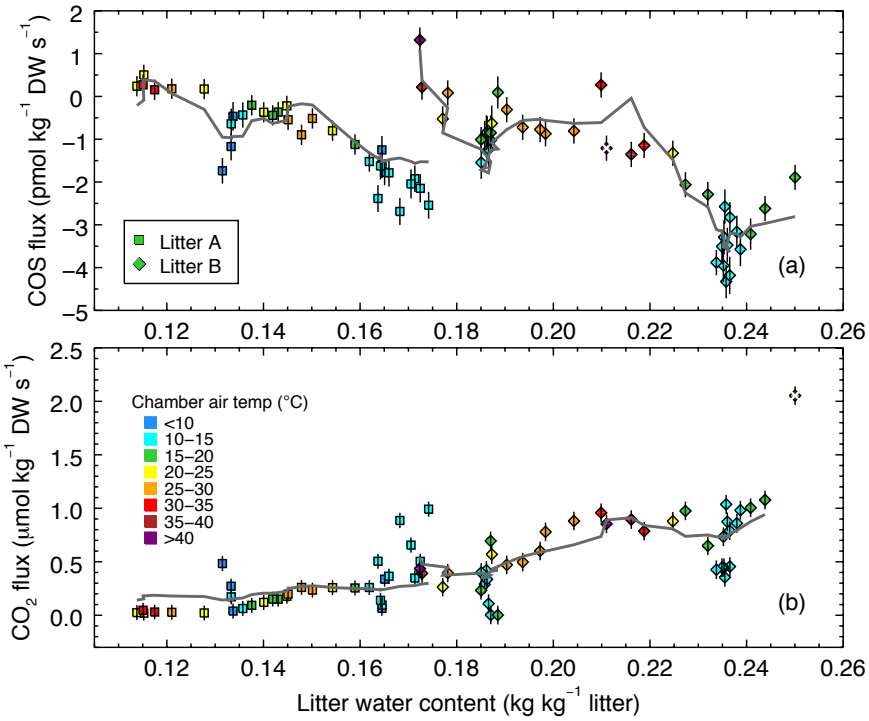

Figure 3.3: Litter COS (a) and CO_2 (b) fluxes observed in two incubation experiments using litter collected at the site. Error bars show ±1 σ ranges with blank chamber effect included. Colors of data points indicate temperature bins. Also shown are fitted litter fluxes (grey, Eqs. 3.1 and 3.2). Outliers (marked by white crosses) were excluded from the regressions.

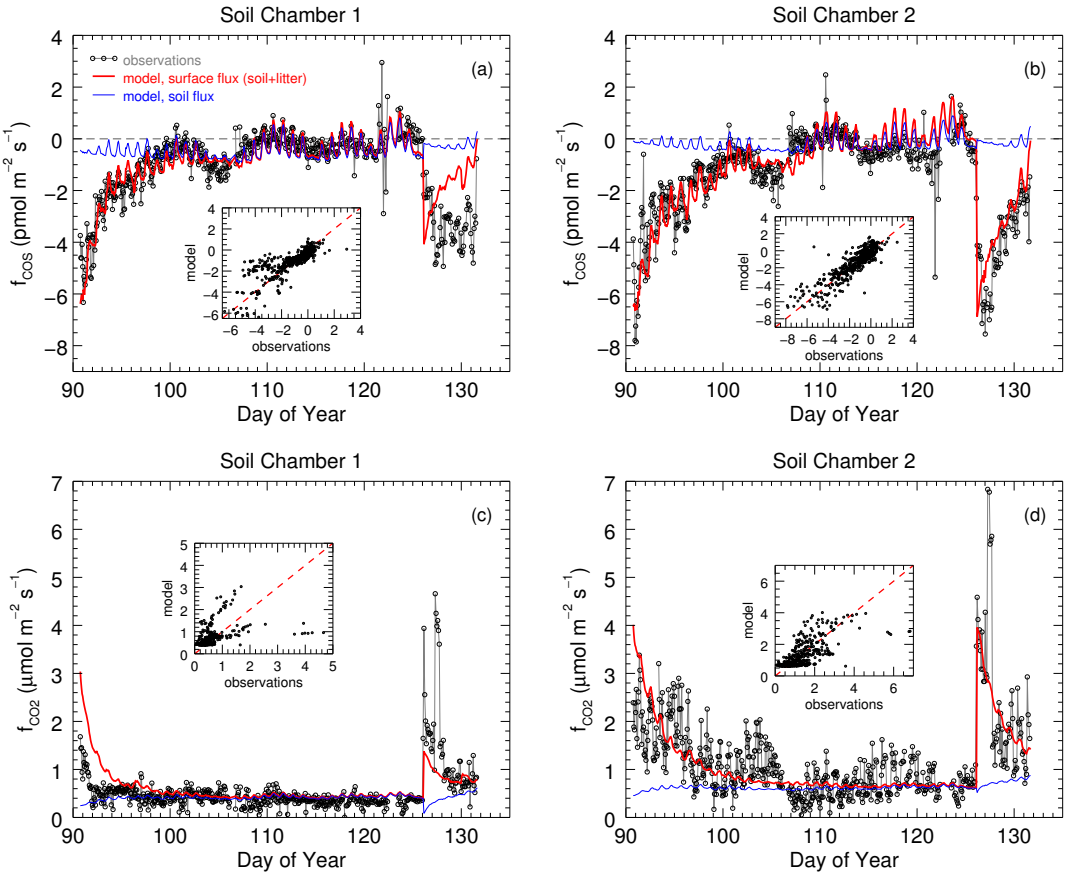

Figure 3.4: Modeled surface (soil + litter) COS (a–b) and CO_2 (c–d) fluxes (red) in the two soil chambers agree well with observations (black) during most of the campaign (panel insets show modeled vs. observed fluxes). Also shown are the fluxes simulated at the litter-soil interface, i.e. resulting from soil-only gas exchange (blue).

Table 3.1: Summary of observations and model results for chamber fluxes

	SC1	SC2
Max. surface COS flux (pmol m^{-2} s^{-1})	2.95	2.47
Min. surface COS flux (pmol m^{-2} s^{-1})	−6.33	−7.85
Mean surface COS flux (pmol m^{-2} s^{-1})	−1.13	−1.43
Mean surface CO_2 flux, observed (µmol m^{-2} s^{-1})	0.54	1.19
Mean soil water content (m^{-3} m^{-3})	0.138	0.035
Litter thickness (cm)	2	6
Mean modeled surface COS flux (pmol m^{-2} s^{-1})	−1.02	−1.28
Mean modeled surface CO_2 flux (µmol m^{-2} s^{-1})	0.63	1.13
RMSE of modeled COS fluxes (pmol m^{-2} s^{-1})	0.85	0.83
RMSE of modeled CO_2 fluxes (µmol m^{-2} s^{-1})	0.49	0.63
Pearson correlation, model vs obs. COS fluxes	0.801	0.884
Pearson correlation, model vs obs. CO_2 fluxes	0.436	0.717
Range of modeled litter COS fluxes (pmol m^{-2} s^{-1})	−5.95 to +0.25	−6.85 to +0.74
Mean modeled litter COS flux (pmol m^{-2} s^{-1})	−0.58	−1.10
Mean litter contribution to COS soil + litter uptake	56.9%	85.7%
Mean litter contribution to COS soil + litter uptake, first 5 days (after rain)	83.5%	95.6%
Mean modeled litter CO_2 flux (µmol m^{-2} s^{-1})	0.21	0.51
Mean litter contribution to CO_2 emissions	34.2%	44.8%
Mean litter contribution to CO_2 emissions, first 5 days (after rain)	71.7%	74.2%

3.4 Discussion

3.4.1 Litter is a major contributor to surface COS fluxes

Using the depth-resolved model to quantify the contributions from litter and soil to net surface fluxes (Figure 3.4), we found that litter uptake accounted for the majority of COS fluxes during wet periods, and nearly the entire flux for SC2 (Table 3.1 and Figure 3.5). During the dry period, litter still contributed substantially to fluxes in SC2 but very little in SC1. The net surface COS fluxes should therefore be plotted against the litter moisture as the relevant parameter in Figure 3.2a. Since we did not record continuous litter moisture data, the fluxes are plotted against soil moisture that has similar changes over time, but the plots appear shifted since the soil moisture was significantly lower in SC2 throughout the campaign.

Several factors may explain the stronger role of litter fluxes in SC2. Since SC2 was located directly under the large tree, it had a much thicker litter layer than SC1 (6 cm vs. 2 cm) and hence more litter COS uptake. The litter in SC2 should also have a lower rate of water loss because of the insulating effect of the thicker layer, and due to the lower temperatures (Figure 3.1c) in its shaded location next to a tree. The resulting higher litter moisture in SC2 during the dry period is represented in the model (Figure 3.13, Supplement). The stronger COS uptake in the thicker and more humid litter in SC2 then leads to a stronger COS drawdown across the litter layer so that less COS reaches the soil (Figure 3.18, Supplement). In addition, SC2 had lower soil moisture due to water uptake by the roots of the nearby tree. The soil under SC2 should therefore have lower microbial activity due to the lower moisture, and additionally lower microbial COS uptake due to the lower soil COS concentration. However, the stronger litter COS uptake more than compensates for the lower soil uptake in SC2, particularly during wet periods. In oak woodlands and other ecosystems with a sparse or open canopy, we thus expect overall stronger, and more litter-dominated, surface COS fluxes near and under the trees than in the inter-canopy space. As discussed below, we also expect that litter COS uptake plays a major role in surface COS fluxes, and thus surface COS fluxes

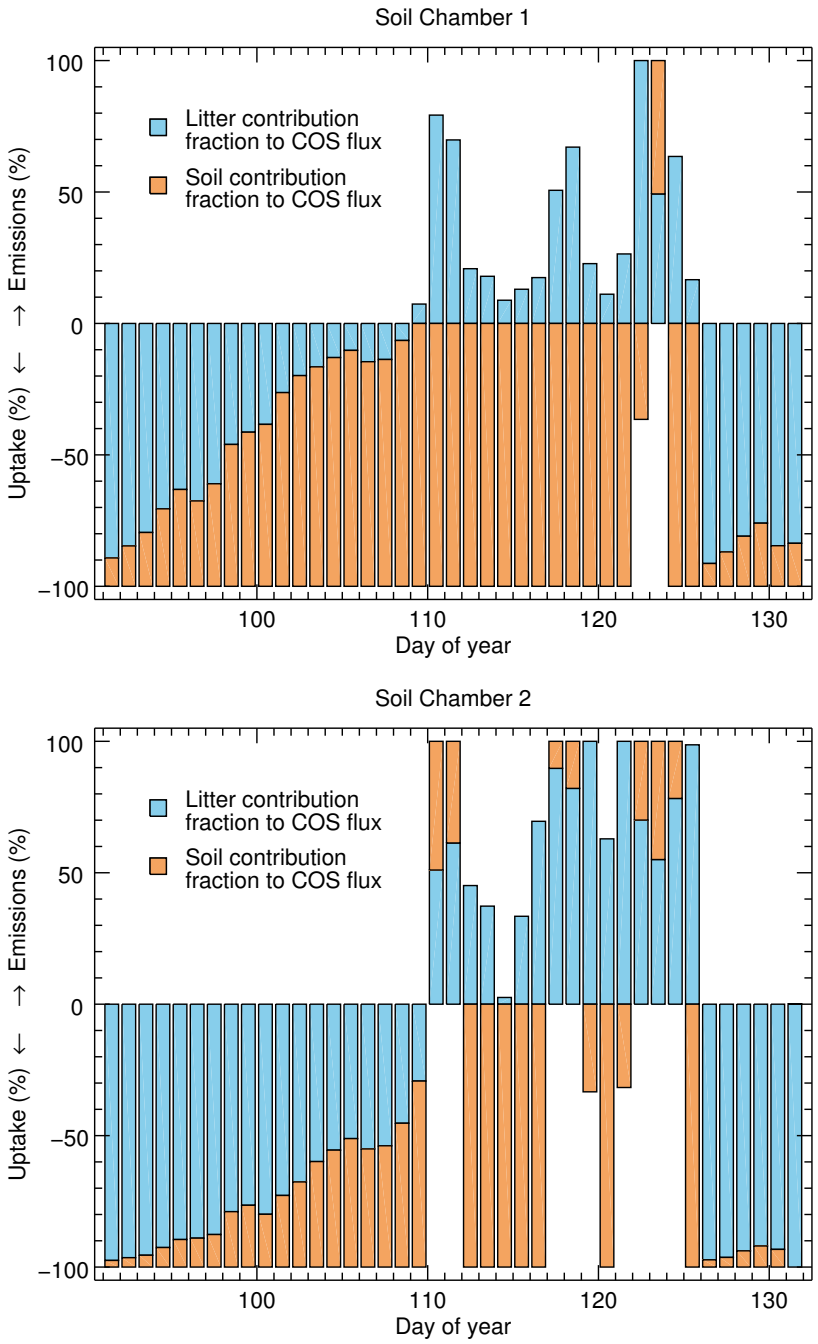

Figure 3.5: Relative contributions of litter and soil components to daily mean chamber COS fluxes from model results. Note that emissions were much smaller than uptake fluxes (see Figure 3.4). Litter and soil fluxes with different signs were normalized against the larger component (e.g. between DOY 110 and 125).

to reflect the distribution and timing of litter fall and decomposition across many ecosystems.

The litter in our field incubations had fluxes ranging from −4.3 to +1.3 pmol s^{-1} kg^{-1} dry weight (section 3.2), comparable to litter fluxes of −2.7 to +1.6 pmol s^{-1} kg^{-1} dry weight from a beech forest measured in laboratory incubations [*Kesselmeier and Hubert*, 2002]. *Kesselmeier and Hubert* [2002] also observed increasing litter COS uptake with litter moisture up to approximately 25–45%, although the litter moisture in our field incubations (10–25%) was at the lower end of their range. For soil samples from our site, the largest observed COS uptake rate was about 0.3 pmol kg^{-1} s^{-1} from laboratory incubations, with a similar range as measured for samples from other natural ecosystems [*Whelan et al.*, 2016].

3.4.2 Litter moisture changes drive variations in surface COS and CO_2 fluxes

We observed strong concurrent increases in surface COS uptake and CO_2 emissions after rain (Figure 3.6). Combining the surface flux and litter incubation data with model simulations indicates this increase predominantly originated from the litter layer (Figure 3.4), with more than 80% of COS uptake and more than 70% of CO_2 emissions attributed to the litter layer in the first five days after the rain event (Table 3.1). The response of both fluxes to rainfall is similar to the Birch effect—the burst of CO_2 efflux after rewetting of dry soils [*Birch*, 1958; *Jarvis et al.*, 2007]. However, at our site the flux spike was dominated by litter fluxes, with only a minor contribution from soil fluxes. In addition to the model analysis, our attribution is supported by the fact that the COS and CO_2 fluxes responded simultaneously (Figure 3.6). Secondly, the flux responses in SC2 were much stronger for both COS and CO_2 even though there was very little change in soil moisture underneath the tree canopy and thick litter layer (Figure 3.1).

Bursts of CO_2 emissions from litter following rewetting have been reported from laboratory studies [e.g. *Clein and Schimel*, 1994] but their contributions to surface fluxes in natural ecosystems have not been identified yet. Based on our findings, we propose that leaf litter in the field can

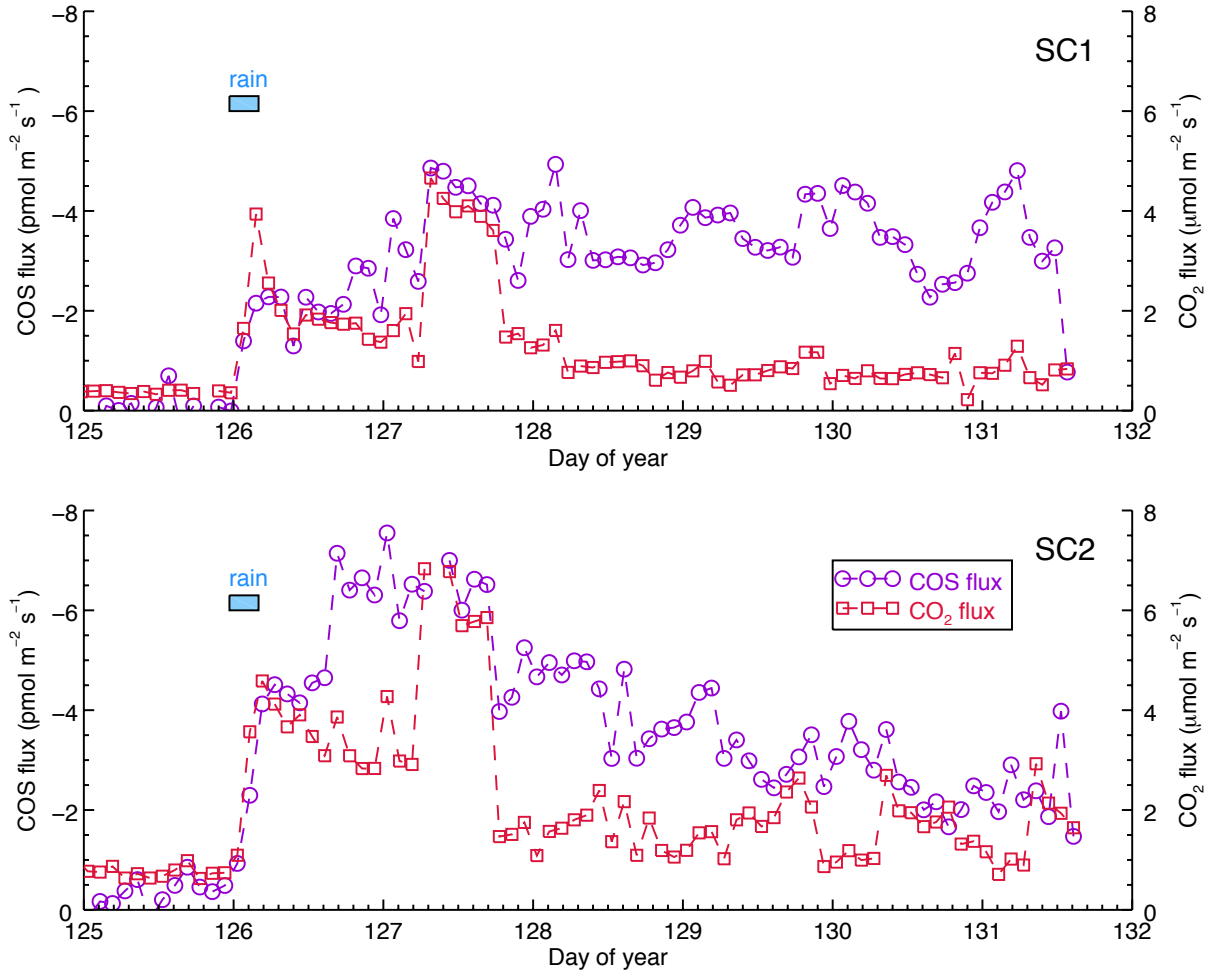

Figure 3.6: Rapid increases in COS and CO_2 fluxes immediately after the onset of rain on DOY 126 observed in both soil chambers. The peak fluxes occur with a lagged response, about 1 day after the rain. Note that the COS uptake is plotted on a reversed *y*-axis.

generate a Birch effect similar to that observed in soils. This litter Birch effect can occur even after light rainfall that is intercepted largely by the aboveground litter, with very little change in soil moisture. At the ecosystem scale, the rewetting of leaf litter may be an important contributor to the Birch effect observed in ecosystems with drying-rewetting cycles, for example in mediterranean regions.

The physical destruction of soil aggregates should not play a role in the litter Birch effect, in contrast to the contribution of this process to the Birch effect in the soil [*Denef et al.*, 2001; *Navarro-García et al.*, 2012]. In the litter, labile carbon may have accumulated due to other mechanisms such as photodegradation [e.g. *Rutledge et al.*, 2010; *Wang et al.*, 2015] or the physical breaking up of leaves. The rapid mineralization of microbial compounds in response to rewetting identified in the soil [*Fierer and Schimel*, 2003] could also play a role in the litter. Further research is needed to identify which of these mechanisms may contribute to the litter Birch effect.

About one day after the rain, both COS and CO_2 fluxes show a second increase, with an earlier onset in the COS uptake than the CO_2 emissions (Figure 3.6). The difference in the timing of the second increase is likely due to the higher temperature sensitivity of litter respiration whereas the enzyme activity responsible for COS uptake appears to be less sensitive to temperature. The time lag between first and second increase could indicate a sequential resuscitation of fast and slow responding microorganisms as observed in other ecosystems in California [*Placella et al.*, 2012], or a sequence of re-activation of microbes from dormancy followed by new microbial growth [*Fierer and Schimel*, 2003; *Blazewicz et al.*, 2014]. Microbial dynamics will need to be included explicitly to improve our capacity to simulate COS fluxes in environments with drying-rewetting cycles.

For the litter water content immediately after the rain (not measured), we used a best estimate of 0.3 g g^{-1} litter dry weight. This value fits well with the observed litter water content a few days after the rain (Figure 3.13), and is about half of the measured saturated litter water content of 0.5 to 0.6 g g^{-1} (Table 3.6, Supplement). To assess the potential effects of uncertainties in litter moisture on the litter–soil partitioning of COS uptake, we used an idealized simulation with no

litter flux and enhanced soil uptake. However, even increasing the V_{max} for soil COS uptake by an order of magnitude cannot account for the high uptake after the rain because COS uptake does not respond linearly to V_{max}, but rather logarithmically as it is limited by diffusion [*Sun et al.*, 2015]. Considering that litter uptake draws down the COS concentration at the litter–soil boundary, it is even less likely that soil contributes a significant portion to the COS uptake after the rain.

We also observed an increase in COS uptake in both chambers during DOY 103–105, coincident with decreased soil temperatures and high relative humidity (Figure 3.1a, and Figure 3.19, Supplement). This increase was likely caused by the lower soil and litter temperature that reduced COS production, and possible dew formation on the litter surface that stimulated litter COS uptake.

3.4.3 Implications of litter fluxes for soil chamber measurements

Chamber measurements of surface fluxes have been made either with the litter layer intact [*Castro and Galloway*, 1991; *Kuhn et al.*, 1999; *Yi et al.*, 2007], or with the aboveground litter removed from treatment plots [*Yi et al.*, 2007]. Litter fluxes have been reported separately in only one study so far [*Berkelhammer et al.*, 2014]: litter fluxes (-2.04 ± 0.4 pmol m^{-2} s^{-1}) were nearly identical to litter + soil fluxes (-2.1 ± 0.2 pmol m^{-2} s^{-1}), although the bare soil fluxes were larger (-4.4 ± 0.6 pmol m^{-2} s^{-1}). Our model simulations provide some insight into the mechanisms that may be responsible for this pattern. The strong uptake of COS in the litter layer leads to a significantly lower COS concentration at the litter–soil interface than in the ambient air at the litter surface (see Figure 3.18, Supplement). As enzymatic uptake depends on the COS concentration, the removal of the litter layer results in a much larger soil uptake flux due to the increased COS concentration in the soil air. Measuring soil fluxes with the litter removed therefore yields information on the potential soil uptake rather than the actual soil fluxes. Hence, removing the litter layer may lead to biases in measured COS uptake and CO_2 emissions, particularly in ecosystems with drying-rewetting cycles. Only during dry periods with small or no litter COS uptake does the litter layer behave as a diffusion barrier without a large effect on soil fluxes themselves.

As demonstrated by the results reported here and in *Berkelhammer et al.* [2014], the COS uptake of a soil–litter system is typically not the sum of fluxes measured from bare soil and litter samples. We therefore suggest that future studies report three fluxes: the surface flux from the intact litter–soil system, the bare soil flux after removing the litter, and the litter flux isolated from the soil underneath. A depth resolved diffusion-reaction model can then be used to assess the contributions of litter and soil fluxes to the net surface COS flux [*Sun et al.*, 2015; *Ogée et al.*, 2016].

3.4.4 Dynamics of surface COS exchange in an oak woodland

The surface COS flux is controlled by physical and biological properties of the soil and overlying litter layers. At the Stunt Ranch site, water content was the dominant factor controlling the long-term trend of surface COS fluxes, whereas diurnal variations were mostly driven by temperature. We hypothesize that surface COS fluxes in ecosystems with seasonal rainfall such as mediterranean or other semi-arid regions will have pronounced seasonal variations, with peaks in COS uptake following rain, and weak COS uptake or emissions during the dry season. Strong variations in the isotopic composition of soil CO_2 fluxes have also been reported in semi-arid ecosystems [e.g. *Wingate et al.*, 2008; *Maseyk et al.*, 2009], indicating moisture-driven variations in microbial respiration and CA enzyme activity.

Litter phenology is likely another key factor controlling the seasonality of surface COS fluxes. In mediterranean ecosystems, many drought-deciduous species shed their leaves in the hot, dry summer period. Microbial activity is severely water-limited during those months, and photochemical degradation plays a major role in litter decomposition [e.g. *Austin and Vivanco*, 2006]. The air-dried leaf litter accumulated on the ground provides structure and material (dormant microbial biomass or labile carbon) for the rapid onset of microbial activity after rainfall, i.e. the litter Birch effect associated with spikes in litter COS uptake. In contrast, in temperate ecosystems litter fall typically occurs in the autumn, and we would expect enhanced surface COS uptake around that time. However, litter decomposition then proceeds more gradually as long as there

is sufficient soil moisture, hence litter COS fluxes should be less variable than in semi-arid systems. We therefore expect distinct patterns in the seasonality of surface COS fluxes for semi-arid compared to other ecosystems.

3.4.5 Implications for COS-enabled land biosphere models

Incorporating COS as tracer into biosphere models has the potential to separate the responses of photosynthesis and respiration at large scales. However, few land surface models represent the litter as a separate layer even though a significant portion of land area is covered by aboveground litter [*Matthews*, 1997]. The lack of a litter layer may bias the net surface COS uptake if soil fluxes are parameterized from chamber measurements where the litter has been removed. For example, surface fluxes would be overestimated by a factor of two if based on the soil flux data instead of the soil + litter data reported in *Berkelhammer et al.* [2014]. Hence, neglecting litter uptake may lead to a potentially large bias in estimates of global surface COS fluxes. This would result in an equally large bias in vegetation COS uptake derived from flux budgets, and be propagated into the COS-derived gross photosynthetic carbon uptake [see *Whelan et al.*, 2016].

In addition, our findings indicate that surface COS and CO_2 fluxes could be decoupled due to the effects of litter COS uptake. In the first study using a COS-enabled global biosphere model [*Berry et al.*, 2013], soil COS uptake was parameterized using the empirical relationship between COS uptake and microbial respiration [*Yi et al.*, 2007] and soil moisture limitation to diffusion [*Van Diest and Kesselmeier*, 2008]. Litter fluxes or soil COS production were not included. We tested two empirical COS-CO_2 relationships [*Berry et al.*, 2013; *Berkelhammer et al.*, 2014] using data from SC1, and found that they did not capture well the fluxes in the wet period (Figure 3.20, Supplement). The decoupling result as litter fluxes dominate the net surface COS exchange while both litter and soil contribute to CO_2 emissions. For example, soil CO_2 production could proceed with very little associated COS uptake when a large amount of COS has already been converted in the litter layer. COS emitted during photodegradation [*Whelan and Rhew*, 2015] and soil COS production

[*Maseyk et al.*, 2014] may additionally decouple COS and CO_2 fluxes at high solar radiation or soil temperatures.

Similar to the empirical COS-CO_2 relationships, the relationship with H_2 deposition that has been used to parameterize soil COS fluxes [*Launois et al.*, 2015a] is likely an indirect link. In the soil, H_2 is mostly consumed by microbial hydrogenases (e.g. in *Streptomycetes* spp., see *Constant et al.* [2010]), and sometimes by methanogens and sulfate reducers [*Conrad*, 1996]. These processes do not appear to be directly linked to CA enzyme activity. Instead, the observed similarities in large-scale COS and H_2 deposition [*Belviso et al.*, 2013] could result from variations in microbial activity that affect different enzymes and hence both fluxes.

Instead of empirical relationships, depth-resolved models that treat COS as independent tracer [*Sun et al.*, 2015; *Ogée et al.*, 2016] are better suited for global COS simulations. However, we currently lack data on many of the model parameters. In our study, we were able to fit a single set of optimized COS uptake and production parameters for both chambers (Table 3.8, Supplement), indicating that similar mechanisms determine the flux patterns despite the differences in litter thickness and soil moisture. The optimized fluxes agreed well with observations in both chambers, which is encouraging for the use of biome-specific sets of parameters in large scale models. Both chambers also had a similar optimum temperature for COS uptake of around 13°C (Figure 3.16, Supplement), comparable to a temperate arable soil (15°C) but lower than boreal soils (25°C) in lab incubations [*Van Diest and Kesselmeier*, 2008]. Temperature optima could be affected by changes in microbial community as well as varying contributions from different COS-converting enzymes [*Smeulders et al.*, 2011; *Ogawa et al.*, 2013] that may be present in addition to CA. COS models would therefore strongly benefit from data on enzyme activity linked to microbial community dynamics across biomes and seasons.

3.5 Chapter conclusion

Our results indicate that litter plays a major role in determining surface COS fluxes in a mediterranean oak woodland. Litter water content was the most important driving factor for litter uptake, and thus also for net surface COS fluxes. Following a rainfall event, we observed a litter Birch effect with peaks in both COS and CO_2 fluxes, implying a rapid reactivation of litter microbes after rainfall. Surface COS fluxes are likely to show a distinct and pronounced seasonality in semi-arid ecosystems. Due to the uptake of COS in the litter layer, combined with the concentration-dependent nature of soil COS uptake, the COS uptake by the intact litter–soil system is not the sum of the separate litter and soil components. It is therefore important to keep the litter–soil structure intact when installing chambers for surface COS measurements. Similarly, it is important to account for the litter–soil structure as well as litter fluxes in model simulations. Characterizing net surface, litter and bare soil COS fluxes separately will provide valuable new data and insights for model development, and help to improve ecosystem to global COS budgets.

3.6 Supplement

3.6.1 Meteorological conditions

The meteorological station at Stunt Ranch Reserve is located approximately 80 m NW from the measurement site. Two precipitation events were observed during the campaign—2 mm on 31 March 2013 and 13.5 mm on 5 and 6 May 2013.

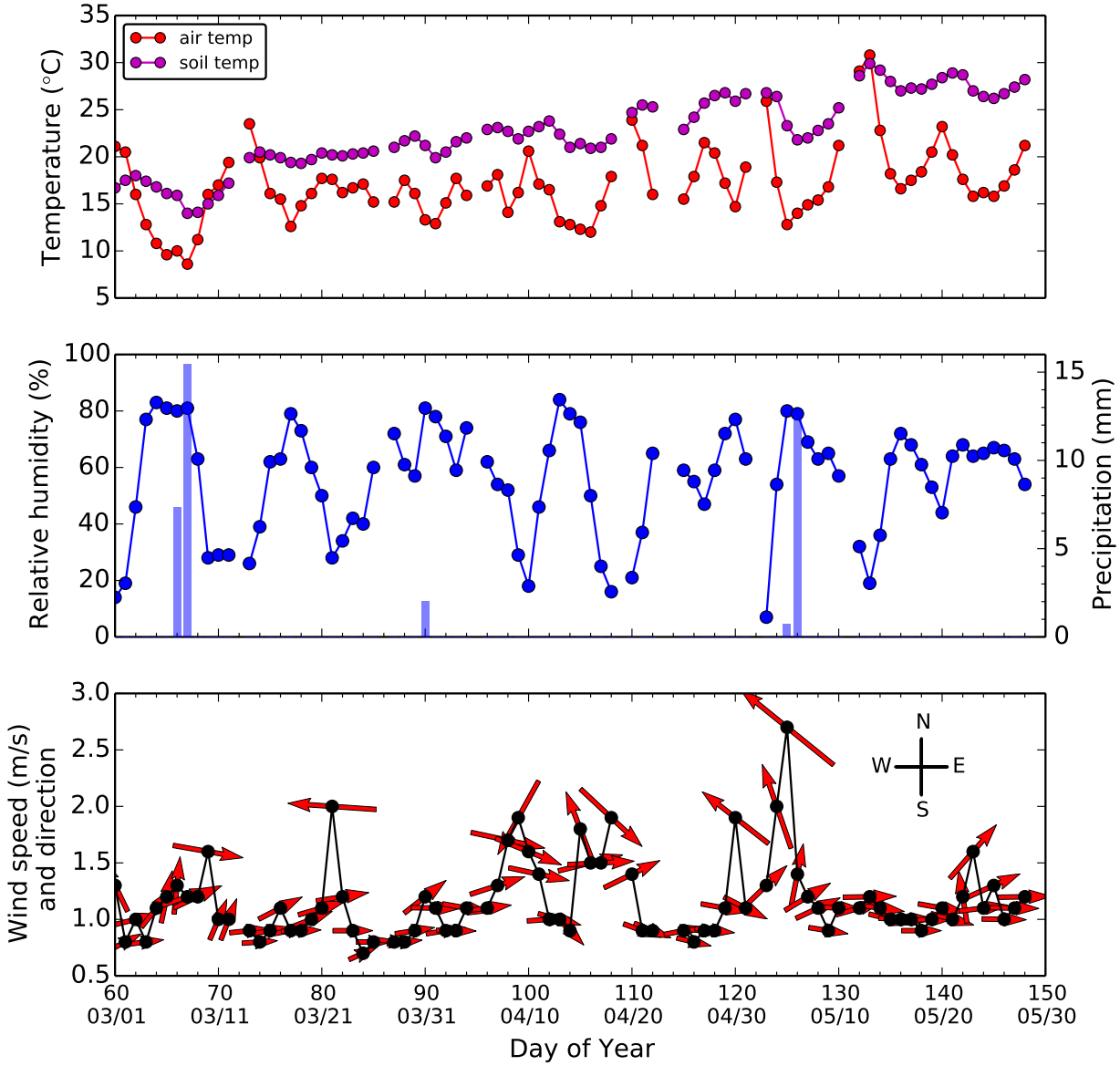

Figure 3.7: Daily mean meteorological conditions at Stunt Ranch Reserve in March to May 2013. (a) Air (red) and soil (purple) temperature; (b) relative humidity (circles) and precipitation (bars); (c) wind direction (arrows) and speed (circles). Our field measurements were conducted between DOY 90 and 132.

3.6.2 Chamber flux measurements

During each 15-min chamber measurement period, the sampling sequence was allocated as in Figure 3.8. We calculated chamber COS, CO_2 and H_2O fluxes based on mass balance:

$$V\frac{dC}{dt} = f(C_{in} - C_{out}) + FA \tag{3.5}$$

where C is the chamber concentration of the measured gas, V and A are the chamber volume and surface area, f is the air flow rate, F is the flux rate of the gas, and C_{in} and C_{out} are the chamber inlet and outlet concentrations. Assuming well-mixed chamber air, the outlet concentration must equal the chamber headspace concentration, i.e., $C_{out} = C$. The flux rate F is assumed constant in the measurement period. To account for changes in Cin during chamber closure, we interpolated linearly C_{in} (Figure 3.8) and subtracted this zero-flux baseline from the changes in chamber concentration.

There were no significant chamber effects on COS and CO_2 fluxes. The average COS effect from a blank chamber was 0.15 ± 0.44 pmol m^{-2} s^{-1} (Figure 3.9). The chamber effects were not correlated with temperature ($r^2 = 0.03$), and small even at high air temperatures. However, chamber effects had larger variations at lower temperatures (5–15°C). The reason is not entirely clear, but could be due to COS adsorption/desorption on chamber walls and vapor condensation in the chamber at night that slightly bias the mass balance. For CO_2 flux, the average chamber effect (–0.02 ± 0.13 µmol m^{-2} s^{-1}) was not statistically different from zero. Standard deviations of the chamber effects were included in the calculation of chamber flux errors.

3.6.3 Modeling litter COS and CO_2 fluxes from field incubations

In modeling litter COS flux, the following assumptions were considered:

1. COS uptake rate is proportional to its concentration [*Kesselmeier et al.*, 1999]
2. Enzymatic COS hydrolysis is an aqueous reaction [*Notni et al.*, 2007; *Elliott et al.*, 1989], which

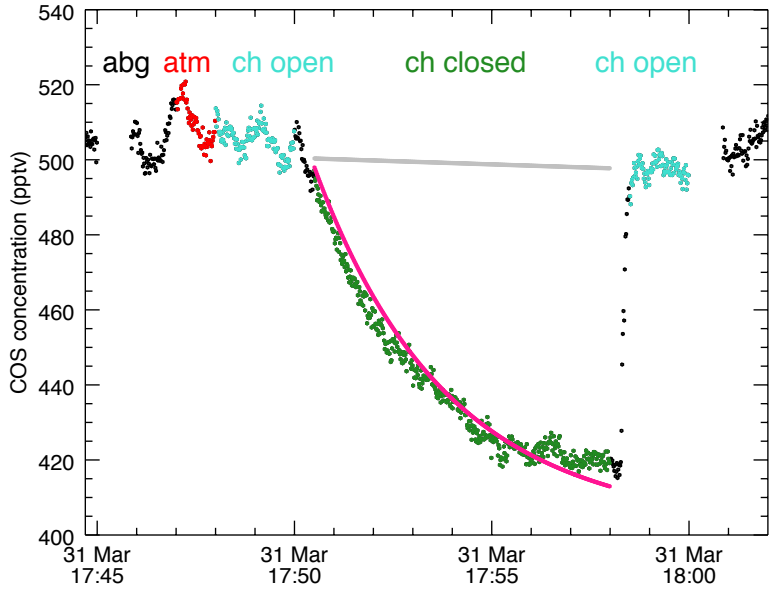

Figure 3.8: Sampling sequence during a sampling period (15 min), illustrated with data from soil chamber 1. The first 2 min are allocated to auto-background calibration (abg), followed by 1 min of sampling on the atmosphere line (atm). Then the system switches to the chamber line, and samples the air in the open chamber (ch open) for 2 min. The chamber is then closed (ch closed) for 8 min, and opened for the last 2 min. The light gray line represents the zero-flux baseline correction to account for changes in ambient concentrations between the two chamber-open intervals.

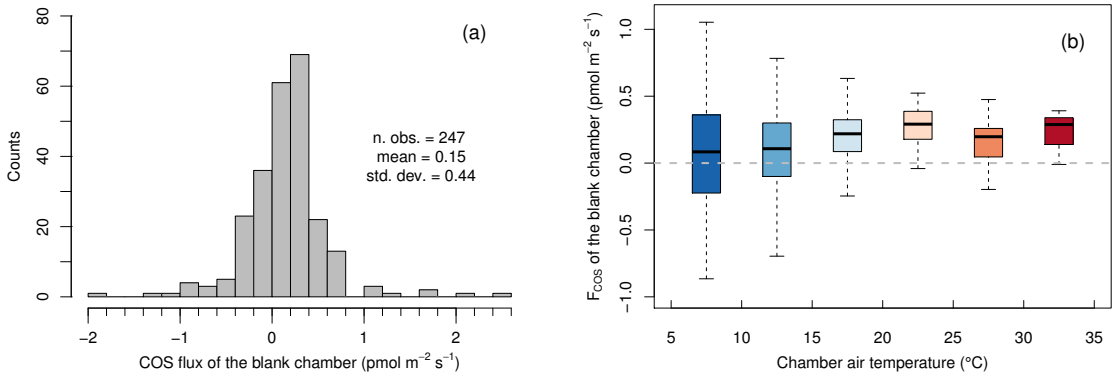

Figure 3.9: COS fluxes produced by the blank chamber shown in a histogram (a), and boxplot with 5°C bins (b). The boxes in (b) indicate the interquartile ranges (IQR) bounded by 25th and 75th quantiles (Q_1 and Q_3). The upper whiskers are at the smaller of the data maximum and Q_3 + 1.5 IQR, and the lower whiskers are at the larger of the data minimum and Q_1 − 1.5 IQR.

means COS uptake rate depends on its aqueous concentration $k_{H,S}C_{S,a}$

3. Temperature dependence of the uptake rate can be described by Arrhenius equation, proportional to $\exp\left(-\frac{E_{act}}{RT_L}\right)$, where E_{act} is the apparent activation energy
4. COS uptake increases exponentially with litter water content w_L, as observed from the incubation data
5. COS production is present since COS emissions were observed

We therefore formed the following nonlinear regression model of litter COS flux F_{SL},

$$F_{SL}(w_L, T_L, C_{S,a}) = V_{SLU,max} \cdot \sinh(k_{SL} w_L) \cdot k_{H,S}(T_L) C_{S,a} + V_{SLP,max} \cdot \exp\left[k_T (T_L - T_{ref})\right] \quad (3.6)$$

The explicit temperature dependence of COS uptake, $\exp\left(-\frac{E_{act}}{RT_L}\right)$, was tested but dropped since it was not statistically significant. The uptake rate is thus implicitly dependent on T_L since $k_{H,S}$ is a function of temperature. A hyperbolic sine function was used for water content dependence, because uptake flux should approach zero in completely dry conditions ($w_L \to 0$).

Since the relationship between litter COS production and temperature has not yet been determined, COS production of leaf litter was assumed to depend exponentially on temperature simi-

lar to that of root COS production [*Maseyk et al.*, 2014] and soil abiotic COS production [*Whelan and Rhew*, 2015]. In *Maseyk et al.* [2014], two regression lines of COS fluxes against temperature under different soil moisture conditions give Q_{10} values of 1.7 and 2.1, therefore we used the average Q_{10} = 1.9 here (equivalent to k_T = 0.064).

The fitted parameters for the regression models of litter COS and CO_2 fluxes are shown in Table 3.3. When fitting the two litter incubation experiments separately, the parameters are different due to heterogeneity between the litter samples. We therefore combined the data from both experiments for regressions to parameterize litter COS fluxes in the soil–litter COS flux model. The models trained with the combined data average out the heterogeneity, and do not significantly increase RMSEs.

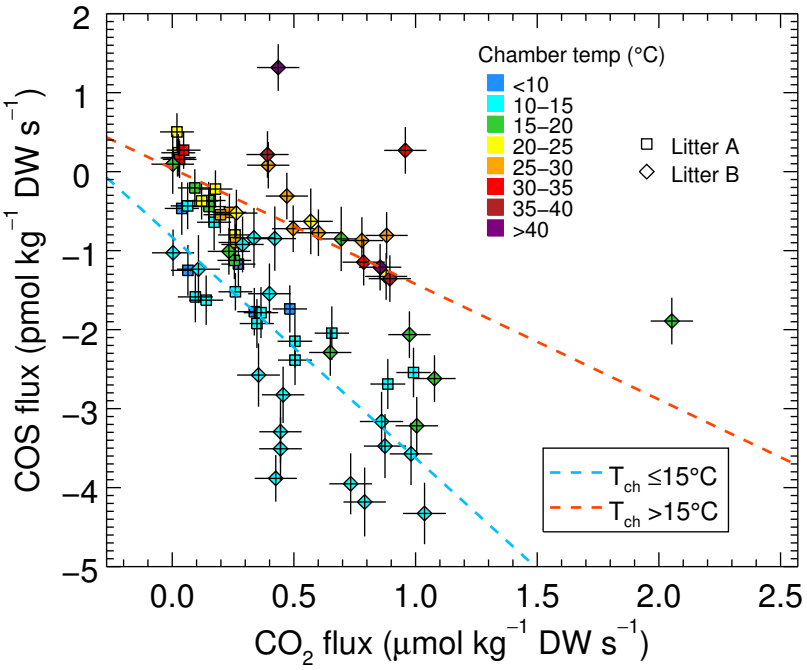

Figure 3.10: Litter COS and CO_2 fluxes ($\pm 1\,\sigma$) are well correlated. Data points are colored for temperature bins, with square symbols indicating litter incubation experiment A (DOY 127–129), and diamond symbols for experiment B (DOY 129–131). Litter COS flux has weaker sensitivity to CO_2 flux when chamber temperature > 15°C, due to different temperature dependence of the two fluxes.

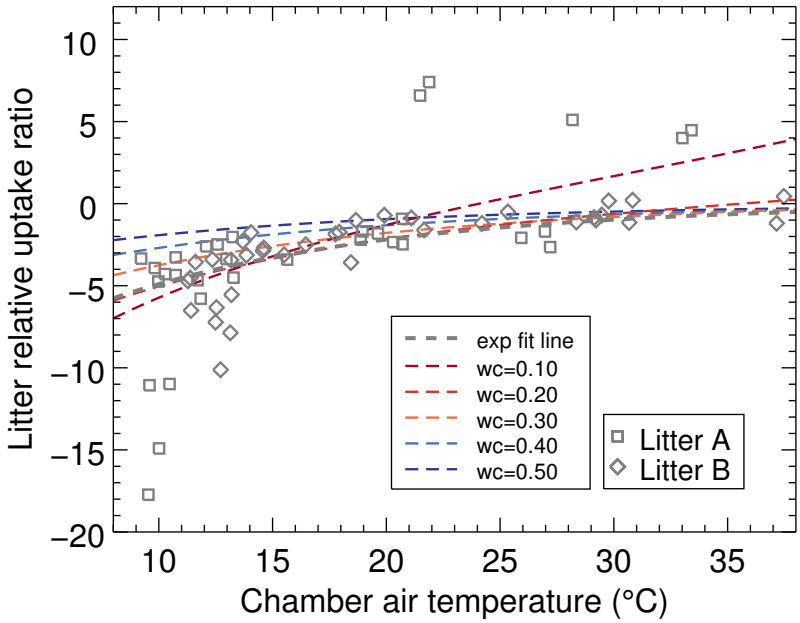

Figure 3.11: Litter relative uptake ratio versus chamber temperature. The relative uptake ratio, defined as the flux ratio of COS to CO_2 normalized by their respective concentrations, generally increases with temperature, and asymptotically approaches zero at high temperature. The thick gray line indicates the fitted function for relative uptake vs. temperature, $RU = -\exp(2.40 - 0.0808\,T)$ ($r^2 = 0.42$, RMSE = 2.77). Note only negative litter relative uptake values are used for the regression. Other colored thin lines are simulated curves at various constant litter water contents, χ_{COS} = 500 pptv and χ_{CO_2} = 400 ppmv, based on Eqs. (S1) and (S2).

Table 3.2: Litter dry weight and thickness

Litter sample no.	Dry weight (g)	Thickness (cm)	Dry bulk density (kg dry weight m^{-3})†
Litter in SC1	20.201	2	31.8
Litter in SC2	58.733	6	30.8
Litter incubation A	59.265	N/A	N/A
Litter incubation B	47.505	N/A	N/A

† Chamber bottom area is 317.8 cm^2.

Table 3.3: Model parameters for fluxes from litter incubation experiments

Sample no.	$V_{SLU,max}$ $m\ s^{-1}$	k_{SL}	$V_{SLP,max}$ $pmol\ kg^{-1}\ s^{-1}$	$V_{SLP,max}$ $\mu mol\ kg^{-1}\ s^{-1}$	k_{CL}	E_{RL} $kJ\ mol^{-1}$	RMSE(F_{SL}) $pmol\ kg^{-1}\ s^{-1}$	RMSE(F_{CL}) $\mu mol\ kg^{-1}\ s^{-1}$
Litter A	$\underline{6.667 \times 10^{-7}}$ [a]	35.02	<u>0.2147</u>	$\underline{3.084 \times 10^{-4}}$	49.37	<u>20.80</u>	0.33	0.16
Litter B	$\underline{2.286 \times 10^{-6}}$	22.10	<u>0.1376</u>	$\underline{2.327 \times 10^{-2}}$	19.08	21.42	0.45	0.19
Combined [b]	2.818×10^{-5}	11.56	0.4247	5.651×10^{-2}	15.00	14.88	0.54	0.21

[a] Underlined parameters are not statistical significant, based on $p < 0.05$ criterion.

[b] This is the same parameter set used in soil–litter flux model, but they are transformed to per unit volume basis using the dry bulk density of litter (31.3 kg m^{-3}) and $K_m = 1.9$ mol m^{-3}.

3.6.4 Parameterizing litter water fluxes and litter water content

The litter density was measured to be 530 kg m^{-3} after grinding the litter into fine powder. With the average dry bulk density of litter layers estimated as 31.3 kg m^{-3} (Table 3.2), we calculated litter porosity as 0.94 $m^3\ m^{-3}$. Because we did not measure litter water content in the two soil chambers (SC1 and SC2), we reconstructed litter water content using the empirical relationship between litter water fluxes, $F_{WL} = f(T, w_L)$ and environmental variables (temperature T (°C) and litter water content w_L), from multiple regression using litter incubation data:

$$F_{WL} = (-0.00766 + 0.00152\,T) \cdot \sinh(7.64\,w_L) \tag{3.7}$$

Here F_{WL} is in mmol s^{-1} kg^{-1} dry weight, normalized by the dry weight of the litter. The comparison of modeled versus observed litter water flux is shown in Figure 3.12.

We divided the litter into two layers, a top layer spanning 0–1 cm (model layers 0–2) and a bottom layer spanning 1–2 cm (model layers 3–5) in SC1, and 1–5.5 cm (model layers 3–10) in SC2. In the top 1 cm of the litter, we assumed the evaporation rate is 1.5 times of that described in Eq. (S3), and in the lower layer of the litter, the evaporation rate is 50% of that in Eq. (S3).

The following ordinary differential equation was formed for w_L in each litter layer,

$$\frac{d}{dt}\left[\frac{w_L m_d}{1 - w_L}\right] = m_d F_{WL}(T, w_L) M_w \tag{3.8}$$

where m_d is the dry weight of litter. Litter water content of the two chambers were solved numerically with the assumed conditions of w_L after rain events (Figure 3.13).

We assumed the initial water content was 0.35 g g^{-1} for the litter in SC1, and 0.30 g g^{-1} for the litter in SC2, across different vertical layers. These assumptions of initial litter water content lead to a good agreement between the simulated and the observed high COS fluxes, which is not attainable by simply increasing soil flux parameters. Similarly, we assumed that the litter water content was vertically uniform immediately after the rain on 5–6 May 2013 (DOY 125–126). We also included nighttime condensation of water on the litter surface. The amount of condensation was calculated by assuming that the over-saturated water vapor in a 10 m air column above the chamber would be condensed out and added to the top 1 cm of the litter. Although there are uncertainties in litter water content after the rain due to lack of continuous data, the parameterized litter water content is within the range constrained by the data from the litter incubation experiments (Figure 3.13).

Table 3.4: Litter water content measured in a follow-up field visit on April 19, 2014.

Litter sample no.	Description (location, depth)	Gross weight (g)	Dry weight (g)	Litter water content (g g^{-1})	Soil moisture below (m^3 m^{-3})
LTR-SC1-1	SC1, top layer (0–1 cm)	14.915	12.830	0.140	0.106
LTR-SC1-2	SC1, bottom layer (1–2 cm)	20.163	17.360	0.139	
LTR-SC2-1	SC2, top layer (0–1 cm)	15.033	13.423	0.107	
LTR-SC2-2	SC2, middle layer (1–3 cm)	30.518	26.701	0.125	0.120
LTR-SC2-3	SC2, bottom layer (~ 3–6 cm)	66.876	56.706	0.152	

Table 3.5: Water content of fresh leaves from coast live oak (*Quercus agrifolia*) at the site, sampled on March 2, 2015.

Sample no.	Fresh weight (g)	Water loss (g)	Leaf water content (g g^{-1})
Sample set LF1: sunlit, big leaves (5 pieces each subsample)			
LF1-V1	2.348	1.213	0.517
LF1-V2	1.857	0.959	0.516
LF1-V3	1.671	0.813	0.487
LF1-V4	1.670	0.877	0.525
Mean ± S.D.		N/A	0.511 ± 0.014
Sample set LF2: shaded, big leaves (5 pieces each subsample)			
LF2-V1	1.607	0.810	0.504
LF2-V2	2.009	1.049	0.522
LF2-V3	1.669	0.797	0.477
LF2-V4	1.287	0.588	0.457
Mean ± S.D.		N/A	0.490 ± 0.025
Sample set LF3: small leaves (5 pieces each subsample)			
LF3-V1	0.597	0.294	0.492
LF3-V2	0.742	0.357	0.481
LF3-V3	0.473	0.217	0.459
LF3-V4	0.409	0.202	0.494
Mean ± S.D.		N/A	0.481 ± 0.014

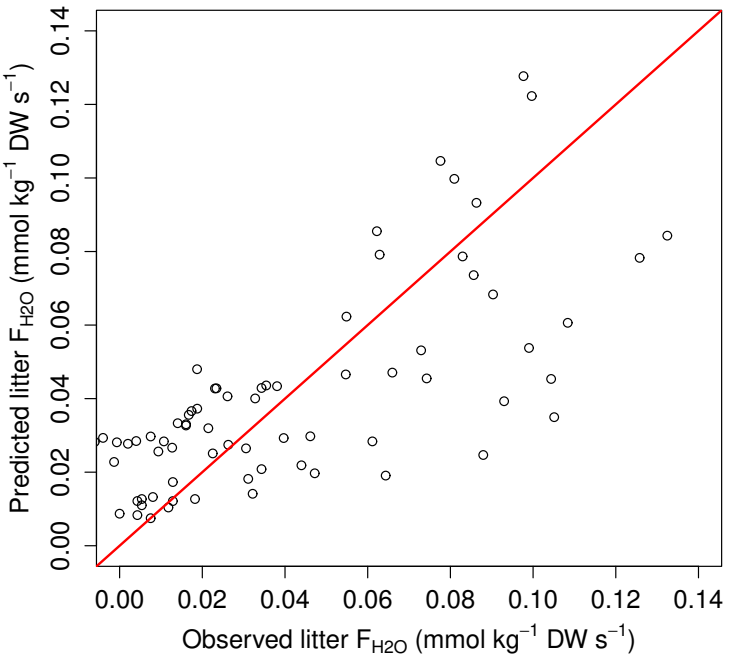

Figure 3.12: Predicted vs. measured litter water fluxes in field incubations.

Table 3.6: Saturated water content of the litter measured from a soaking experiment on March 2, 2015. Litter samples were soaked in water overnight, and then taken out for water content measurements. The soaked samples were wiped before weighing to remove water droplets on the litter surface.

Sample no.	Saturated weight (g)	Dry weight (g)	Water content (g g^{-1})
LTRSAT-1	6.677	2.544	0.619
LTRSAT-2	5.013	2.635	0.474
Mean	N/A		0.547

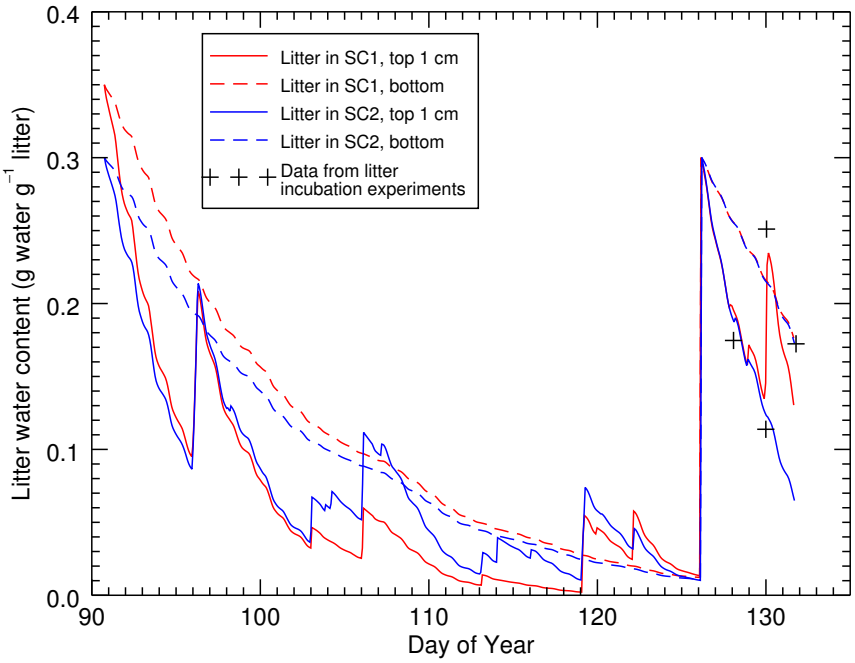

Figure 3.13: Modeled water content changes of the litter in the two soil chambers during the campaign. Data calculated from litter incubation experiments were used to constrain litter water content after rain events.

3.6.5 Site-specific parameters for soil variables and fluxes

Soil/litter water content profiles are shown in Figure 3.14. Soil temperature profiles of SC1 and SC2 were simulated empirically from those measured at 5 cm depth, and compared with data from a nearby meteorological station (Figure 3.15). The temperature signals were assumed as a superposition of fast varying diurnal signals (T_F) and slowly varying synoptic scale signals (T_S) [*Van Wijk and de Vries*, 1963],

$$T(z,t) = T_S + T_F \exp(-z/z_T) \sin(\omega t + \phi - z/z_T) \tag{3.9}$$

where z_T (m) is the damping depth for diurnal temperature waves, $\omega = 2\pi$ day^{-1} is the angular frequency, and ϕ is the phase constant. z_T can be calculated from,

$$z_T = \sqrt{2\alpha/\omega} \tag{3.10}$$

where α (m^2 s^{-1}) is the soil thermal diffusivity. Based on *Peters-Lidard et al.* [1998] and *Johansen* [1975], we calculated α to be 6.8–8.1 $\times 10^{-7}$ m^{-2} s^{-1} for SC1, and 2.0–3.9 $\times 10^{-7}$ m^{-2} s^{-1} for SC2. An average damping depth $z_T = 0.14$ m was used for modeling soil temperature profiles at SC1, while $z_T = 0.085$ m was used for SC2. Temperatures of the litter layers were interpolated between soil temperatures and chamber air temperatures by assuming logarithmic temperature profiles.

Soil COS flux terms include a sink term, depending on soil temperature, moisture and COS concentration, and a source term depending on soil temperature only. The exact function forms are described in detail in [*Sun et al.*, 2015]. The sink term has an optimum temperature, assumed to be about 13°C in this study (Figure 3.16), and an optimum water content at 0.14 m^3 m^{-3}, estimated from lab incubations of soil samples from Stunt Ranch [*Whelan et al.*, 2016]. The source term responds exponentially to temperature, with a Q_{10} parameter of 1.9 [see *Sun et al.*, 2015].

An empirical approach to parameterizing soil COS flux has been proposed based on an exponential relationship between the ratio of concentration-normalized fluxes of COS and CO_2 with temperature [*Berkelhammer et al.*, 2014]. In contrast, in our study the variability of this ratio was not well explained by temperature (Figure 3.17b), probably due to the inclusion of litter COS fluxes.

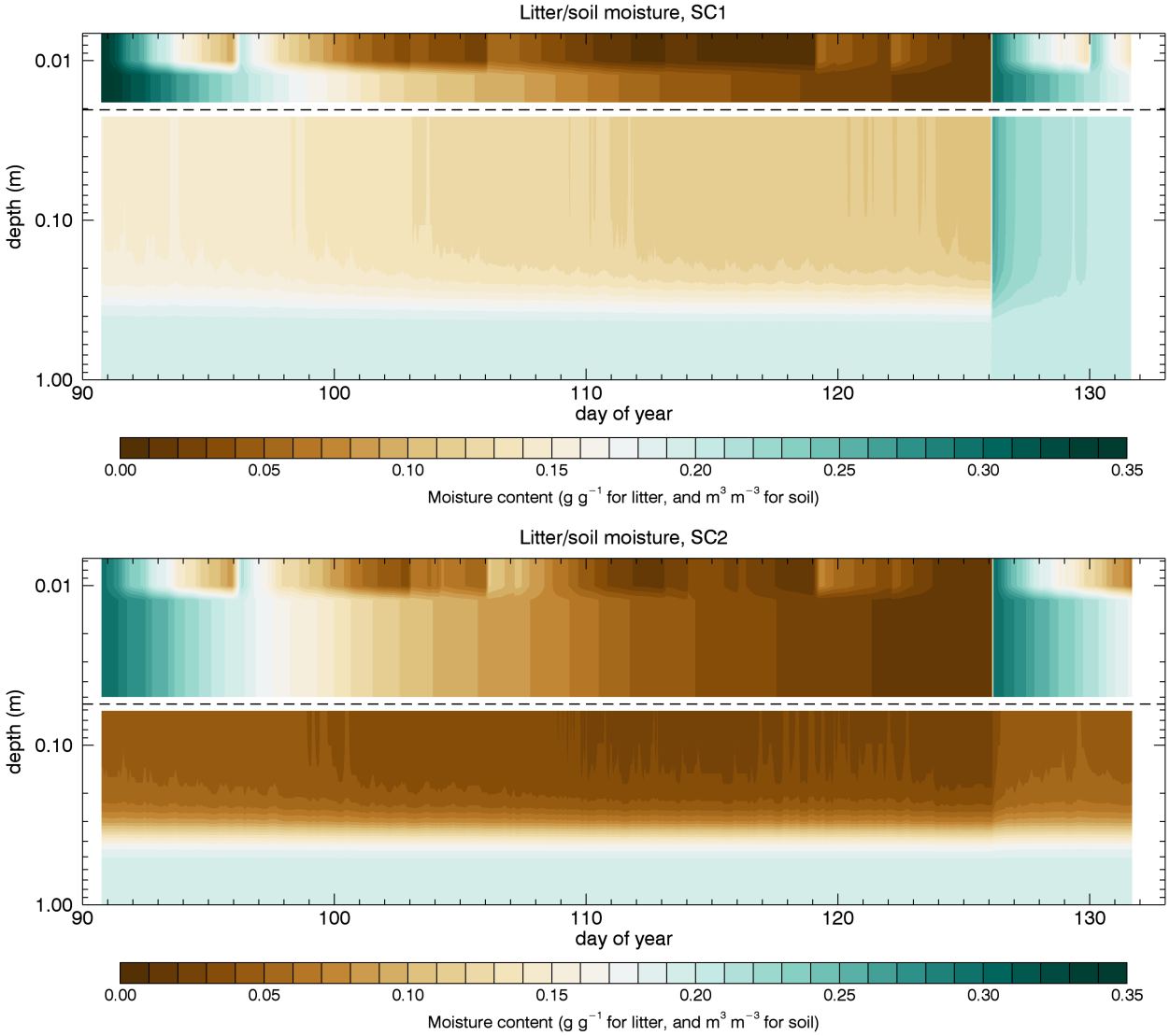

Figure 3.14: Parameterized water content profiles for SC1 and SC2. The dashed lines denote litter–soil interfaces. In the litter layers, water content is shown as mass fraction (g g^{-1}), whereas in soil layers it is shown as volumetric fraction (m m^{-3}). Note that the y-axis is in logarithmic scale.

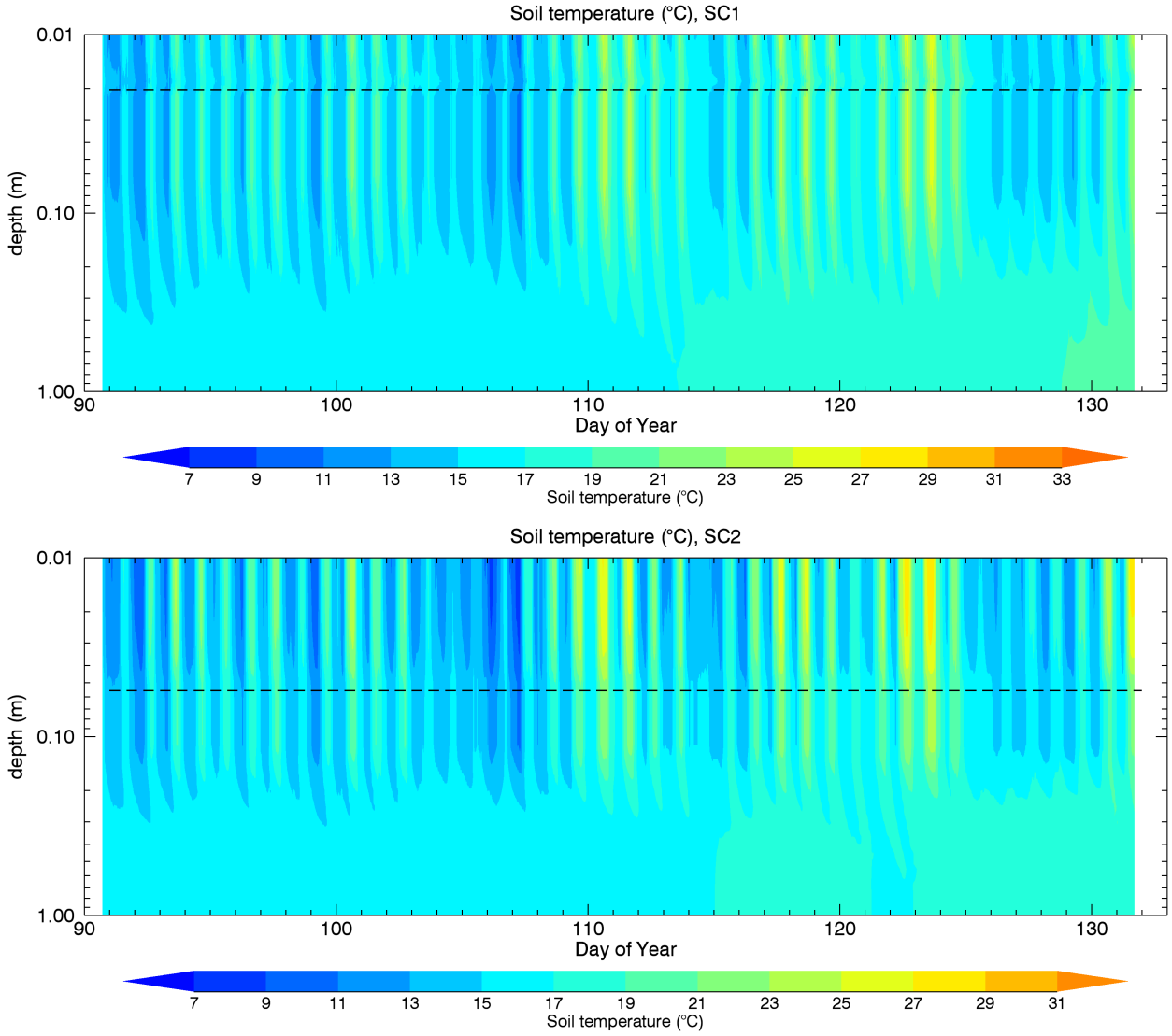

Figure 3.15: Parameterized soil temperature profiles for SC1 and SC2 (top and middle panels), and the interpolated profile at the nearby meteorological station measured at 5, 10, 20, and 50 cm (bottom panel). Note that the y-axis is in logarithmic scale. The litter–soil interfaces are marked by dashed lines. Since the area around the meteorological station is exposed to the sun, soil temperatures there are higher than at the mostly shaded soil chambers. The two areas show generally consistent patterns of variation.

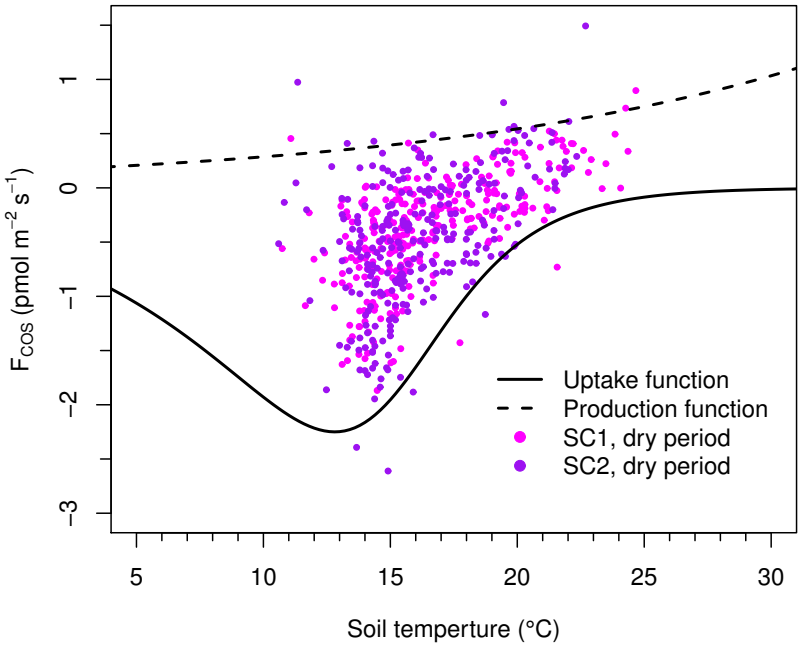

Figure 3.16: Temperature dependence functions of soil COS uptake and production compared with data in the dry period (DOY 100–120). The dry period was chosen to minimize the effects of moisture changes on fluxes. The functions are shown with arbitrary magnitude to match the envelope of the data. We set parameters of the uptake function to give an optimum temperature $T_{opt} \approx 13°C$ that is consistent with the data.

Table 3.7: Soil temperatures and moisture near the surface and 20 cm depth near SC1 measured on April 19, 2014.

Depth (cm)	Temperature (°C)	Moisture (m^3 m^{-3})
5	22.0	0.085
20	22.9	0.108

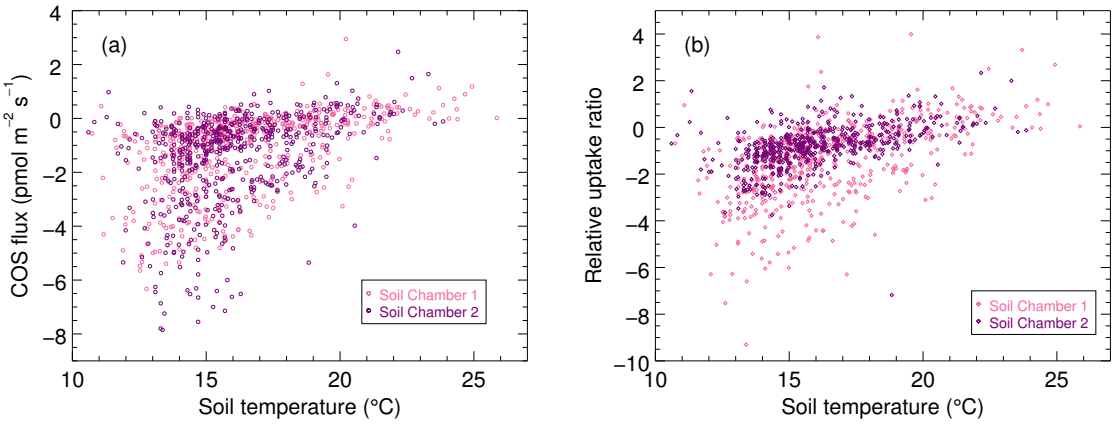

Figure 3.17: Temperature dependence of (a) surface COS flux and (b) relative uptake ratio of concentration-normalized COS to CO_2 fluxes.

3.6.6 Modeled COS profiles in wet and dry periods

Because COS uptake rates strongly depend on litter and soil moisture content, the differences of fluxes in wet and dry conditions lead to different COS profiles. In wet conditions, steeper vertical COS gradients develop in the upper layers as a result of strong COS uptake and high diffusivity in the litter (Figure 3.18). The gradients are reduced in dry conditions, with much higher COS concentration in the litter and upper soil. Due to the assumed soil COS production, COS concentrations are at the compensation point in the deeper soil. The compensation point is higher in the dry period, when COS uptake becomes weaker.

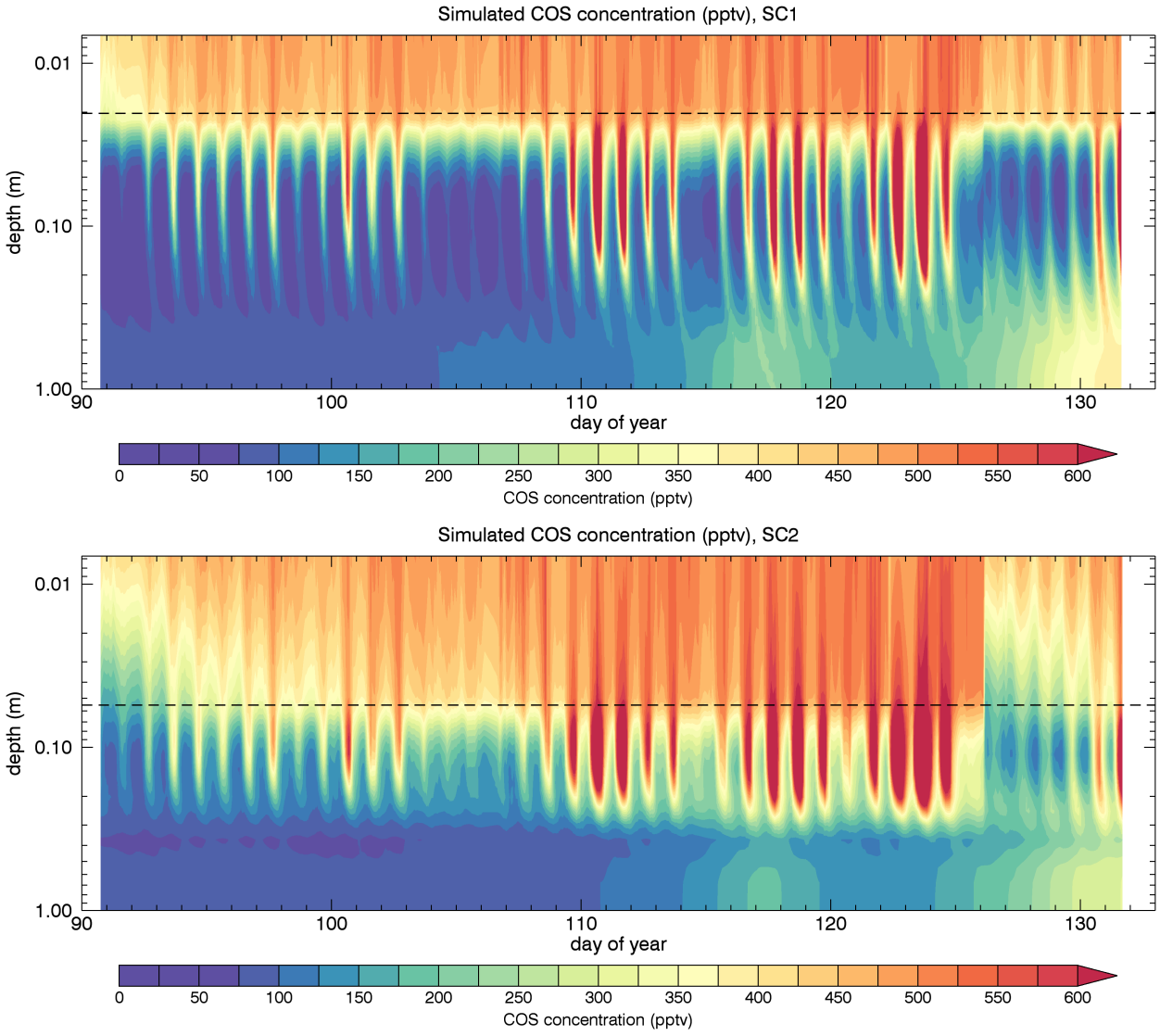

Figure 3.18: Simulated COS concentration profiles at the two chambers. The litter–soil interfaces are marked with a dashed line. The y-axis is in logarithmic scale.

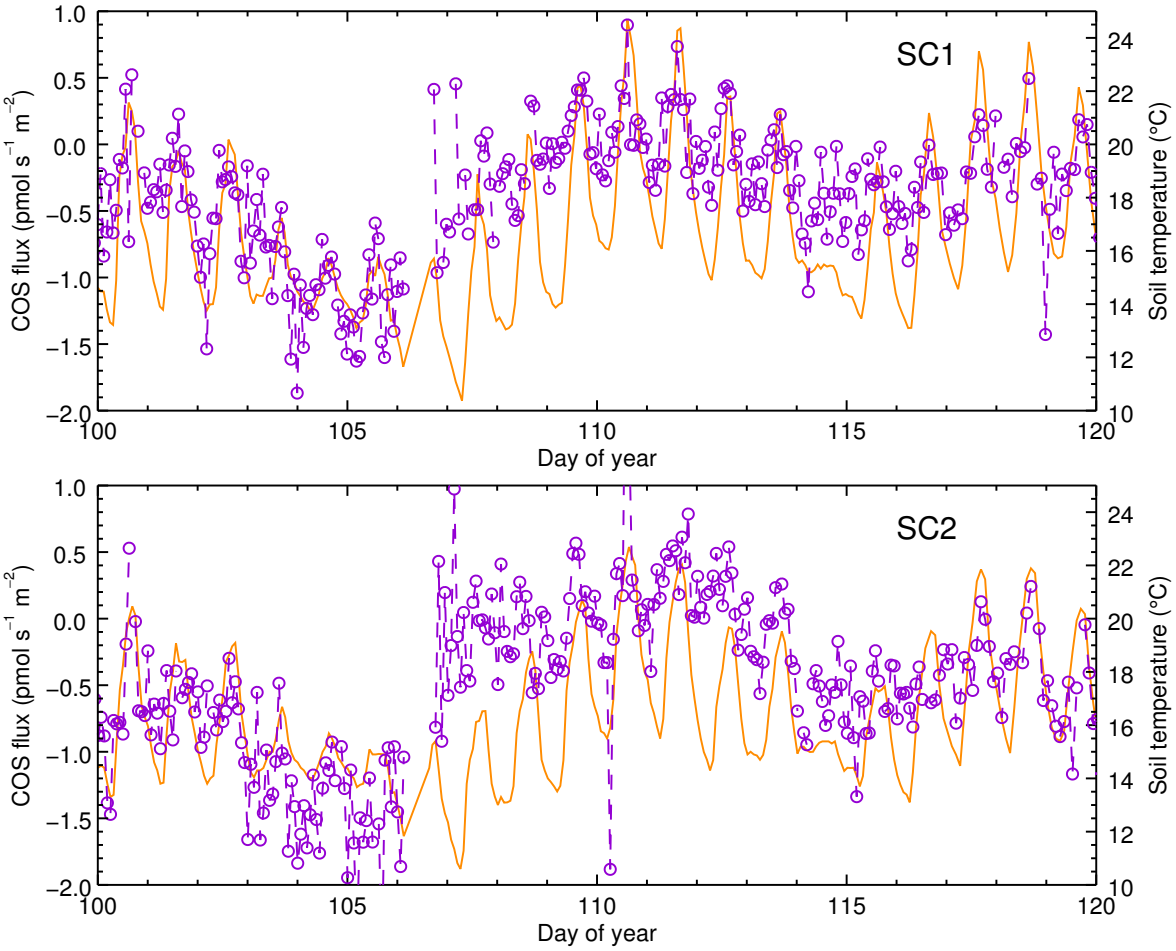

Figure 3.19: The transient increase in net surface COS uptake (purple dots) during dry conditions between DOY 103 and 106 was mainly caused by reduced COS production due to lower soil temperature (orange lines).

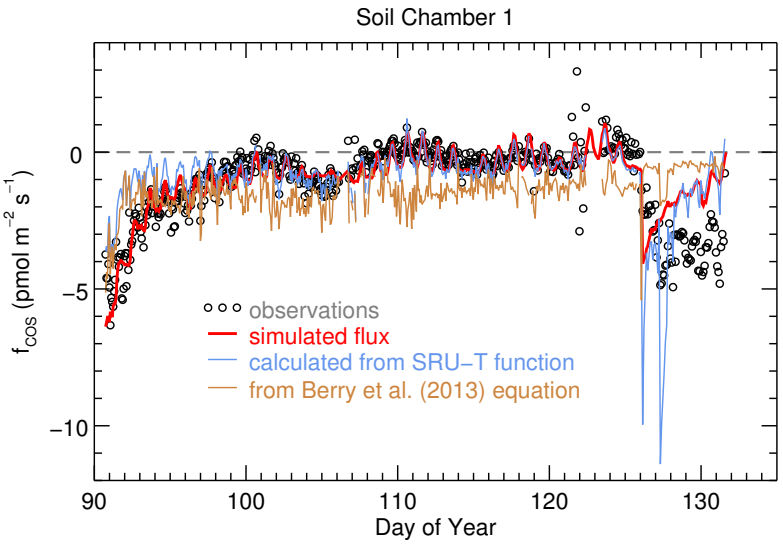

Figure 3.20: Observations (black) and model results (red) for chamber 1 compared with estimates from two empirical relationships used to calculate soil COS uptake: based on heterotrophic respiration, a WFPS dependence function, and a proportionality factor linking the COS to the CO_2 flux, here 4 pmol COS µmol^{-1} CO_2 [*Berry et al.*, 2013] (brown), and based on a function which links the concentration-normalized ratio of COS to CO_2 flux (soil uptake ratio, SRU) to soil temperature [*Berkelhammer et al.*, 2014] (blue). Here, a linear SRU–T function was used (see Figure 3.17).

Table 3.8: List of variables and parameters.

	Value and unit	Description	Reference
Physical and biological constants			
T_{ref}	298.15 K	Reference temperature	
R	8.3145 J K^{-1} mol^{-1}	Universal gas constant	
$k_{\mathrm{H,C}}(T)$	dimensionless	Henry's law constant of CO_2	*Weiss* [1974]
$k_{\mathrm{H,S}}(T)$	dimensionless	Henry's law constant of COS	*Sun et al.* [2015]; *Elliott et al.* [1989]
K_{m}	1.9 mol m^{-3}	Michaelis–Menten constant for COS hydrolysis by carbonic anhydrase	*Ogawa et al.* [2013]
Soil and litter properties			
θ_{a}	m^3 m^{-3}	Volumetric air content	
θ_{w}	m^3 m^{-3}	Volumetric water content	
θ_{sat}	0.35 m^3 m^{-3}	Soil porosity	This study
	0.94 m^3 m^{-3}	Litter porosity	This study
T	K	Soil temperature	
T_{S}	K	Slow varying component of soil temperature	

continued on the next page

continued from the previous page

	Value and unit	Description	Reference
T_F	K	Fast varying component of soil temperature	
T_L	K	Litter temperature	
w_L	g g^{-1}	Litter water content	
z_T	m	Damping depth for diurnal temperature waves	This study
α	m^2 s^{-1}	Soil thermal diffusivity	*Peters-Lidard et al.* [1998]; *Johansen* [1975]
Chamber mass balance calculation			
C	mol m^{-3}	Chamber concentration of the gas being measured	
V	m^3	Chamber volume	
A	m^2	Chamber-covered surface area	
f	mol s^{-1}	Flow rate	
F	mol m^{-2} s^{-1}	Flux rate of the gas	
C_{in}	mol m^{-3}	Sampling inlet concentration	
C_{out}	mol m^{-3}	Sampling outlet concentration	
C_a	mol m^{-3}	Ambient concentration	
Fluxes and model parameters			
F_{SL}	pmol s^{-1} kg^{-1} litter dry weight	COS fluxes from litter incubation	

continued on the next page

continued from the previous page

	Value and unit	Description	Reference
F_{CL}	μmol s^{-1} kg^{-1} litter dry weight	CO_2 fluxes from litter incubation	
$C_{S,a}$	mol m^{-3}	COS concentration in air	
$C_{C,a}$	mol m^{-3}	CO_2 concentration in air	
$V_{SLU,max}$	2.818×10^{-5} m^3 s^{-1} kg^{-1} dry weight	Litter COS uptake capacity, per unit dry weight	Regression model
$V_{SLP,max}$	0.4247 pmol s^{-1} kg^{-1} dry weight	Litter COS production capacity, per unit dry weight	Regression model
$V_{CLP,max}$	5.651×10^{-2} μmol s^{-1} kg^{-1} dry weight	Litter CO_2 production capacity, per unit dry weight	Regression model
k_{SL}	11.56	Factor for moisture dependence of litter COS uptake	Regression model
k_{CL}	15.00	Factor for moisture dependence of litter CO_2 fluxes	Regression model
E_{RL}	14.88 kJ mol^{-1}	Apparent activation energy of litter respiration	Regression model
z_D	0.2 m	Exponential decay depth of respiration	
$V_{SLU,max}$	1.68×10^{-3} mol m^{-3} s^{-1}	Litter COS uptake capacity	Converted from regression model
$V_{SLP,max}$	1.33×10^{-11} mol m^{-3} s^{-1}	Litter COS production capacity	Converted from regression model

continued on the next page

continued from the previous page

	Value and unit	Description	Reference
$V_{CLP,max}$	1.77×10^{-6} mol m^{-3} s^{-1}	Litter CO_2 production capacity	Converted from regression model
$V_{SSU,max}$	9.56×10^{-3} mol m^{-3} s^{-1}	Soil COS uptake capacity	Model optimization
$V_{SSP,max}$	1.62×10^{-11} mol m^{-3} s^{-1}	Soil COS production capacity	Model optimization
$V_{CSP,max}$	2.63×10^{-6} mol m^{-3} s^{-1} for SC1; 7.87×10^{-6} mol m^{-3} s^{-1} for SC2	Soil CO_2 production capacity	Model optimization

CHAPTER 4

Soil COS and CO fluxes in a boreal pine forest in southern Finland

4.1 Chapter introduction

Soil is a significant sink of the trace gases carbonyl sulfide (COS) and CO [*Conrad*, 1996; *Schlesinger and Bernhardt*, 2013], contributing to 26–33% of the global COS sink [*Berry et al.*, 2013; *Launois et al.*, 2015a], and 10–15% of the global CO sink [*Conrad and Seiler*, 1985; *Khalil and Rasmussen*, 1990; *King and Weber*, 2007]. In the atmosphere, COS is a major precursor to the stratospheric sulfate aerosols that exert negative radiative forcing [*Brühl et al.*, 2012; *Kremser et al.*, 2016], and CO affects concentrations of methane and other important greenhouse gases by regulating their sinks through the OH radical [*Daniel and Solomon*, 1998]. Soil fluxes influence the mean concentrations and distributions of COS and CO in the atmosphere, and consequently atmospheric chemical processes and the Earth's radiative balance.

COS participates in land carbon cycle processes due to its chemical similarities to CO_2 [*Kettle et al.*, 2002; *Montzka et al.*, 2007; *Berry et al.*, 2013]. In leaf chloroplasts and soil microbes, COS as a substrate of carbonic anhydrase is hydrolyzed irreversibly to CO_2 and H_2S [*Protoschill-Krebs and Kesselmeier*, 1992; *Protoschill-Krebs et al.*, 1996; *Stimler et al.*, 2010a, 2011; *Kesselmeier et al.*, 1999; *Saito et al.*, 2002; *Kato et al.*, 2008; *Ogawa et al.*, 2013]. The hydrolysis occurs as a side reaction of CO_2 hydration, the main function of carbonic anhydrase in living organisms [*Badger and Price*, 1994;

Henry, 1996]. Because of the irreversible COS hydrolysis in leaves, COS is taken up concurrently with CO_2 through stomata and is not emitted back from leaves [*Sandoval-Soto et al.*, 2005; *Stimler et al.*, 2010a]. This allows COS to serve as a tracer to quantify terrestrial photosynthesis independently from respiration [*Montzka et al.*, 2007; *Campbell et al.*, 2008; *Seibt et al.*, 2010; *Wohlfahrt et al.*, 2012; *Asaf et al.*, 2013; *Berry et al.*, 2013; *Billesbach et al.*, 2014; *Maseyk et al.*, 2014].

Globally, the largest COS sink is leaf uptake, followed by soil uptake [*Berry et al.*, 2013], whereas the major COS sources include ocean emissions from biogenic and photochemical processes [*Ferek and Andreae*, 1984; *Launois et al.*, 2015b], and anthropogenic emissions from industrial activities and biomass burning [*Campbell et al.*, 2015]. Since ocean COS emissions are geographically separated from the terrestrial COS sinks (leaf and soil), and anthropogenic emissions are usually concentrated as point sources, the spatial separation of dominant COS sources and sinks enables us to constrain land COS fluxes, and hence photosynthetic carbon uptake, from large-scale atmospheric COS observations [*Campbell et al.*, 2008; *Berry et al.*, 2013; *Hilton et al.*, 2015]. However, for the use of COS as a photosynthetic tracer, soil COS flux, which is unrelated to photosynthesis, needs to be understood and separated from the ecosystem COS flux that is the sum of leaf and soil fluxes [*Maseyk et al.*, 2014; *Commane et al.*, 2015; *Wehr et al.*, 2017].

Soils vary from COS sinks to sources depending on physical and biogeochemical conditions [*Maseyk et al.*, 2014; *Whelan and Rhew*, 2015; *Whelan et al.*, 2016; *Devai and DeLaune*, 1995]. Aerated upland soils are primarily weak COS sinks, whereas anoxic wetland soils are COS sources [*Whelan et al.*, 2013]. In unmanaged upland soils, the uptake rates range from 0 to 12 pmol m^{-2} s^{-1} in field studies [e.g., *Steinbacher et al.*, 2004; *Yi et al.*, 2007; *Berkelhammer et al.*, 2014]. Soil COS uptake depends nonlinearly on soil temperature and moisture, with optimal conditions that maximize the uptake [*Kesselmeier et al.*, 1999; *Van Diest and Kesselmeier*, 2008; *Whelan et al.*, 2016]. Soil COS uptake also correlates positively with soil respiration [*Yi et al.*, 2007; *Berkelhammer et al.*, 2014; *Sun et al.*, 2016], suggesting a link through microbial activity between them.

It has been assumed that soil COS flux is a minor component in the total COS budget of non-

wetland ecosystems when using COS for photosynthesis measurements [e.g., *Asaf et al.*, 2013]. However, recent discoveries defy this assumption. Strong net emissions of COS have been observed from cropland soils at high temperature [*Maseyk et al.*, 2014; *Whelan et al.*, 2016] and in an alpine grassland under solar radiation [*Kitz et al.*, 2017], highlighting the crucial role of abiotic COS production in soil COS flux. In semi-arid ecosystems, the rewetting of leaf litter after rainfall can stimulate pulses in COS uptake that temporarily overwhelm leaf COS uptake [*Sun et al.*, 2016]. Understanding factors controlling soil COS flux variability is therefore essential to the prediction of soil COS fluxes. In ecosystems where soil COS flux takes a potentially significant and variable fraction of the ecosystem COS budget, failure to account for soil COS flux may lead to significant biases in the photosynthesis estimates from the COS approach [*Whelan et al.*, 2016]. Ensuring accurate photosynthesis measurements from the COS approach requires understanding how soil COS flux is controlled by soil temperature, moisture, and biotic factors.

Soil CO flux is also the net balance between concurrent uptake and production activities [*Conrad and Seiler*, 1980, 1985; *Sanhueza et al.*, 1998; *King*, 1999; *King and Crosby*, 2002; *Bruhn et al.*, 2013; *van Asperen et al.*, 2015; *Pihlatie et al.*, 2016]. Soil CO uptake is primarily due to microbial activity [*Inman et al.*, 1971; *Conrad and Seiler*, 1980; *Whalen and Reeburgh*, 2001] and involves more diverse metabolic pathways compared with those in COS uptake [*Mörsdorf et al.*, 1992; *King and Weber*, 2007; *Ogawa et al.*, 2013]. The key environmental factors controlling CO uptake rates include soil moisture and temperature [*Conrad and Seiler*, 1985; *King*, 1999; *Yonemura et al.*, 2000a]. Similarly, there can exist an optimal condition of soil moisture and temperature that maximizes the soil CO uptake [*Moxley and Smith*, 1998; *King*, 1999], but this feature has not been evaluated extensively on different soil types. The moisture optimum can sometimes be lower than the annual soil moisture range in natural conditions [e.g., *King*, 1999], and thus may not be well defined in field observations. Soil CO uptake has also been shown to correlate with soil respiration in the laboratory (Hendrickson and Kubiseski, 1991), but such correlation is yet to be investigated in field conditions.

Soil can show net CO emissions. CO production in soils have been considered largely abiotic [*Conrad and Seiler*, 1985; *Zepp et al.*, 1997], but microbes on fine roots have also been reported to con-

tribute significant CO production in the laboratory [*King and Crosby*, 2002]. Soil CO emissions generally increases with temperature and solar radiation in field conditions [*King*, 1999; *Yonemura et al.*, 2000a; *Zepp et al.*, 1997; *van Asperen et al.*, 2015], indicating dominant contributions from photochemical and thermal production. Because most studies on soil CO flux are laboratory incubations of altered soil samples or short-term, sporadic field experiments, how environmental factors control the variability of soil CO flux in the field remain poorly understood.

In general, soil fluxes of COS and CO are controlled by gas transport in the soil column that responds to soil moisture [e.g., *Sun et al.*, 2015; *Yonemura et al.*, 2000a], and by in situ reactions including uptake and production. Both COS and CO uptake processes are mainly due to microbial activities [*Kesselmeier et al.*, 1999; *Kato et al.*, 2008; *Bartholomew and Alexander*, 1979; *Whalen and Reeburgh*, 2001] and may correlate with soil respiration through microbial activity link [*Yi et al.*, 2007; *Berkelhammer et al.*, 2014; *Hendrickson and Kubiseski*, 1991], whereas their production processes are predominantly abiotic and should respond to physical drivers. Based on previous studies, we hypothesize soil COS flux to respond to soil temperature, moisture, and microbial activity indicated by the heterotrophic respiration. Despite limited knowledge of soil CO processes, we expect similarities in the responses of soil CO flux to soil physical variables and microbial activity compared to the responses of COS flux, based on the reactive transport mechanism in the soil column [*Sun et al.*, 2015; *Ogée et al.*, 2016; *Yonemura et al.*, 2000b]. Here we report continuous field measurements of soil COS, CO, and CO_2 fluxes in a Scots pine forest in southern Finland over the late growing season. We explore diurnal and seasonal variabilities of the fluxes and identify the major physical and biological drivers of the variabilities.

4.2 Materials and methods

4.2.1 Site description

Field measurements were made at the SMEAR II site (Station for Measuring Forest Ecosystem–Atmosphere Relations) at Hyytiälä Forestry Field Station of the University of Helsinki (61.845°N, 24.288°E, 181 m above sea level). The station features a largely homogeneous stand of Scots pine (*Pinus sylvestris*) planted in 1962 [*Suni et al.*, 2003; *Vesala et al.*, 2005]. The forest floor is covered by mosses (*Dicranum polysetum*, *Hylocomium splendens*, and *Pleurozium schreberi*) and understory herbs including bilberry (*Vaccinium myrtillus*) and lingonberry (*Vaccinium vitis-idaea*) [*Kulmala et al.*, 2011]. The climate is boreal, with 30-year average January and July temperatures of −7.2°C and 16.0°C, respectively [*Pirinen et al.*, 2012]. The average annual precipitation is 711 mm, with summer and fall receiving somewhat more than winter and spring [*Pirinen et al.*, 2012]. Meteorological and ancillary data such as surface pressure, air temperature, relative humidity, radiation, precipitation, and soil temperature and moisture are continuously monitored at the SMEAR II site (see *Hari and Kulmala*, 2005 for description of the site infrastructure). These data are available online at http://avaa.tdata.fi/web/smart/smear/.

Soils at the site are podzols of depths varying from 0.5 to 1.6 m, developed from glacial deposits. The O horizon is a porous mor-humus layer laden with fine roots and mycorrhizae, distinct from the mineral soil underneath. Its thickness varies from 1 to 5 cm [*Pihlatie et al.*, 2007; *Pumpanen et al.*, 2008], bulk density is 0.10 g cm^{-3}, and porosity is 0.67 m^3 m^{-3} [*Pumpanen and Ilvesniemi*, 2005]. The O horizon is highly acidic (pH = 2.9 to 3.6) and rich in carbon content (31–45 wt%). The mineral soil underneath is of sandy loam texture, but also has a high fraction of gravels and stones [*Haataja and Vesala*, 1997]. The A horizon is 4–8 cm thick, and has the total porosity of 0.61 m^3 m^{-3} and the carbon content of 3–6 wt%. Beneath the A horizon, porosity and carbon content decrease with depth. The mineral soil is less acidic than the humus layer, with pH around 4 to 5.

4.2.2 Experimental setup

A quantum cascade laser spectrometer (QCLS, Aerodyne Research Inc., Billerica, MA, USA) was used to measure concentrations of COS, CO, CO_2, and H_2O at 1 Hz. The instrument has overall uncertainty (1 s.d.) of 7.5 ppt (parts per trillion) for COS, 3.3 ppb for CO, and 0.23 ppm for CO_2 [*Kooijmans et al.*, 2016]. An oil-free dry scroll pump (Varian TriScroll) was connected to the QCLS to pull the sampling air through the analyzer. The QCLS was housed inside a small cabin that was not air conditioned. An automatic background correction was performed every 6 hours with an ultrahigh-purity (99.99999%) nitrogen cylinder to remove the curvature effect in the baseline spectra. An air purifier (Gatekeeper CE-500K-I-4R) was used to scrub trace amounts of CO from the cylinder air. The instrument was calibrated against three working standards that had been calibrated to the NOAA or WMO scale in the laboratory [*Kooijmans et al.*, 2016].

Soil fluxes were measured in two automated soil chambers (LI-8100A-104, LI-COR Biosciences, Lincoln, NE, USA) modified to avoid COS emission artifacts from chamber materials and operated in a flow-through configuration [*Maseyk et al.*, 2014]. These modifications included replacing the chamber bowl and soil collar with stainless steel components, and removing or replacing other small COS-producing parts. Dark chambers were selected to prevent photochemical production of COS [e.g., *Whelan and Rhew*, 2015] or CO [e.g., *van Asperen et al.*, 2015] at the soil surface during chamber measurements. The two chambers were placed in similar environments, about 10 m apart. The moss layer or any other vegetation was removed to expose the humus layer inside the chambers.

The sampling system used a multi-position valve (Valco Instruments Co., Inc.) to sample each soil chamber once per hour. Air was sampled from the open chamber for 3 minutes, then the chamber was closed and the headspace air was sampled for 9–10 minutes, followed by sampling from the open chamber for 2 minutes. Soil chamber 2 was added to the sampling system on 30 July 2015. Prior to this date, soil chamber 1 was measured twice per hour.

To ensure that the chamber materials do not show apparent fluxes that bias the measurements, we conducted blank chamber tests with soil chamber 1 at the start of the campaign. The chamber footprint was sealed off with a Teflon FEP film to exclude soil fluxes and measure only the fluxes from chamber materials. We found that the apparent fluxes of CO and CO_2 from the blank chamber were 0.00 ± 0.10 nmol m^{-2} s^{-1} and -0.05 ± 0.15 µmol m^{-2} s^{-1}, respectively (Figure 4.7, Supplement), and hence were not statistically different from zero. However, we found a small positive COS flux (0.66 ± 0.48 pmol m^{-2} s^{-1}) that was statistically different from zero in a one-sample t-test (t = 3.40 and p = 0.02). We did not observe the blank chamber COS emissions to depend on temperature as in *Maseyk et al.* [2014], since daily temperature changes were small at the site. Because the same chamber was previously used at a site with strong diurnal temperature variations but did not show temperature-dependent COS emissions [*Sun et al.*, 2016], we assumed the blank chamber COS flux to be constant throughout the campaign period. We therefore subtracted the mean blank chamber COS flux from the measured COS fluxes in both chambers, and included the uncertainty term from the blank chamber COS flux. In doing so, we also assumed soil chamber 2 to have the same blank chamber COS flux as soil chamber 1, since the chamber materials were the same.

The tubing connecting the chambers to the QCLS (Synflex 1/4″) was flushed continuously to minimize wall effects for the sampled gases. The segment of inlet tubing inside the chambers was perforated to enhance the mixing of chamber air. The outlet tubing was pushed into the center of the chamber bowl, with a filter attached to it. Airflow into the chambers was provided by a diaphragm pump (KNF N811) with inlet at 0.5 m height in the vicinity of the chambers. The air flowing through the pump did not show enhanced COS or CO concentrations. The flow rates into the chambers were set to 1.5 standard liter per minute (slm) before, and 2.1 slm after 19 August 2015. Flow rates at the chambers, and pressure and flow rate at the pump inlet were checked during regular site visits. To correct for drifts, we interpolated the time series of chamber flow rate linearly from a set of discrete field measurements, including the measured flow rate values and the estimated values derived from linear correlations with pump flow rates and inlet pressure. The residence time of the air in the chamber was 3–4 minutes, as calculated from the chamber

effective volume (6.1 L) and the flow rate.

In flow-through chambers, any imbalance between inlet and outlet flows creates pressurization in the chamber headspace that drives vertical advection in the soil column, leading to biases in measured fluxes [*Lund et al.*, 1999]. For soil fluxes, underpressure seems more problematic than overpressure, because it would siphon up the soil pore air that is usually enriched in CO_2 by a few orders of magnitude. To prevent pressure-related flux biases, we set the inlet flow slightly higher than the outlet flow, with the small residual flow (approx 0.1 slm) equilibrated through the vent at the top of the chamber [*Xu et al.*, 2006]. The residual flow that was dissipated would not affect the mass balance calculation, because flux values were always calculated using the flow rates measured at the inlet.

4.2.3 Flux calculation

Fluxes were calculated from the mass balance equation of chamber headspace concentrations during chamber closure. Assuming the chamber air is well mixed, the rate of change of headspace concentration of a gas species is the balance of the inlet flux, the outlet flux, and the soil flux. The inlet concentration is assumed to be the ambient concentration measured before chamber closure, and the outlet concentration is what the analyzer measures during chamber closure. We therefore obtain an equation of mass balance in the chamber,

$$V\frac{\mathrm{d}C}{\mathrm{d}t} = q(C_\mathrm{a} - C) + FA \tag{4.1}$$

where C [mol m^{-3}] is the chamber headspace concentration, C_a [mol m^{-3}] is the ambient concentration, q [m^3 s^{-1}] is the inlet flow rate, V [m^3] and A [m^2] are the chamber volume and footprint area, respectively, and F [mol m^{-2} s^{-1}] is the flux rate to determine. By solving the differential equation of mass balance, the soil flux rate F is then obtained from least square fit of the chamber headspace concentration versus time.

We implemented a baseline correction to account for changes in ambient concentrations during chamber closure and instrument drift. The inlet concentration was interpolated between the two opening periods before and after chamber closure. This zero-flux baseline was subtracted from chamber concentrations before calculating the flux from least square fitting. Some measurement periods had wavelike noises in all measured gas concentrations, likely due to instrument instability, which prevented the calculation of reliable fluxes. Causes of the instrument instability were unclear and we did not find it to be related to condensation in the chamber. The affected flux data points were filtered out by diagnosing the concentration versus time plots, and conspicuous outliers were also removed (Table 4.3, Supplement).

4.2.4 Treatment of soil moisture data

Soil moisture data were measured with the Campbell TDR100 time-domain reflector (Campbell Scientific, Logan, UT, USA) and provided by the SMEAR II database. Sensors were in close proximity to the chambers ($\sim$ 5 m). Since soil moisture measurements were associated with high-frequency random noises, we ran a Savitzky–Golay filter with a one-day window to smooth them while retaining the daily trends. After early September 2015, soil moisture measurements had frequent gaps. A more complete time series was available from soil profile measurements about 30 m north from the chamber site. Soil A horizon moisture at this site in August was highly correlated with both the A horizon ($r^2 = 0.88$) and humus layer ($r^2 = 0.93$) moisture measurements near the chambers. We reconstructed the missing measurements at our soil plots from the linear regressions using August data. The gapfilled soil moisture data of both layers generally agreed well with the intermittent measurements during that period (RMSE = 0.042 $m^3\ m^{-3}$ for the humus layer and 0.015 $m^3\ m^{-3}$ for the A horizon, respectively).

4.2.5 Statistical analysis

To extract smooth patterns of temperature and moisture dependence of soil fluxes, we ran a 2D local regression (LOESS) on COS, CO, and CO_2 fluxes against humus layer temperature and moisture (predictors). Unlike linear regression, LOESS is a non-parametric method that does not require any analytical expression of the underlying relationships. At each data point, a low-degree polynomial is fitted to all its neighboring points, weighted by distances, to give a smoothed estimate at the current point [*Cleveland et al.*, 1992].

Table 4.1: A statistical summary of fluxes from the two soil chambers.

	mean	s.d.	1st qtl.	median	3rd qtl.	Jun/Jul mean	Aug mean	Sep mean	Oct/Nov mean
SC1									
F_{COS} (pmol m^{-2} s^{-1})	−2.83	1.01	−3.38	−2.75	−2.17	−2.55	−2.74	−3.25	−3.76
F_{CO} (nmol m^{-2} s^{-1})	−1.00	0.43	−1.27	−0.93	−0.69	−0.78	−1.02	−1.39	−1.18
F_{CO_2} (µmol m^{-2} s^{-1})	3.18	1.29	2.29	3.12	4.02	2.97	4.13	3.23	1.10
SC2									
F_{COS} (pmol m^{-2} s^{-1})	−2.47	1.18	−3.12	−2.38	−1.75	n/a	−2.15	−2.80	−2.79
F_{CO} (nmol m^{-2} s^{-1})	−0.76	0.43	−1.01	−0.69	−0.44	n/a	−0.64	−0.94	−0.72
F_{CO_2} (µmol m^{-2} s^{-1})	3.84	1.92	2.42	3.58	5.23	n/a	3.73	5.12	1.94

4.3 Results

4.3.1 COS flux

Soils in both chambers behaved as COS sinks, with average fluxes of −2.8 (± 1.0) and −2.5 (± 1.2) pmol m^{-2} s^{-1} for SC1 and SC2, respectively (Figure 4.1; Table 4.1). The two chambers exhibited

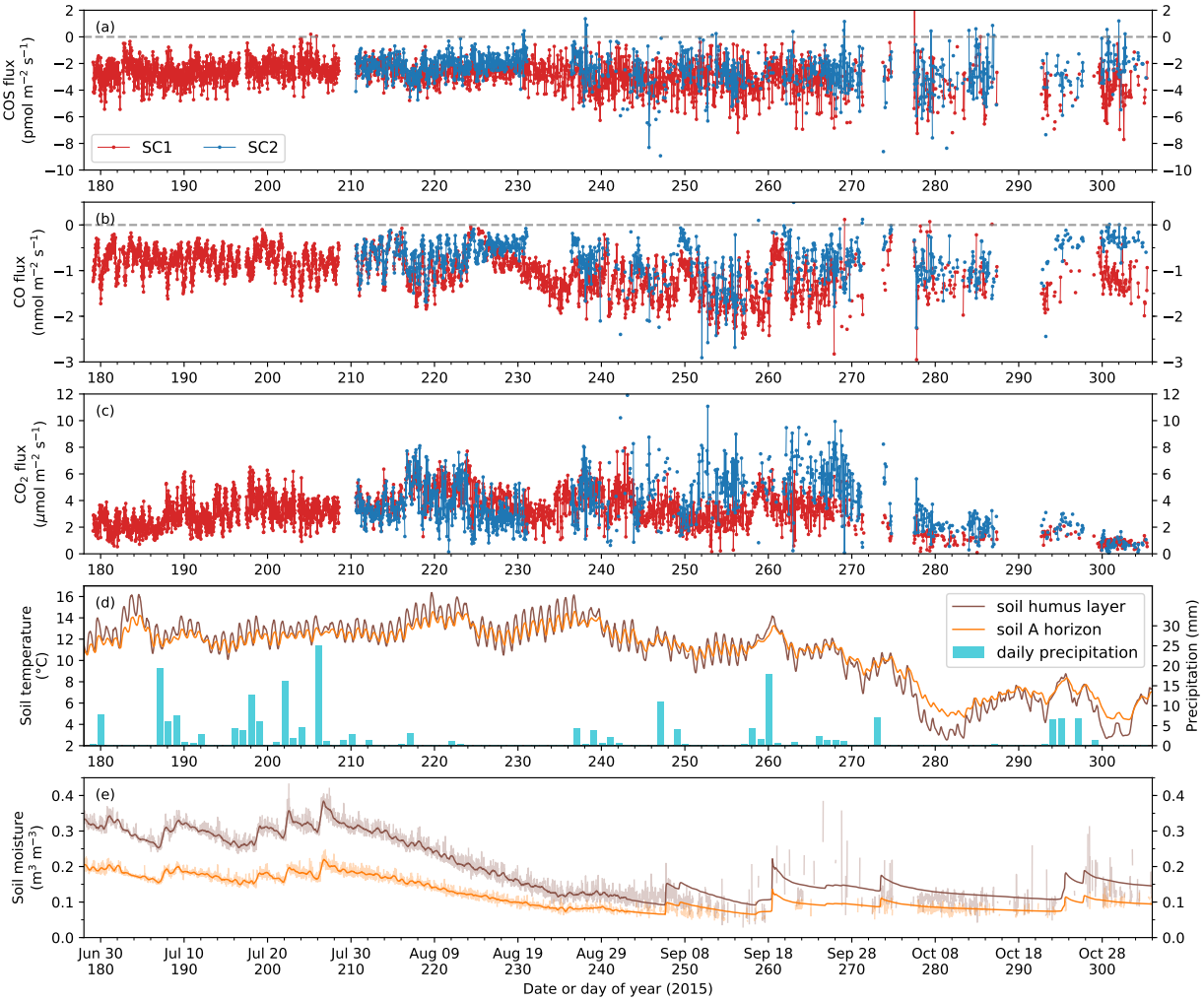

Figure 4.1: Soil fluxes of (a) COS, (b) CO, and (c) CO_2 from two chambers in a pine forest in southern Finland in summer and fall 2015. Also shown are (d) soil humus layer (1 to 5 cm) and A horizon (2 to 5 cm below the humus layer) temperatures (lines) and daily precipitation (bar plot), and (e) gapfilled and smoothed soil moistures in the humus layer and A horizon. Frequent gaps in raw soil moisture data (shown in transparent colors) from September 2015 onwards were gapfilled (solid lines) based on the correlation with soil moisture from a nearby location (see Sect. 4.2.4 for details).

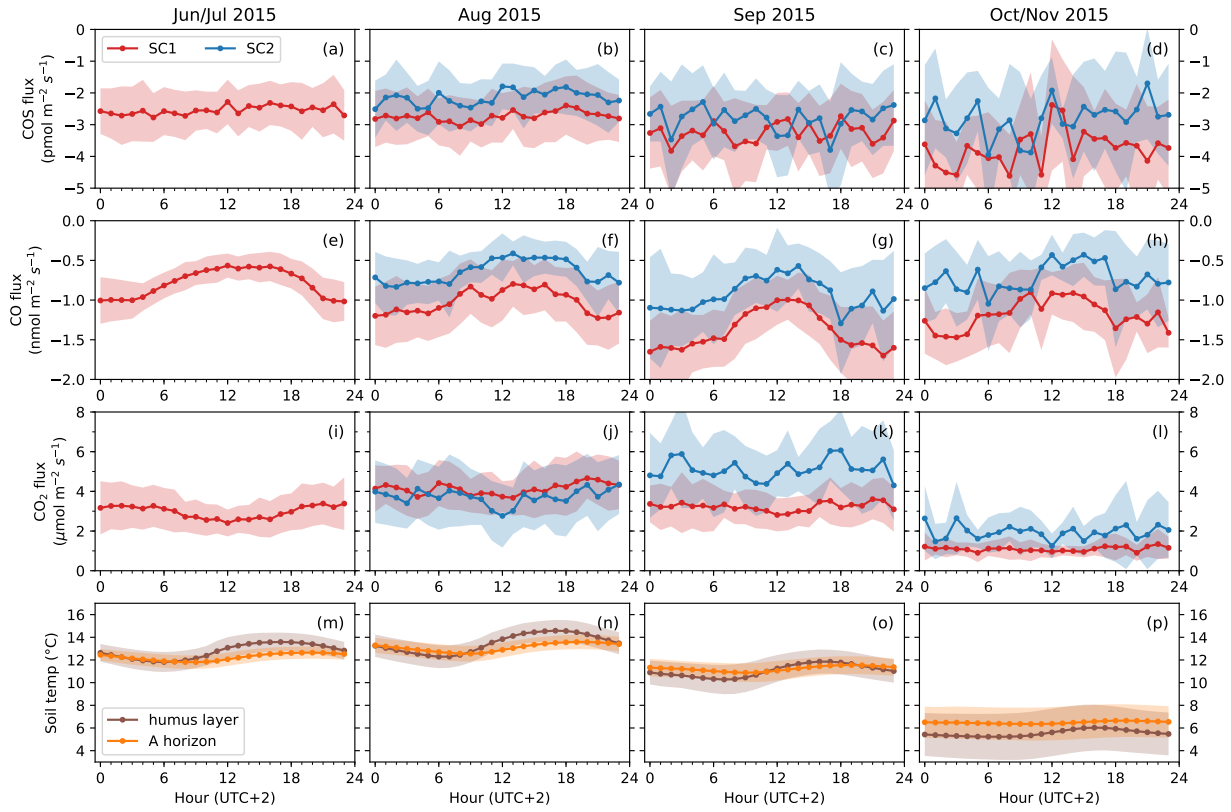

Figure 4.2: Monthly-mean diurnal trends of soil chamber fluxes of COS (a–d), CO (e–h), and CO_2 (i–l), and temperature in the humus layer and in the A horizon (m–p), averaged in one-hour bins. The x-axes are local winter time (UTC+2). Red and blue curves are mean diurnal trends of SC1 and SC2, respectively (a–l). Brown and orange represent temperature in the humus layer and in the A horizon, respectively (m–p). All shaded areas indicate standard deviations (± 1 s.d.). Note that for soil temperature the y-axis ranges change by month. The July 2015 subset includes two days of data from June, and the October 2015 subset includes two days from November.

broadly similar patterns of COS fluxes (Figures 4.1a and 4.2a–d). COS emissions happened rarely, accounting for only 0.1% cases of SC1 and 1.5% cases of SC2, respectively. Most emission cases were not statistically different from zero, and the few large emissions appeared to be transient and isolated cases unrelated to temperature or moisture change. Overall, soil COS fluxes at this site were comparable to reported values in similar ecosystems, for example, -2.5 pmol m^{-2} s^{-1} from a Swedish boreal forest soil in *Simmons et al.* [1999].

There was a weak increasing trend in soil COS uptake (or decreasing net COS flux) throughout the campaign (Table 4.1). This increasing trend was not significant during the peak growing months (July and August), but became stronger towards the end of the growing season (September and October). Such trend in COS uptake appeared to coincide with the decreasing trends in soil temperature and moisture (Figure 4.1d, e). However, soil COS uptake in October might have been affected by more frequent instrument instabilities (Sect. 4.2.3) and power outages, and likely had larger uncertainty than other periods.

No significant diurnal trend was observed in COS fluxes (Figure 4.2a–d), although surface (0.5 m) COS concentration often changed from around 300 pmol mol^{-1} at night to 400 pmol mol^{-1} at midday. Interesting, we found no correlation between COS fluxes and ambient COS concentrations ($r = 0.005$; Figure 4.8, Supplement), indicating that COS uptake was not concentration limited at the daily timescale. The deposition velocity of COS (uptake normalized by concentration) showed weak diurnal variability (Figure 4.3a, b), as a result of the depleted canopy COS concentration at night due to the stable boundary layer conditions and nocturnal canopy COS uptake [*Kooijmans et al.*, 2017].

Smoothed 2D patterns of soil COS uptake as a function of soil temperature and moisture were constructed with the LOESS method (Sect. 4.2.5). Soil moisture rather than temperature was the dominant physical driver of soil COS uptake, with uptake rates decreasing with increasing moisture (Figure 4.4a). There was only a weak tendency of increasing COS uptake with decreasing temperature. Soil COS uptake was positively correlated with soil respiration (Figure 4.5), consis-

tent with previous observations [*Yi et al.*, 2007; *Berkelhammer et al.*, 2014; *Sun et al.*, 2016]. However, the relationship between soil COS uptake and respiration seemed to divide into different branches delimited by soil temperature bins (Figure 4.5).

4.3.2 CO flux

CO was also taken up by soils in both chambers, with average fluxes of −1.00 (± 0.43) and −0.76 (± 0.43) nmol m^{-2} s^{-1} in SC1 and SC2, respectively (Table 4.1). Although the two chambers were placed in similar conditions, SC1 always had slightly stronger uptake than SC2, indicating small scale heterogeneity. Both chambers had only a few and very weak CO emission cases (0.1% of SC1 and 0.5% of SC2).

In contrast to soil COS flux, there was clear diurnal variability in CO flux, consistent across all months (Figure 4.2). CO uptake was significantly lower during the daytime than at night, with up to 0.5 nmol m^{-2} s^{-1} difference (30–50% of nighttime CO uptake). We found weak correlations between soil CO flux and ambient CO concentration ($r = -0.590$ and -0.317 for SC1 and SC2, respectively, Table 4.2; Figure 4.8, Supplement). However, the relative diurnal amplitudes of CO concentration were too small (less than 10% in monthly-mean diurnal trends; not shown) to explain the diurnal variability in CO uptake. Significant diurnal variability was also present in CO deposition velocity (Figure 4.3c, d), with the midday values about 40% smaller than those around midnight. This further supported that the diurnal variability in CO uptake was not driven by ambient CO concentration. The diurnal variability in CO uptake was also unrelated to soil temperature, since it was out of phase with soil temperature variations (Figure 4.2). Instead, CO uptake was weakly correlated with the below-canopy radiation (rank correlation = 0.51 and 0.35 for SC1 and SC2, respectively; Figure 4.12, Supplement), which varied diurnally, suggesting that the midday reduction in CO uptake might be partially due to photochemical CO production at the soil surface.

During the campaign period, soil CO uptake was the highest in September compared with other months (Table 4.1; Figure 4.2). The increase of CO uptake in September appeared to result from the decrease of soil moisture rather than changes in soil temperature (Figure 4.4). CO uptake was also weakly correlated with CO_2 flux (Figure 4.5; Table 4.2), branching into different clusters depending on temperature bins. Such pattern resembled the relationship between COS and CO_2 fluxes (Figure 4.5).

4.3.3 CO_2 flux

The average CO_2 fluxes during the campaign period were 3.2 (± 1.3) and 3.8 (± 1.9) μmol m^{-2} s^{-1} for SC1 and SC2, respectively. Soil respiration showed strong seasonal variations that correlated with soil temperature changes (Table 4.2 and Figure 4.4; Figures 4.9 and 4.10, Supplement). Monthly mean soil respiration in SC1 increased from 3.0 μmol m^{-2} s^{-1} in July to 4.1 μmol m^{-2} s^{-1} in August, the warmest month. As soil temperature began to decrease in September, soil respiration dropped to 3.2 μmol m^{-2} s^{-1} in SC1 but increased in SC2, indicating possible small-scale differences between the two chamber locations. There was no well-defined relationship between soil moisture and respiration (Figure 4.4).

We did not see strong temperature-driven diurnal trends in soil respiration (Figure 4.2), mainly because daily temperature variations were small (2–3°C diurnal amplitude in the humus layer). Temperature dependence of soil respiration at the daily timescale was generally weak since most of the days had low correlations between CO_2 flux and temperature (see Figure 4.14, Supplement for a histogram of the corresponding daily r^2-values), despite the correlation between soil respiration and temperature over the campaign period. Interestingly, a small decrease in respiration at midday was found in the July diurnal trend of CO_2 flux in SC1 (Figure 4.2i). Daytime CO_2 flux in July was on average 0.44 μmol m^{-2} s^{-1} lower than nighttime CO_2 flux, and such difference was statistically significant ($p = 1 \times 10^{-8}$ in a two-sample t-test). The slightly higher nighttime respiration in July might be related with A horizon temperature that peaked at midnight. Other

months did not see such pattern.

Figure 4.3: Monthly-mean diurnal trends of apparent deposition velocities of COS and CO ($-F_{COS}/[COS]_{0.5\,m}$ and $-F_{CO}/[CO]_{0.5\,m}$) in the two chambers, averaged in one-hour bins. Different monthly periods are color-coded.

4.4 Discussion

4.4.1 Physical and biological factors controlling COS and CO fluxes

The net soil flux of COS or CO is generally the balance of concurrent sink and source activities. Here we explore how physical and biological factors drive the variability in the net fluxes of COS

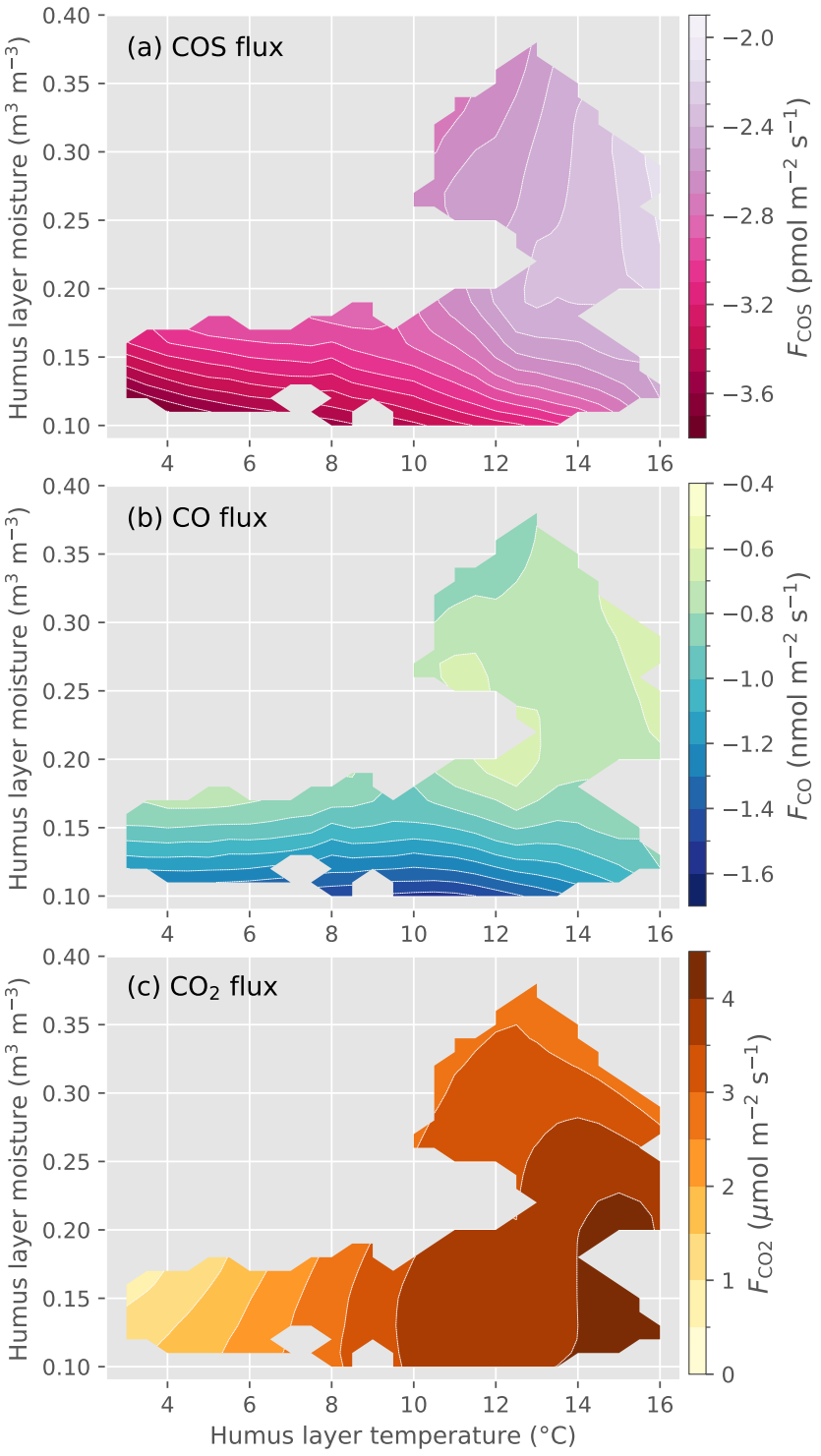

Figure 4.4: Smoothed patterns of soil COS (a), CO (b) and CO_2 (c) fluxes as functions of soil humus layer temperature and moisture, constructed using 2D local regression. Darker colors indicate stronger COS or CO uptake, or stronger CO_2 emission.

Table 4.2: Pearson correlations between fluxes and environmental variables for the two soil chambers. $T_{soil,O}$ and $T_{soil,A}$ are soil temperatures in the humus layer and in the A horizon, respectively. Similarly, $w_{soil,O}$ and $w_{soil,A}$ are soil moistures ($m^3\ m^{-3}$) in the humus layer and in the A horizon.

	COS ($pmol\ mol^{-1}$)	CO ($nmol\ mol^{-1}$)	$T_{soil,O}$ (°C)	$T_{soil,A}$ (°C)	$w_{soil,O}$ ($m^3\ m^{-3}$)	$w_{soil,A}$ ($m^3\ m^{-3}$)	F_{CO_2} ($\mu mol\ m^{-2}\ s^{-1}$)
SC1							
F_{COS} ($pmol\ m^{-2}\ s^{-1}$)	0.022	−0.096	0.327	0.307	0.308	0.293	−0.212
F_{CO} ($nmol\ m^{-2}\ s^{-1}$)	0.592†	−0.590	0.254	0.180	0.560	0.555	−0.205
F_{CO_2} ($\mu mol\ m^{-2}\ s^{-1}$)	−0.204	0.249	0.462	0.524	−0.007	−0.033	1
SC2							
F_{COS} ($pmol\ m^{-2}\ s^{-1}$)	0.019	−0.060	0.163	0.161	0.184	0.178	−0.491
F_{CO} ($nmol\ m^{-2}\ s^{-1}$)	0.531	−0.317	0.075	0.041	0.231	0.226	−0.474
F_{CO_2} ($\mu mol\ m^{-2}\ s^{-1}$)	−0.223	0.373	0.388	0.399	−0.041	−0.038	1

† For pairs which we do not expect an underlying mechanistic reason for their correlations, for example, CO flux and COS concentration, the correlation values are underlined.

and CO, and infer their effects on the gross uptake of COS and CO.

Soil moisture is the key determinant of the net soil COS flux (Figure 4.4a). Since COS production is controlled mainly by temperature [*Whelan et al.*, 2016], the absence of temperature-driven diurnal variability in COS flux (Figure 4.2a–d) indicates that COS production, if present at all, was likely a minor component. Hence, the observed soil moisture dependence of COS flux should result from the variability in gross COS uptake not COS production. The moisture dependence of COS uptake activity typically manifests as a bell-shaped curve with a moisture optimum [*Kesselmeier et al.*, 1999; *Van Diest and Kesselmeier*, 2008; *Whelan et al.*, 2016]. Below the moisture optimum, microbial uptake of COS is limited by water availability, whereas above it, COS uptake is limited by the diffusional supply of COS from the atmosphere because soil gas diffusivity decreases with moisture content [*Sun et al.*, 2015; *Ogée et al.*, 2016]. In this study, the decrease of COS uptake with increasing soil moisture (Figure 4.4a) is characteristic of the diffusion-limited regime in COS uptake. The diffusion-limited regime indicates that the moisture optimum for COS uptake was likely below the observed soil moisture range and that most COS uptake happened beneath the surface humus layer.

There is only a weak tendency of decreasing net COS uptake with increasing temperature (Figure 4.4a). The lack of strong temperature dependence is not surprising given that 90% of the data were measured in the narrow temperature range of 8.3–16.4°C (humus layer). A temperature optimum for COS uptake cannot be identified within the observed temperature range, but likely exists below this range since COS uptake tends to increase slightly with decreasing temperature (Figure 4.4a). The low temperature optimum would differ from previous laboratory studies that report temperature optimum values of around 20° [*Kesselmeier et al.*, 1999; *Van Diest and Kesselmeier*, 2008], suggesting a need to constrain such parameter under field conditions.

Soil CO flux variability is also dominated by moisture dependence and did not show any significant temperature dependence (Figure 4.4b). Previous studies show that the moisture dependence of CO uptake also follows a bell-shaped curve with a moisture optimum, which qualitatively re-

sembles that of soil COS uptake [*Moxley and Smith*, 1998; *King*, 1999]. Because CO uptake in the soil is subject to the same reactive transport mechanism as in COS uptake, the decrease of CO uptake with increasing soil moisture indicates that CO uptake was also diffusion-limited and the majority of uptake activity should happen below the surface humus layer. The absence of temperature-driven variability in net CO uptake suggests the lack of significant abiotic thermal production of CO, yet other production activity may still exist.

A unique feature of soil CO flux is the diurnal cycle showing reduced daytime net uptake (Figure 4.2e–h), contrasting with soil COS flux that shows no significant diurnal variability. The correlation between CO uptake and below-canopy radiation (Sect. 4.3.2; Figure 4.8, Supplement) implies that there might be photochemical production at the surface humus layer during the campaign. Although opaque chambers were used to prevent photochemical production of CO during measurements (Sect. 4.2.2), when the chamber was open and not being measured, the soil surface was exposed in the sun and photochemical production might happen. CO production at the surface, if present, may alter the vertical CO profile and consequently affects surface flux measurements, because gas transport in the soil column is a slow process. Strong diurnal variability in soil CO flux due to photochemical production has previously been reported in a boreal forest [*Zepp et al.*, 1997], a temperate mixedwood plain [*Constant et al.*, 2008], and a reed canary grass cropland [*Pihlatie et al.*, 2016]. Hence, photochemical production is a possible daytime source of CO that can be responsible for the diurnal cycle of net CO flux. Future studies on soil CO flux will need to operate the chamber in constant darkness to confirm or falsify the existence of photochemical CO production.

Both COS and CO fluxes appear to correlate well with soil respiration when divided into specific temperature bins (Figure 4.5). To characterize the sensitivities of COS and CO fluxes to respiration, mean flux ratios ($F_{COS} : F_{CO_2}$ and $F_{CO} : F_{CO_2}$) are calculated in each temperature bin, approximated by the slope of no-intercept linear regression (Figure 4.6). The sensitivity of COS or CO uptake to respiration is stronger at lower temperature, as indicated by the more negative $F_{COS} : F_{CO_2}$ or $F_{CO} : F_{CO_2}$ ratio (Figure 4.6). The asymptotic nature of the temperature dependence

of $F_{COS} : F_{CO_2}$ ratio corresponds well with that of the concentration-normalized COS to CO_2 flux ratio (termed the soil uptake ratio, SRU, which differs from the flux ratio by a factor of 1 to 1.15) reported from a temperate forest [*Berkelhammer et al.*, 2014]. This suggests that the temperature dependence of the $F_{COS} : F_{CO_2}$ ratio can be a generalizable feature for soils. Interestingly, the transition from linear increase to constant ratio occurs around 10°C at our site (Figure 4.6) compared to 30°C in the temperate sites, indicating a soil or site-specific feature for further investigation. The newly discovered relationship between the $F_{CO} : F_{CO_2}$ ratio and temperature can be used to simulate soil CO uptake empirically.

Why does the relationship between COS or CO uptake and respiration divide into different branches defined by soil temperature (Figure 4.5), despite that COS or CO uptake itself does not show strong temperature dependence (Figure 4.4)? Since microbial activity underpins COS or CO uptake, each branch in the uptake–respiration pattern may represent the behavior of a distinct microbial group. The temperature dependence of flux ratios hence may indicate shifts in active COS and CO-consuming microbial groups caused by temperature. For example, microbial groups that have optimal uptake at a lower temperature may have a stronger sensitivity of COS (or CO) uptake to respiration than groups active at higher temperature. The asymptote values of $F_{COS} : F_{CO_2}$ and $F_{CO} : F_{CO_2}$ (Figure 4.6) hence would reflect the uptake to respiration sensitivity behavior of microbial groups active at higher temperature. Collectively, the sum of COS uptake (or CO uptake) contributions from the ensemble of microbial groups may not show a well-defined temperature response like that in respiration. Although we cannot rule out the possibility that the flux ratio vs. temperature pattern is influenced by divergent temperature responses of microbial uptake and abiotic production [e.g., *Whelan et al.*, 2016; *King*, 1999; *van Asperen et al.*, 2015], abiotic production is unlikely to correlate with respiration. A mechanistic explanation for the temperature dependence of flux ratios requires a clear-cut separation of uptake and production processes and further understanding on the microbial communities involved in COS uptake or CO uptake.

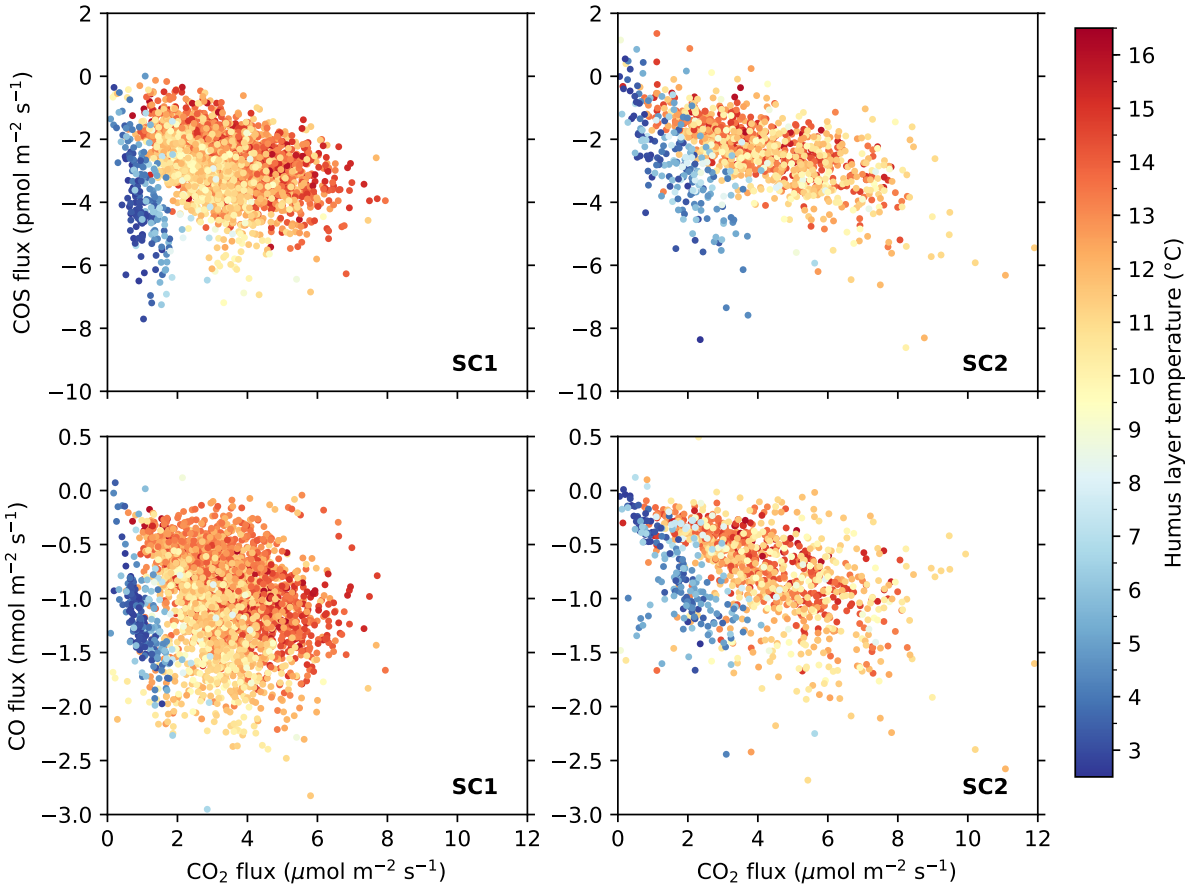

Figure 4.5: Relationships between COS and CO_2 fluxes (top row) and that between CO and CO_2 fluxes (bottom row). The slopes are modulated by soil humus layer temperatures (colored).

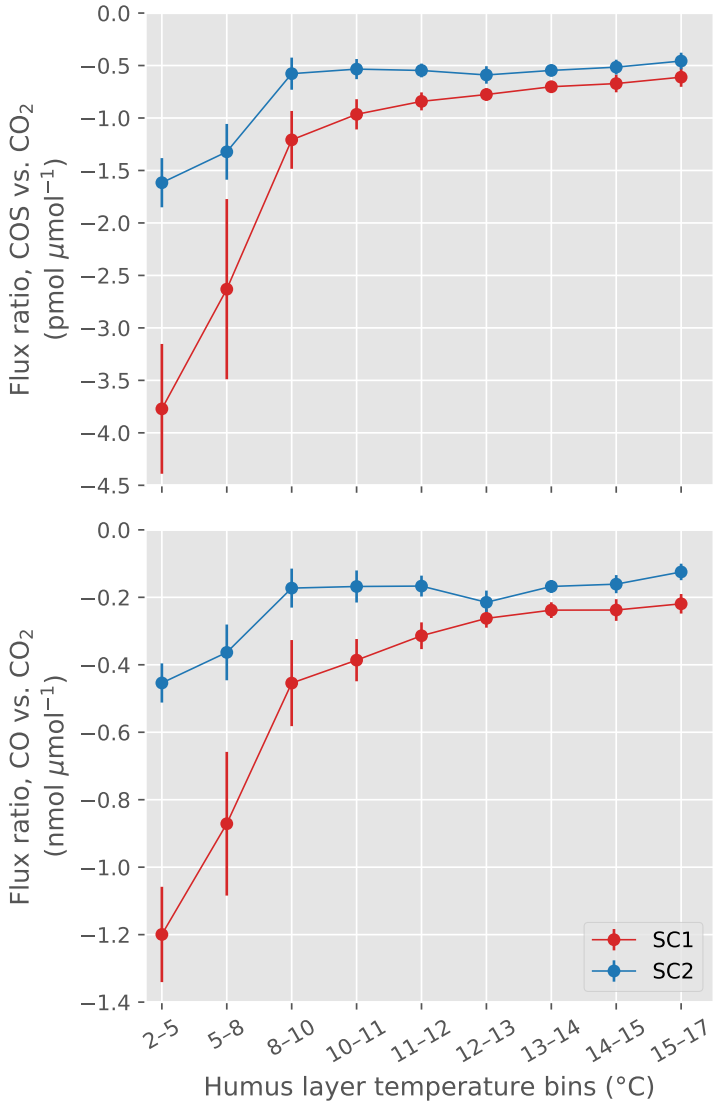

Figure 4.6: Ratios of COS vs. CO_2 and CO vs. CO_2 fluxes determined from no-intercept linear regressions across soil temperature bins. Error bars are showing ± 2 standard errors (or 95.5% C.I.). Flux ratios are generally smaller in SC2 because of higher CO_2 fluxes.

4.4.2 Variations of soil fluxes over the late growing season

Neither COS flux nor CO flux exhibits strong seasonality, mainly because soil temperature variation was not strong and soil moisture was not low enough to severely limit microbial activity. For example, *Whelan et al.* [2016] has shown that COS uptake is inhibited when soil moisture is below around 0.10 m^3 m^{-3} in incubation experiments, yet in this campaign soil moisture was above this threshold most of the time. From August to October, monthly mean net soil uptake of COS increased slightly from 2.7 to 3.8 pmol m^{-2} s^{-1}, and that of CO increased from 1.0 to 1.2 nmol m^{-2} s^{-1}, despite a significant drop in humus layer temperature from 13.5 to 5.5°C. As discussed previously, the increase was due to increased gas diffusivity caused by declining soil moisture. Soil microbial activities for COS and CO uptake at this site appeared tolerant of low temperature at the end of the growing season. Given the lack of temperature-related seasonality in COS or CO uptake, it is possible that a shift in active microbial groups might have acted to stabilize the overall uptake against changes in soil physical variables.

Soil respiration in SC1 increased significantly from July to August (3.0 to 4.1 µmol m^{-2} s^{-1}), concurrent with a slight increase in the mean soil temperature (12.8 to 13.5°C). As shown in *Pumpanen et al.* [2008], soil respiration at the site is not only controlled by temperature but also by gas diffusivity and photosynthate input from the vegetation. Since soil moisture dropped greatly after July (Figure 4.1), the increase in respiration was more likely driven by the aeration of soil than by just a slight increase in soil temperature. In early October, soil respiration was suppressed by the abrupt decrease in soil temperature, and gradually dropped to below 1 µmol m^{-2} s^{-1} (Figure 4.1). In addition, the declining ecosystem photosynthetic activity after August [*Vesala et al.*, 2010] would reduce photosynthate input to the soil, and therefore might also contribute to the decrease in respiration. However, since the soil plots in both chambers were cleared of understory vegetation before the campaign, autotrophic fraction in total soil respiration should be much smaller than soil plots with intact vegetation, and would rely on photosynthate supply from trees in a distance. The smaller contribution of autotrophic respiration is also supported by the lower August soil respiration of around 4 µmol m^{-2} s^{-1} in our campaign compared with the August soil

respiration of around 6 μmol m^{-2} s^{-1} in *Pumpanen et al.* [2015] from a vegetated area at the same site. Overall, the seasonal pattern of CO_2 flux is mainly driven by soil temperature and moisture, and to a lesser extent, photosynthate input.

4.4.3 Implications on using COS as a photosynthetic tracer

The soil at this boreal forest site (podzol) was consistently a weak sink of COS during the late growing season (July to November). Soil uptake of COS was around 8–16% of the daytime mean ecosystem uptake of about 24 pmol m^{-2} s^{-1} [*Kooijmans et al.*, 2017, with daytime defined as the period with solar elevation angle $> 20^{\circ}$ therein]. Soil COS uptake did not show strong diurnal and seasonal variations, nor did it show any abrupt increase induced by rain events [cf. *Sun et al.*, 2016; *Whelan and Rhew*, 2016]. Moreover, soil COS uptake variability was well explained by changes in soil moisture and respiration, and it would be possible to construct an empirical model for soil COS flux based on its relationship with soil moisture, temperature, and CO_2 flux (Figures 4.4 and 4.5). Hence, we expect that soil COS uptake can be reliably accounted for when using COS as a photosynthetic tracer at this site.

Since soil COS uptake did not show a well-defined response to soil temperature or moisture but correlates well with respiration when divided into specific temperature bins (Figures 4.4 and 4.5), simulating soil COS uptake in this boreal forest will rely on using soil respiration as an important statistical predictor. In this case, the parameterization scheme used in *Berry et al.* [2013] and the empirical relationship based on soil relative uptake ratio (COS uptake to CO_2 emission ratio normalized by their concentrations) as in *Berkelhammer et al.* [2014] will be useful in predicting COS uptake, provided that diffusion in the soil column is properly resolved.

4.4.4 Implications on soil–atmosphere CO exchange

The global soil CO budget remains uncertain due to limited field observations and the lack of modeling studies. Our results from the boreal forest site help bridge the gap in the understanding of soil CO exchange in this important biome. CO uptake by soil is usually characterized by the deposition velocity of CO, because ambient CO concentration varies spatially. At this site, CO deposition velocity lies in the range of 0.1–0.35 mm s^{-1} (Figure 4.3), similar to previous studies in boreal forests [*Zepp et al.*, 1997; *Kuhlbusch et al.*, 1998] and slightly less than in temperate forests [*Sanhueza et al.*, 1998; *Yonemura et al.*, 2000a]. CO deposition velocity shows a weak decreasing trend with increasing soil moisture (Figure 4.13, Supplement), which is broadly similar to the negative correlation found in *Yonemura et al.* [2000a], indicating a prominent diffusional control on CO uptake.

Globally, soils contribute to a significant but poorly constrained CO sink. The current estimate of global soil CO uptake ($\sim$ 300 Tg yr^{-1} in *King and Weber*, 2007) is equivalent to a global mean uptake of 2.3 nmol m^{-2} s^{-1}, averaged over the total land area (1.49×10^8 km^2). This global mean value is significantly higher than the mean CO uptake ($\sim$ 1 nmol m^{-2} s^{-1}) observed at this boreal forest in the late growing season. Recent field observations of soil CO uptake in temperate ecosystems are also smaller than this global mean, for example, less than 1 nmol m^{-2} s^{-1} in a grassland in Italy [*van Asperen et al.*, 2015], and 0.78 nmol m^{-2} s^{-1} in a grassland in Denmark [*Bruhn et al.*, 2013]. If we assume soil at this site is representative of boreal forest soils, it follows that temperate and tropical soils must have higher CO uptake capacity to compensate for the relatively low soil CO uptake in the boreal forest compared with the global mean, or the current estimate of global soil CO uptake needs to be revisited.

4.5 Chapter conclusion

The boreal forest soil studied here behaves consistently as a sink of COS and CO during the late growing season. Soil COS and CO uptake appear to be largely insensitive to temperature, at least within the narrow temperature (3–16°C) and moisture range (0.10–0.38 m^3 m^{-3}) at this site. In contrast to laboratory experiments, controls on fluxes can be difficult to identify in field conditions due to concurrent changes in temperature, moisture, and microbial community. We find that soil moisture is the dominant physical driver for soil COS and CO uptake, and the uptake rate generally decreases with soil moisture, suggesting that microbial uptake is limited by the diffusional supply of COS and CO into the soil column. The relationship between COS uptake and respiration and that between CO uptake and respiration are regulated by soil temperature, leading to the temperature dependence of COS : CO_2 and CO : CO_2 flux ratios. In future studies, measuring soil vertical profiles of COS and CO will help resolve the interplay between physical transport and biological uptake. Furthermore, studies on microbial dynamics are needed to shed light on the mechanisms relating COS and CO uptake with respiration.

Compared with total ecosystem uptake of COS, soil COS uptake is a small fraction (8–16%). Soil COS uptake does not show significant diurnal or long-term variability in the peak growing season (July and August), and thus will not be a dominant source of uncertainty when inferring photosynthesis from COS measurements.

Soil CO uptake shows reduced midday uptake rate and deposition velocity, possibly related to the photochemical production of CO at the surface organic layer. A comparison of soil CO uptake in this boreal forest with the estimated global mean shows that boreal forest soils have relatively low CO uptake activity. Similar studies on soil CO fluxes are needed in other biomes to better constrain the magnitude and distribution of global biosphere–atmosphere CO exchange.

4.6 Supplement

Table 4.3: Numbers of valid observations from the two chambers (SC1 and SC2).

	no. of total possible obs.			no. of missing obs.			no. of misfit obs. and outliers†			no. of valid obs.			% of valid obs.		
	SC1	SC2	both	SC1	SC2	both	SC1	SC2	both	SC1	SC2	both	SC1	SC2	both
F_{COS}	3768	1992	5760	143	98	241	549	859	1408	3076	1035	4111	81.63	51.96	71.37
F_{CO}	3768	1992	5760	143	98	241	601	870	1471	3024	1024	4048	80.25	51.41	70.28
F_{CO_2}	3768	1992	5760	143	98	241	544	868	1412	3081	1026	4107	81.77	51.51	71.30
F_{H_2O}	3768	1992	5760	143	98	241	534	854	1388	3091	1040	4131	82.03	52.21	71.72

†Misfits are measurements affected by severe instrument drift or fluctuation, whereas outliers are unusual peaks in the time series of the calculated fluxes identified from the Iglewicz–Hoaglin modified Z-score statistic.

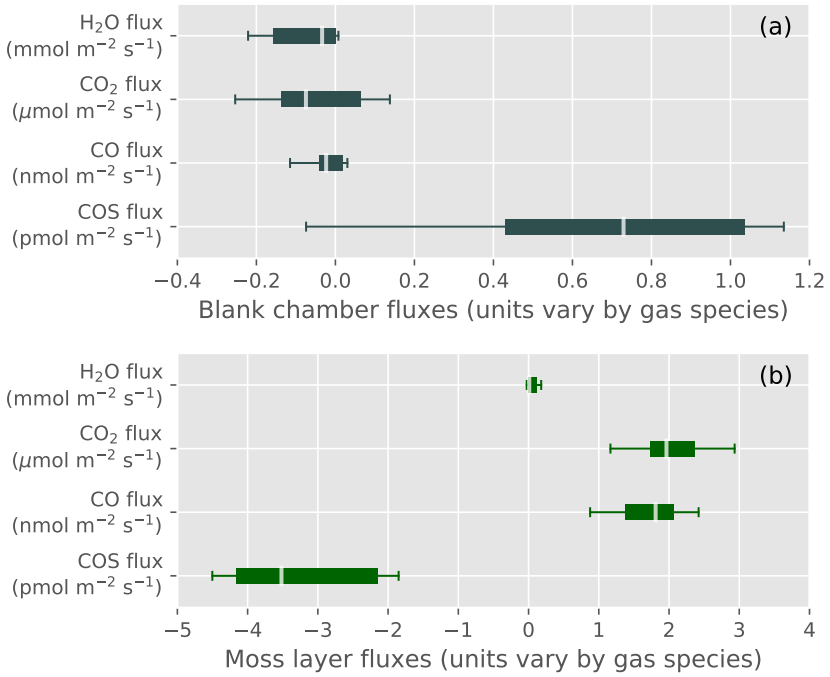

Figure 4.7: Boxplots of the fluxes of COS, CO, CO_2, and H_2O from (a) a blank chamber test for the apparent fluxes caused by chamber materials (see Sect. 4.2.2 in the main text), and from (b) an incubation of the moss layer in the field. Flux rates are normalized with respect to the chamber footprint area. For each flux term, the thin white bar marks the median value, the box represents the interquartile range, and the whiskers delimit the inlier range. Note that the units of fluxes differ by gas species, as shown on the y-axes.

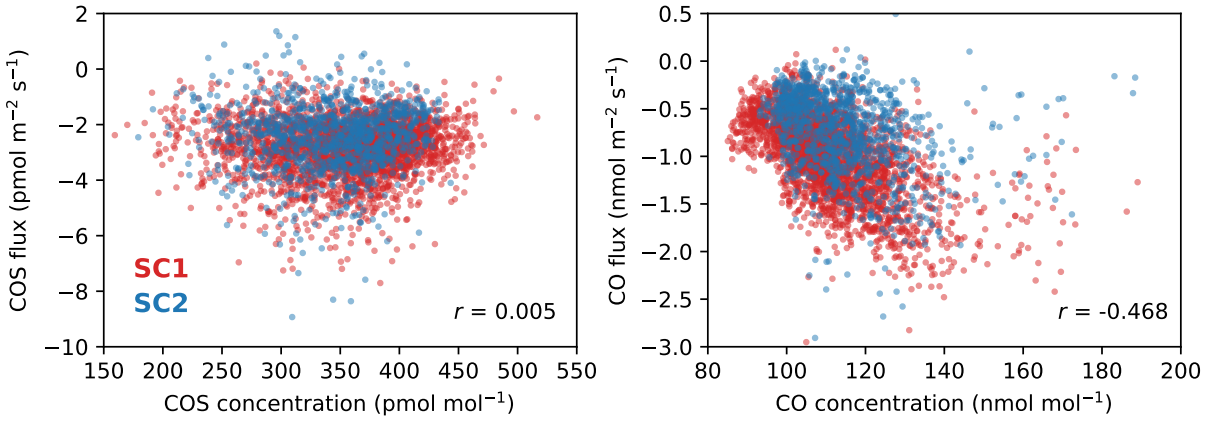

Figure 4.8: COS and CO fluxes versus their respective concentrations. COS uptake do not show a correlation with COS concentration ($r = 0.005, p = 0.738$), whereas CO uptake is weakly correlated with CO concentration ($r = -0.468, p < 1 \times 10^{-16}$).

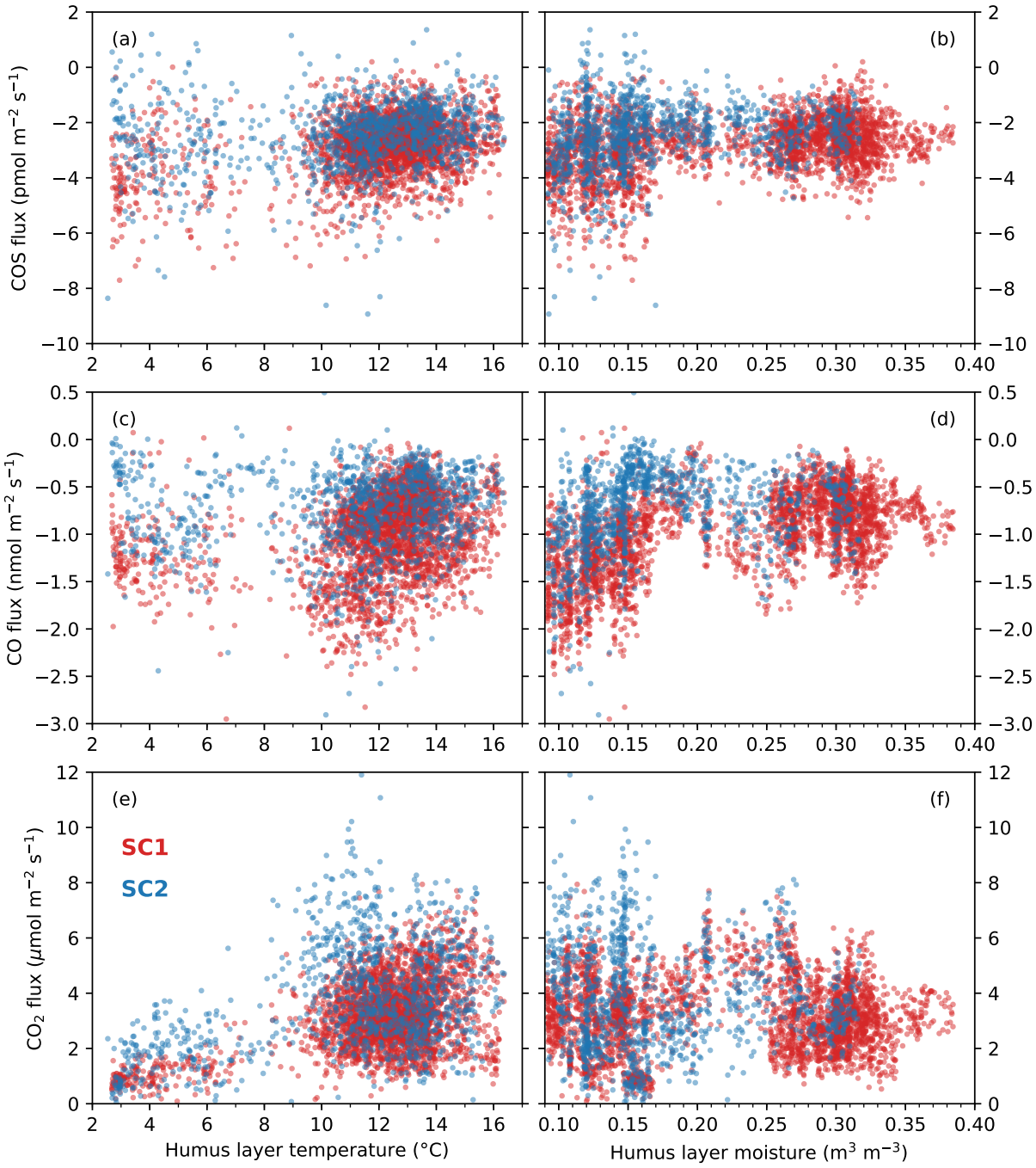

Figure 4.9: Soil fluxes of COS, CO, and CO_2 versus temperature and moisture in soil humus layer.

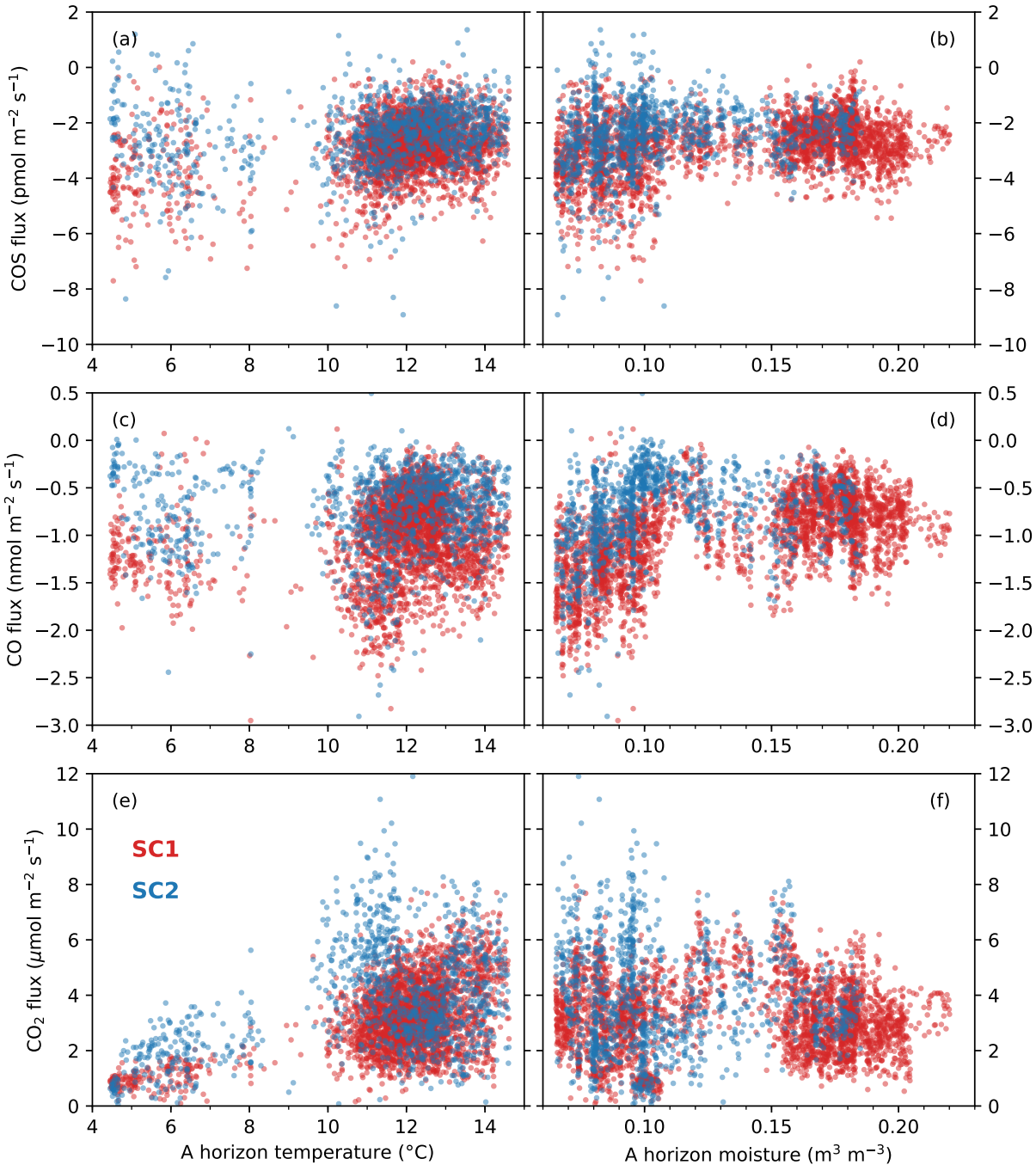

Figure 4.10: Soil fluxes of COS, CO, and CO_2 versus temperature and moisture in soil A horizon.

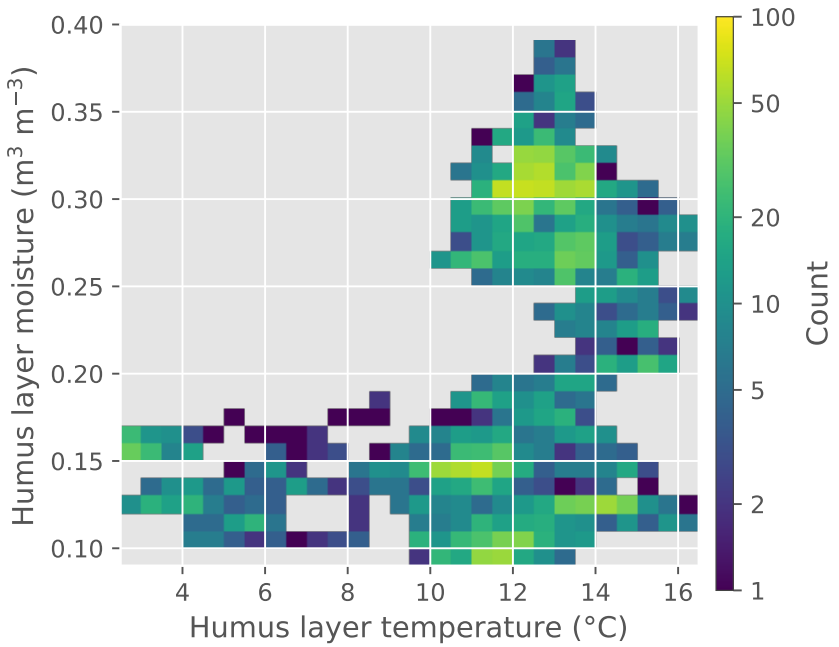

Figure 4.11: A 2D histogram for sample counts in temperature and moisture bins. Note that the scale is logarithmic for better visualization.

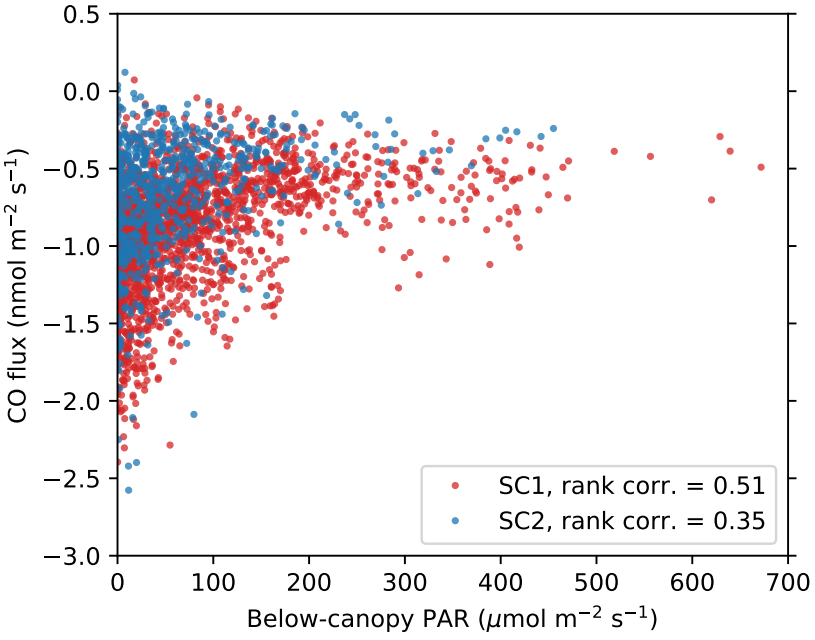

Figure 4.12: Daytime CO flux correlates weakly with below-canopy photosynthetically available radiation (PAR), as indicated by the Spearman's rank correlations shown on the figure legend.

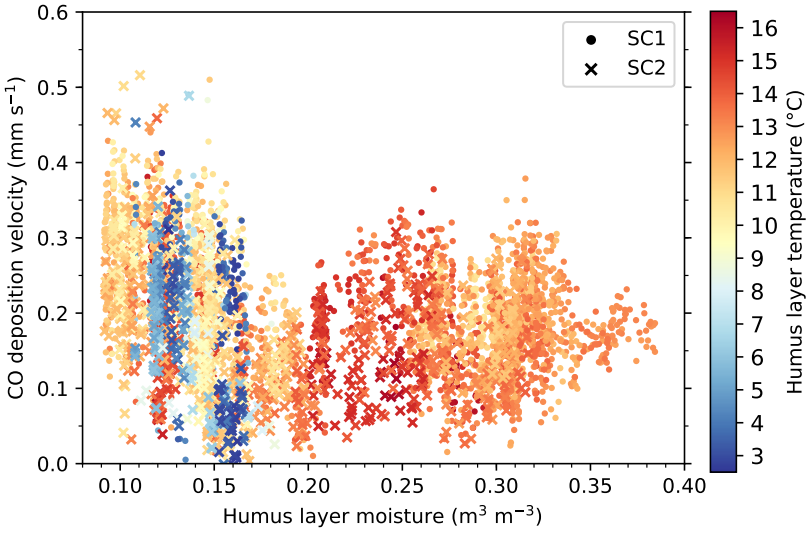

Figure 4.13: Apparent CO deposition velocity ($-F_{CO}/[CO]_{0.5\ m}$) as a function of soil humus layer moisture (x-axis) and temperature (colors).

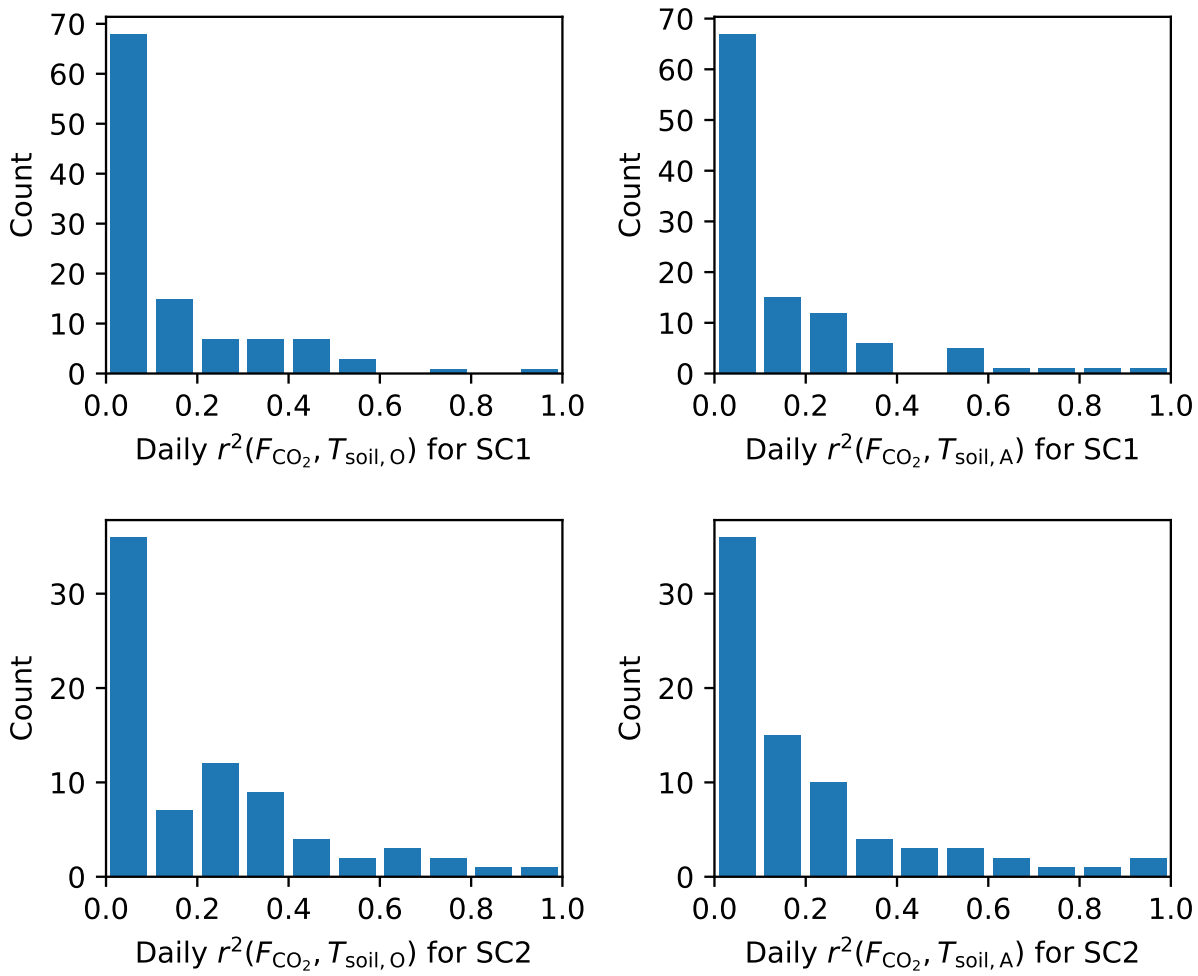

Figure 4.14: Histograms of the daily r^2 values of the correlation between CO_2 flux and humus layer temperature (left column) or A horizon temperature (right column) for the two soil chambers (top row: SC1; bottom row: SC2). Most days showed insignificant or weak correlations between CO_2 flux and soil temperature variables.

CHAPTER 5

Conclusion

5.1 The determinants of soil COS flux

Soil COS flux is governed by two types of processes: physical transport and (bio)chemical reactions. Physical transport processes do not create or destroy COS, but shift COS distribution in the soil column. The main environmental factor controlling the physical transport is soil moisture because the effective diffusivity is related to soil texture, porosity, and moisture. At the Hyytiälä forest site where soil moisture is not limiting microbial activity, soil COS uptake decreases with increasing soil moisture (decreasing diffusivity), showing a diffusion limited regime (Chap. 4). Reactions that consume or produce COS may have complicated responses to environmental parameters. Enzymatic uptake of COS is expected to be related to the microbial activity. At the Stunt Ranch site in the dry season, the most important determinant of soil (with litter) COS exchange is moisture content, as it is a limiting factor of the microbial activity (Chap. 3). The responses of soil COS flux to moisture are different between a dry climate and a moist climate. However, a common feature between the two climates is the correlation between soil COS flux to soil respiration. Naturally, soil respiration is an indicator of microbial activity. The flux relationships between COS and CO_2 may be a more generalized feature for soils. In summary, soil moisture and respiration strength are two important environmental determinants of soil COS flux and the responses are likely universal to various soil types.

5.2 Implication for ecosystem COS exchange

The ability to predict soil COS flux from soil variables, which are routinely measured as part of biometeorological data at flux tower sites, shall lend support to the practical goal of inferring gross primary productivity from COS flux measurements. The soil COS flux model (Chap. 2) may be integrated as part of an ecosystem model driven by meteorological and ecological parameters to simulate COS and CO_2 flux components. It is hoped that a modeling framework can be built to assimilate field data of COS and CO_2 soil and canopy fluxes for carbon flux partitioning into photosynthesis and respiration and for the improvement of model representation of coupled stomatal conductance and photosynthesis processes.

5.3 Future research

One and half centuries have passed since the first reported separation of COS by C. Than in 1867 [*Berthelot*, 1868]. COS is now recognized as an interesting species in the atmosphere for its influences on the climate as a precursor to stratospheric sulfate aerosols, its participation in the biogeochemical cycle, and its applications as a carbon cycle tracer. For COS, the realm of knowledge continues to expand, as well as the terra incognita. The understanding of soil COS exchange has been advanced in the past few years, but with these discoveries, more questions have surfaced. Strong emissions of COS from soils have been observed and the mechanisms of COS production are not well understood [*Maseyk et al.*, 2014; *Whelan and Rhew*, 2015; *Whelan et al.*, 2016; *Kitz et al.*, 2017]. Most field observations of soil COS exchange have been done in the temperate zones in the northern hemisphere, while soils in tropical ecosystems such as rainforests and savannas are very underrepresented in COS studies. Current global estimate of soil COS budget needs to be revisited with a process-based soil COS flux model.

Here I list a few important open questions on soil–atmosphere COS exchange. For researchers

studying on this topic, I suggest that the following questions may be prioritized in future research.

On soil COS production mechanisms

- What are the main agents responsible for soil COS emissions? Abiotic production, plant roots, or soil microbes?
- What is the mechanism of photochemical production of COS in soils? What are the precursors of COS?
- How do soil microbes produce COS? Do the mechanisms differ between wetland soils (anoxic) and upland soils (oxic)?

On relationships between flux and environmental variables

- How does soil COS uptake activity respond to soil variables that are less often observed: organic carbon content, O_2 concentration, redox potential, pH, etc.?
- How does abiotic production respond to temperature, moisture, and solar radiation?
- What are the environmental determinants of microbial COS production?

On ecosystem applications

- With more field observations of soil COS flux, can we identify a set of ecosystem-dependent parameters for predicting soil COS flux in representative ecosystems?
- What are the global soil source strength and sink strength of COS?

In summary, future research should continue advancing the understanding of soil COS processes and the use of COS as a tracer for terrestrial carbon cycle processes.

References

Aerodyne Research (2017), Carbonyl Sulfide Monitors, http://www.aerodyne.com/products/carbonyl-sulfide-monitors, accessed April 9, 2017.

Asaf, D., E. Rotenberg, F. Tatarinov, U. Dicken, S. A. Montzka, and D. Yakir (2013), Ecosystem photosynthesis inferred from measurements of carbonyl sulphide flux, *Nature Geoscience*, *6*(3), 186–190, doi:10.1038/ngeo1730.

Austin, A. T., and L. Vivanco (2006), Plant litter decomposition in a semi-arid ecosystem controlled by photodegradation, *Nature*, *442*, 555–558, doi:10.1038/nature05038.

Aydin, M., T. J. Fudge, K. R. Verhulst, M. R. Nicewonger, E. D. Waddington, and E. S. Saltzman (2014), Carbonyl sulfide hydrolysis in Antarctic ice cores and an atmospheric history for the last 8000 years, *Journal of Geophysical Research: Atmospheres*, *119*(13), 8500–8514, doi:10.1002/2014JD021618.

Badger, M. R., and G. D. Price (1990), Carbon oxysulfide is an inhibitor of both CO_2 and HCO_3^- uptake in the cyanobacterium *Synechococcus* PCC7942, *Plant Physiology*, *94*(1), 35–39, doi:10.1104/pp.94.1.35.

Badger, M. R., and G. D. Price (1994), The role of carbonic anhydrase in photosynthesis, *Annual Review of Plant Physiology and Plant Molecular Biology*, *45*, 369–392, doi:10.1146/annurev.pp.45.060194.002101.

Ball, J. T. (1988), An analysis of stomatal conductance, Ph.D. thesis, Stanford University.

Barnes, I., K. Becker, and I. Patroescu (1994), The tropospheric oxidation of dimethyl sulfide: A new source of carbonyl sulfide, *Geophysical Research Letters*, *21*(22), 2389–2392, doi:10.1029/94GL02499.

Bartholomew, G. W., and M. Alexander (1979), Microbial metabolism of carbon monoxide in culture and in soil, *Applied and Environmental Microbiology*, *37*(5), 932–937.

Belviso, S., N. Mihalopoulos, and B. C. Nguyen (1987), The supersaturation of carbonyl sulfide (OCS) in rain waters, *Atmospheric Environment*, *21*(6), 1363–1387, doi:10.1016/0004-6981(67)90083-2.

Belviso, S., M. Schmidt, C. Yver, M. Ramonet, V. Gros, and T. Launois (2013), Strong similarities between night-time deposition velocities of carbonyl sulphide and molecular hydrogen inferred from semi-continuous atmospheric observations in Gif-sur-Yvette, Paris region, *Tellus B*, *65*, 20,719, doi:10.3402/tellusb.v65i0.20719.

Berkelhammer, M., D. Asaf, C. Still, S. Montzka, D. Noone, M. Gupta, R. Provencal, H. Chen, and D. Yakir (2014), Constraining surface carbon fluxes using in situ measurements of carbonyl sulfide and carbon dioxide, *Global Biogeochemical Cycles*, *28*(2), 161–179, doi:10.1002/2013GB004644.

Berry, J., A. Wolf, J. E. Campbell, I. Baker, N. Blake, D. Blake, A. S. Denning, S. R. Kawa, S. A. Montzka, U. Seibt, K. Stimler, D. Yakir, and Z.-X. Zhu (2013), A coupled model of the global cycles of carbonyl sulfide and CO_2: A possible new window on the carbon cycle, *Journal of Geophysical Research: Biogeosciences*, *118*(2), 842–852, doi:10.1002/jgrg.20068.

Berthelot, M. (1868), Über das Kohlenoxysulfid, *Justus Liebigs Annalen der Chemie*, *148*, 266–268, doi:10.1002/jlac.18681480220.

Billesbach, D. P., J. A. Berry, U. Seibt, K. Maseyk, M. S. Torn, M. L. Fischer, M. Abu-Naser, and J. E. Campbell (2014), Growing season eddy covariance measurements of carbonyl sulfide and CO_2 fluxes: COS and CO_2 relationships in Southern Great Plains winter wheat, *Agricultural and Forest Meteorology*, *184*, 48–55, doi:10.1016/j.agrformet.2013.06.007.

Birch, H. F. (1958), The effect of soil drying on humus decomposition and nitrogen availability, *Plant and Soil*, *10*(1), 9–31, doi:10.1007/BF01343734.

Bird, R. B., W. E. Stewart, and E. N. Lightfoot (2002), *Transport Phenomena*, 2nd ed., John Wiley & Sons, Inc., Hoboken, NJ.

Blake, N. J., D. G. Streets, J.-H. Woo, I. J. Simpson, J. Green, S. Meinardi, K. Kita, E. Atlas, H. E. Fuelberg, G. Sachse, M. A. Avery, S. A. Vay, R. W. Talbot, J. E. Dibb, A. R. Bandy, D. C. Thornton, F. S.

Rowland, and D. R. Blake (2004), Carbonyl sulfide and carbon disulfide: Large-scale distributions over the western Pacific and emissions from Asia during TRACE-P, *Journal of Geophysical Research: Atmospheres*, *109*(D15), D15S05, doi:10.1029/2003JD004259.

Blake, N. J., J. E. Campbell, S. A. Vay, H. E. Fuelberg, L. G. Huey, G. Sachse, S. Meinardi, A. Beyersdorf, A. Baker, B. Barletta, J. Midyett, L. Doezema, M. Kamboures, J. McAdams, B. Novak, F. S. Rowland, and D. R. Blake (2008), Carbonyl sulfide (OCS): Large-scale distributions over North America during INTEX-NA and relationship to CO_2, *Journal of Geophysical Research: Atmospheres*, *113*(D9), doi:10.1029/2007JD009163, d09S90.

Blazewicz, S. J., E. Schwartz, and M. K. Firestone (2014), Growth and death of bacteria and fungi underlie rainfall-induced carbon dioxide pulses from seasonally dried soil, *Ecology*, *95*(5), 1162–1172, doi:10.1890/13-1031.1.

Blonquist, J. M., S. A. Montzka, J. W. Munger, D. Yakir, A. R. Desai, D. Dragoni, T. J. Griffis, R. K. Monson, R. L. Scott, and D. R. Bowling (2011), The potential of carbonyl sulfide as a proxy for gross primary production at flux tower sites, *Journal of Geophysical Research: Biogeosciences*, *116*(G4), doi:10.1029/2011JG001723.

Brühl, C., J. Lelieveld, P. J. Crutzen, and H. Tost (2012), The role of carbonyl sulphide as a source of stratospheric sulphate aerosol and its impact on climate, *Atmospheric Chemistry and Physics*, *12*(3), 1239–1253, doi:10.5194/acp-12-1239-2012.

Bruhn, D., K. R. Albert, T. N. Mikkelsen, and P. Ambus (2013), UV-induced carbon monoxide emission from living vegetation, *Biogeosciences*, *10*(12), 7877–7882, doi:10.5194/bg-10-7877-2013.

Campbell, J. E., G. R. Carmichael, T. Chai, M. Mena-Carrasco, Y. Tang, D. R. Blake, N. J. Blake, S. A. Vay, G. J. Collatz, I. Baker, J. A. Berry, S. A. Montzka, C. Sweeney, J. L. Schnoor, and C. O. Stanier (2008), Photosynthetic control of atmospheric carbonyl sulfide during the growing season, *Science*, *322*(5904), 1085–1088, doi:10.1126/science.1164015.

Campbell, J. E., M. E. Whelan, U. Seibt, S. J. Smith, J. A. Berry, and T. W. Hilton (2015), Atmospheric carbonyl sulfide sources from anthropogenic activity: Implications for carbon

cycle constraints, *Geophysical Research Letters*, *42*(8), 3004–3010, doi:10.1002/2015GL063445, 2015GL063445.

Campbell, J. E., J. A. Berry, U. Seibt, S. J. Smith, S. A. Montzka, T. Launois, S. Belviso, L. Bopp, and M. Laine (2017), Large historical growth in global terrestrial gross primary production, *Nature*, *544*, 84–87, doi:10.1038/nature22030.

Castro, M. S., and J. N. Galloway (1991), A comparison of sulfur-free and ambient air enclosure techniques for measuring the exchange of reduced sulfur gases between soils and the atmosphere, *Journal of Geophysical Research*, *96*(D8), 15,427–15,437, doi:10.1029/91JD01399.

Chengelis, C. P., and R. A. Neal (1979), Hepatic carbonyl sulfide metabolism, *Biochemical and Biophysical Research Communications*, *90*(3), 993–999, doi:10.1016/0006-291X(79)91925-9.

Chengelis, C. P., and R. A. Neal (1980), Studies of carbonyl sulfide toxicity: metabolism by carbonic anhydrase, *Toxicology and Applied Pharmacology*, *55*(1), 198–202, doi:10.1016/0041-008X(80)90236-7.

Chin, M., and D. D. Davis (1993), Global sources and sinks of OCS and CS_2 and their distributions, *Global Biogeochemical Cycles*, *7*(2), 321–337, doi:10.1029/93GB00568.

Clapp, R. B., and G. M. Hornberger (1978), Empirical equations for some soil hydraulic properties, *Water Resources Research*, *14*(4), 601–604, doi:10.1029/WR014i004p00601.

Clein, J. S., and J. P. Schimel (1994), Reduction in microbial activity in birch litter due to drying and rewetting events, *Soil Biology and Biochemistry*, *26*(3), 403–406, doi:10.1016/0038-0717(94)90290-9.

Cleveland, W. S., E. Grosse, and W. M. Shyu (1992), Chapter 8 Local Regression Models, in *Statistical Models in S*, edited by J. M. Chambers and T. J. Hastie, Wadsworth & Brooks/Cole, Pacific Grove, California, USA.

Coblentz Society, Inc. (2015), Evaluated Infrared Reference Spectra, in *NIST Chemistry WebBook, NIST Standard Reference Database Number 69*, edited by P. J. Linstrom and W. G. Mallard, National Institute of Standards and Technology, Gaithersburg MD, 20899, doi:10.18434/T4D303.

Collatz, G. J., J. T. Ball, C. Grivet, and J. A. Berry (1991), Physiological and environmental regulation of stomatal conductance, photosynthesis and transpiration: a model that includes a laminar boundary layer, *Agricultural and Forest Meteorology*, *54*(2–4), 107–136, doi:10.1016/0168-1923(91)90002-8.

Commane, R., L. K. Meredith, I. T. Baker, J. A. Berry, J. W. Munger, S. A. Montzka, P. H. Templer, S. M. Juice, M. S. Zahniser, and S. C. Wofsy (2015), Seasonal fluxes of carbonyl sulfide in a midlatitude forest, *Proceedings of the National Academy of Sciences*, *112*(46), 14,162–14,167, doi:10.1073/pnas.1504131112.

Conrad, R. (1996), Soil microorganisms as controllers of atmospheric trace gases (H_2, CO, CH_4, OCS, N_2O, and NO), *Microbiological Reviews*, *60*(4), 609–640.

Conrad, R., and K. Meuser (2000), Soils contain more than one activity consuming carbonyl sulfide, *Atmospheric Environment*, *34*(21), 3635–3639, doi:10.1016/S1352-2310(00)00136-9.

Conrad, R., and W. Seiler (1980), Role of microorganisms in the consumption and production of atmospheric carbon monoxide by soil, *Applied and Environmental Microbiology*, *40*(3), 437–445.

Conrad, R., and W. Seiler (1985), Influence of temperature, moisture, and organic carbon on the flux of H_2 and CO between soil and atmosphere: field studies in subtropical regions, *Journal of Geophysical Research*, *90*(D3), 5699–5709, doi:10.1029/JD090iD03p05699.

Constant, P., L. Poissant, and R. Villemur (2008), Annual hydrogen, carbon monoxide and carbon dioxide concentrations and surface to air exchanges in a rural area (Québec, Canada), *Atmospheric Environment*, *42*(20), 5090–5100, doi:10.1016/j.atmosenv.2008.02.021.

Constant, P., S. P. Chowdhury, J. Pratscher, and R. Conrad (2010), Streptomycetes contributing to atmospheric molecular hydrogen soil uptake are widespread and encode a putative high-affinity [NiFe]-hydrogenase, *Environmental Microbiology*, *12*(3), 821–829, doi:10.1111/j.1462-2920.2009.02130.x.

Cook, R. D. (1977), Detection of influential observation in linear regression, *Technometrics*, *19*(1), 15–18.

Crank, J., and P. Nicolson (1947), A practical method for numerical evaluation of solutions of partial differential equations of the heat-conduction type, *Mathematical Proceedings of the Cambridge Philosophical Society*, *43*, 50–67, doi:10.1017/S0305004100023197.

Crutzen, P. J. (1976), The possible importance of CSO for the sulfate layer of the stratosphere, *Geophysical Research Letters*, *3*(2), 73–76, doi:10.1029/GL003i002p00073.

Daniel, J. S., and S. Solomon (1998), On the climate forcing of carbon monoxide, *Journal of Geophysical Research: Atmospheres*, *103*(D11), 13,249–13,260, doi:10.1029/98JD00822.

Daniel, R. M., M. E. Peterson, M. J. Danson, N. C. Price, S. M. Kelly, C. R. Monk, C. S. Weinberg, M. L. Oudshoorn, and C. K. Lee (2010), The molecular basis of the effect of temperature on enzyme activity, *Biochemical Journal*, *425*(2), 353–360, doi:10.1042/BJ20091254.

De Bruyn, W. J., E. Swartz, J. H. Hu, J. A. Shorter, P. Davidovits, D. R. Worsnop, M. S. Zahniser, and C. E. Kolb (1995), Henry's law solubilities and Śetchenow coefficients for biogenic reduced sulfur species obtained from gas-liquid uptake measurements, *Journal of Geophysical Research*, *100*(D4), 7245–7251, doi:10.1029/95JD00217.

de Mello, W. Z., and M. E. Hines (1994), Application of static and dynamic enclosures for determining dimethyl sulfide and carbonyl sulfide exchange in *Sphagnum* peatlands: Implications for the magnitude and direction of flux, *Journal of Geophysical Research*, *99*(D7), 14,601–14,607, doi:10.1029/94JD01025.

DeLaune, R. D., I. Devai, and C. W. Lindau (2002), Flux of reduced sulfur gases along a salinity gradient in Louisiana coastal marshes, *Estuarine, Coastal and Shelf Science*, *54*(6), 1003–1011, doi:10.1006/ecss.2001.0871.

Denef, K., J. Six, K. Paustian, and R. Merckx (2001), Importance of macroaggregate dynamics in controlling soil carbon stabilization: short-term effects of physical disturbance induced by dry-wet cycles, *Soil Biology and Biochemistry*, *33*(15), 2145–2153, doi:10.1016/S0038-0717(01)00153-5.

Devai, I., and R. D. DeLaune (1995), Formation of volatile sulfur compounds in salt marsh sed-

iment as influenced by soil redox condition, *Organic Geochemistry*, *23*, 283–287, doi:10.1016/0146-6380(95)00024-9.

Durran, D. R. (2010), *Numerical Methods for Fluid Dynamics: With Applications to Geophysics*, 2nd ed., Springer-Verlag, New York.

Elliott, S., E. Lu, and F. S. Rowland (1989), Rates and mechanisms for the hydrolysis of carbonyl sulfide in natural waters, *Environmental Science & Technology*, *23*(4), 458–461, doi:10.1021/es00181a011.

Ensign, S. A. (1995), Reactivity of carbon monoxide dehydrogenase from *Rhodospirillum rubrum* with carbon dioxide, carbonyl sulfide, and carbon disulfide, *Biochemistry*, *34*(16), 5372–5378.

Ferek, R. J., and M. O. Andreae (1984), Photochemical production of carbonyl sulphide in marine surface waters, *Nature*, *307*, 148–150, doi:10.1038/307148a0.

Ferm, R. J. (1957), The chemistry of carbonyl sulfide, *Chemical Reviews*, *57*(4), 621–640, doi:10.1021/cr50016a002.

Fierer, N., and J. P. Schimel (2003), A proposed mechanism for the pulse in carbon dioxide production commonly observed following the rapid rewetting of a dry soil, *Soil Science Society of America Journal*, *67*(3), 798–805, doi:10.2136/sssaj2003.7980.

Fischer, M. L., D. P. Billesbach, J. A. Berry, W. J. Riley, and M. S. Torn (2007), Spatiotemporal variations in growing season exchanges of CO_2, H_2O, and sensible heat in agricultural fields of the Southern Great Plains, *Earth Interactions*, *11*(17), 1–21, doi:10.1175/EI231.1.

Friedl, R. R., W. H. Brune, and J. G. Anderson (1985), Kinetics of mercapto (SH) with nitrogen dioxide, ozone, molecular oxygen, and hydrogen peroxide, *Journal of Physical Chemistry*, *89*(25), 5505–5510, doi:10.1021/j100271a038.

Goulden, M. L., J. W. Munger, S.-M. Fan, B. C. Daube, and S. C. Wofsy (1996), Measurements of carbon sequestration by long-term eddy covariance: methods and a critical evaluation of accuracy, *Global Change Biology*, *2*, 169–182, doi:10.1111/j.1365-2486.1996.tb00070.x.

Haataja, J., and T. Vesala (1997), SMEAR II, Station for Measuring Forest Ecosystem–Atmosphere Relations, *Department of Forest Ecology Publications 17*, University of Helsinki, Aseman Kirjapaino, Orivesi, Finland.

Halmer, M. M., H.-U. Schmincke, and H.-F. Graf (2002), The annual volcanic gas input into the atmosphere, in particular into the stratosphere: a global data set for the past 100 years, *Journal of Volcanology and Geothermal Research*, *115*(3), 511–528, doi:10.1016/S0377-0273(01)00318-3.

Hari, P., and M. Kulmala (2005), Station for Measuring Ecosystem–Atmosphere Relations, *Boreal Environmental Research*, *10*(5), 315–322.

Hendrickson, O. Q., and T. Kubiseski (1991), Soil microbial activity at high levels of carbon monoxide, *Journal of Environmental Quality*, *20*(3), 675–678, doi:10.2134/jeq1991.00472425002000030028x.

Henry, R. P. (1996), Multiple roles of carbonic anhydrase in cellular transport and metabolism, *Annual Review of Physiology*, *58*, 523–538, doi:10.1146/annurev.ph.58.030196.002515.

Hilton, T., A. Zumkehr, S. Kulkarni, J. Berry, M. Whelan, and J. Campbell (2015), Large variability in ecosystem models explains uncertainty in a critical parameter for quantifying GPP with carbonyl sulphide, *Tellus B*, *67*(0), doi:10.3402/tellusb.v67.26329.

Hofmann, U., R. Hofmann, and J. Kesselmeier (1992), Cryogenic trapping of reduced sulfur compounds using a Nafion drier and cotton wadding as an oxidant scavenger, *Atmospheric Environment*, *26*(13), 2445–2449, doi:10.1016/0960-1686(92)90374-T.

Inman, R. E., R. B. Ingersoll, and E. A. Levy (1971), Soil: A natural sink for carbon monoxide, *Science*, *172*(3989), 1229–1231.

Jarvis, P., A. Rey, C. Petsikos, L. Wingate, M. Rayment, J. Pereira, J. Banza, J. David, F. Miglietta, M. Borghetti, G. Manca, and R. Valentini (2007), Drying and wetting of Mediterranean soils stimulates decomposition and carbon dioxide emission: the "Birch effect", *Tree Physiology*, *27*(7), 929–940, doi:10.1093/treephys/27.7.929.

Johansen, O. (1975), Thermal conductivity of soils, Ph.D. thesis, Trondheim, Group for Thermal Analysis of Frost in the Ground, Institute for Kjøleteknikk, Norway, (trans. Rosetta Stone, Nashua, N.H. for U.S. Army Cold Regions Research and Engineering Laboratory, 1977).

Johnson, J. E., and H. Harrison (1986), Carbonyl sulfide concentrations in the surface waters and above the Pacific Ocean, *Journal of Geophysical Research: Atmospheres*, *91*(D7), 7883–7888, doi:10.1029/JD091iD07p07883.

Katayama, Y., Y. Narahara, Y. Inoue, F. Amano, T. Kanagawa, and H. Kuraishi (1992), A thiocyanate hydrolase of *Thiobacillus thioparus*. a novel enzyme catalyzing the formation of carbonyl sulfide from thiocyanate, *Journal of Biological Chemistry*, *267*(13), 9170–9175.

Katayama, Y., T. Kanagawa, and H. Kuraishi (1993), Emission of carbonyl sulfide by *Thiobacillus thioparus* grown with thiocyanate in pure and mixed cultures, *FEMS microbiology letters*, *114*(2), 223–227, doi:10.1111/j.1574-6968.1993.tb06577.x.

Kato, H., M. Saito, Y. Nagahata, and Y. Katayama (2008), Degradation of ambient carbonyl sulfide by *Mycobacterium* spp. in soil, *Microbiology*, *154*(1), 249–255, doi:10.1099/mic.0.2007/011213-0.

Kesselmeier, J., and A. Hubert (2002), Exchange of reduced volatile sulfur compounds between leaf litter and the atmosphere, *Atmospheric Environment*, *36*(29), 4679–4686, doi:10.1016/S1352-2310(02)00413-2.

Kesselmeier, J., N. Teusch, and U. Kuhn (1999), Controlling variables for the uptake of atmospheric carbonyl sulfide by soil, *Journal of Geophysical Research*, *104*(D9), 11,577–11,584, doi:10.1029/1999JD900090.

Kettle, A. J., U. Kuhn, M. von Hobe, J. Kesselmeier, and M. O. Andreae (2002), Global budget of atmospheric carbonyl sulfide: Temporal and spatial variations of the dominant sources and sinks, *Journal of Geophysical Research*, *107*(D22), 4658, doi:10.1029/2002JD002187.

Khalil, M. A. K., and R. A. Rasmussen (1990), The global cycle of carbon monoxide: Trends and mass balance, *Chemosphere*, *20*(1-2), 227–242, doi:10.1016/0045-6535(90)90098-E.

Kim, S.-J., and Y. Katayama (2000), Effect of growth conditions on thiocyanate degradation and emission of carbonyl sulfide by *thiobacillus thioparus* thi115, *Water Research*, *34*(11), 2887–2894, doi:10.1016/S0043-1354(00)00046-4.

King, G. M. (1999), Attributes of atmospheric carbon monoxide oxidation by Maine forest soils, *Applied and Environmental Microbiology*, *65*(12), 5257–5264.

King, G. M., and H. Crosby (2002), Impacts of plant roots on soil CO cycling and soil–atmosphere CO exchange, *Global Change Biology*, *8*(11), 1085–1093, doi:10.1046/j.1365-2486.2002.00545.x.

King, G. M., and C. F. Weber (2007), Distribution, diversity and ecology of aerobic CO-oxidizing bacteria, *Nature Reviews Microbiology*, *5*(2), 107–118, doi:10.1038/nrmicro1595.

Kitz, F., K. Gerdel, A. Hammerle, T. Laterza, F. M. Spielmann, and G. Wohlfahrt (2017), In situ soil COS exchange of a temperate mountain grassland under simulated drought, *Oecologia*, pp. 851–860, doi:10.1007/s00442-016-3805-0.

Kooijmans, L. M. J., N. A. M. Uitslag, M. S. Zahniser, D. D. Nelson, S. A. Montzka, and H. Chen (2016), Continuous and high-precision atmospheric concentration measurements of COS, CO_2, CO and H_2O using a quantum cascade laser spectrometer (QCLS), *Atmospheric Measurement Techniques*, *9*, 5293–5314, doi:10.5194/amt-9-5293-2016.

Kooijmans, L. M. J., K. Maseyk, U. Seibt, W. Sun, T. Vesala, I. Mammarella, P. Kolari, A. Franchin, R. Vecchi, G. Valli, and H. Chen (2017), Canopy uptake dominates nighttime carbonyl sulfide fluxes in a boreal forest, *Atmospheric Chemistry and Physics Discussions*, doi:10.5194/acp-2017-407, in review.

Kremser, S., L. W. Thomason, M. von Hobe, M. Hermann, T. Deshler, C. Timmreck, M. Toohey, A. Stenke, J. P. Schwarz, R. Weigel, S. Fueglistaler, F. J. Prata, J.-P. Vernier, H. Schlager, J. E. Barnes, J.-C. Antuña-Marrero, D. Fairlie, M. Palm, E. Mahieu, J. Notholt, M. Rex, C. Bingen, F. Vanhellemont, A. Bourassa, J. M. C. Plane, D. Klocke, S. A. Carn, L. Clarisse, T. Trickl, R. Neely, A. D. James, L. Rieger, J. C. Wilson, and B. Meland (2016), Stratospheric aerosol—observations, processes, and impact on climate, *Reviews of Geophysics*, *54*(2), 278–335, doi:10.1002/2015RG000511, 2015RG000511.

Kuhlbusch, T. A. J., R. G. Zepp, W. L. Miller, and R. A. Burke (1998), Carbon monoxide fluxes of different soil layers in upland Canadian boreal forests, *Tellus B*, *50*(4), 353–365, doi:10.1034/j.1600-0889.1998.t01-3-00003.x.

Kuhn, U., C. Ammann, A. Wolf, F. Meixner, M. Andreae, and K. J. (1999), Carbonyl sulfide exchange on an ecosystem scale: Soil represents a dominant sink for atmospheric COS, *Atmospheric Environment*, *33*(6), 995–1008, doi:10.1016/S1352-2310(98)00211-8.

Kulmala, L., J. Pumpanen, P. Hari, and T. Vesala (2011), Photosynthesis of ground vegetation in different aged pine forests: Effect of environmental factors predicted with a process-based model, *Journal of Vegetation Science*, *22*(1), 96–110, doi:10.1111/j.1654-1103.2010.01228.x.

Kurylo, M. J. (1978), Flash photolysis resonance fluorescence investigation of the reactions of OH radicals with OCS and CS_2, *Chemical Physics Letters*, *58*(2), 238–242, doi:10.1016/0009-2614(78)80285-1.

Launois, T., P. Peylin, S. Belviso, and B. Poulter (2015a), A new model of the global biogeochemical cycle of carbonyl sulfide – Part 2: Use of carbonyl sulfide to constrain gross primary productivity in current vegetation models, *Atmospheric Chemistry and Physics*, *15*, 9285–9312, doi:10.5194/acp-15-9285-2015.

Launois, T., S. Belviso, L. Bopp, C. Fichot, and P. Peylin (2015b), A new model for the global biogeochemical cycle of carbonyl sulfide–Part 1: Assessment of direct marine emissions with an oceanic general circulation and biogeochemistry model, *Atmospheric Chemistry and Physics*, *15*(5), 2295–2312, doi:10.5194/acp-15-2295-2015.

Lennartz, S. T., C. A. Marandino, M. von Hobe, P. Cortes, B. Quack, R. Simo, D. Booge, A. Pozzer, T. Steinhoff, D. L. Arevalo-Martinez, C. Kloss, A. Bracher, R. Röttgers, E. Atlas, and K. Krüger (2017), Direct oceanic emissions unlikely to account for the missing source of atmospheric carbonyl sulfide, *Atmospheric Chemistry and Physics*, *17*(1), 385–402, doi:10.5194/acp-17-385-2017.

Li, X., J. Liu, and J. Yang (2006), Variation of H_2S and COS emission fluxes from *Calamagrostis angustifolia* wetlands in Sanjiang Plain, Northeast China, *Atmospheric Environment*, *40*(33), 6303–6312, doi:10.1016/j.atmosenv.2006.05.054.

Liu, J., C. Geng, Y. Mu, Y. Zhang, Z. Xu, and H. Wu (2010a), Exchange of carbonyl sulfide (COS) between the atmosphere and various soils in China, *Biogeosciences*, *7*(2), 753–762, doi:10.5194/bg-7-753-2010.

Liu, Y., H. He, and Q. Ma (2008), Temperature dependence of the heterogeneous reaction of carbonyl sulfide on magnesium oxide, *Journal of Physical Chemistry A*, *112*, 2820–2826, doi:10.1021/jp711302r.

Liu, Y., J. Ma, C. Liu, and H. He (2010b), Heterogeneous uptake of carbonyl sulfide onto kaolinite within a temperature range of 220–330 K, *Journal of Geophysical Research*, *115*, D24,311, doi:10.1029/2010JD014778.

Lloyd, J., and J. A. Taylor (1994), On the temperature dependence of soil respiration, *Functional Ecology*, *8*(3), 315–323, doi:10.2307/2389824.

Lorimer, G. H., and J. Pierce (1989), Carbonyl sulfide: an alternate substrate for but not an activator of ribulose-1,5-bisphosphate carboxylase, *Journal of Biological Chemistry*, *264*(5), 2764–2772.

Los Gatos Research (2017), OCS Analyzer Datasheet, http://www.lgrinc.com/documents/OCS_Analyzer_Datasheet.pdf, accessed April 9, 2017.

Lund, C., W. J. Riley, L. L. Pierce, and C. B. Field (1999), The effects of chamber pressurization on soil-surface CO_2 flux and the implications for NEE measurements under elevated CO_2, *Global Change Biology*, *5*(3), 269–281, doi:10.1046/j.1365-2486.1999.00218.x.

Maseyk, K., L. Wingate, U. Seibt, J. Ghashghaie, C. Bathellier, P. Almeida, R. L. de Vale, J. S. Pereira, D. Yakir, and M. Mencuccini (2009), Biotic and abiotic factors affecting the $\delta^{13}C$ of soil respired CO_2 in a Mediterranean oak woodland, *Isotopes in Environmental and Health Studies*, *45*(4), 343–359, doi:10.1080/10256010903388212.

Maseyk, K., J. A. Berry, D. Billesbach, J. E. Campbell, M. S. Torn, M. Zahniser, and U. Seibt (2014), Sources and sinks of carbonyl sulfide in an agricultural field in the Southern Great Plains, *Proceedings of the National Academy of Sciences*, *111*(25), 9064–9069, doi:10.1073/pnas.1319132111.

Massman, W., R. Sommerfeld, A. Mosier, K. Zeller, T. Hehn, and S. Rochelle (1997), A model investigation of turbulence-driven pressure-pumping effects on the rate of diffusion of CO_2, N_2O, and CH_4 through layered snowpacks, *Journal of Geophysical Research*, *102*(D15), 18,851–18,863, doi:10.1029/97JD00844.

Massman, W. J. (1998), A review of the molecular diffusivities of H_2O, CO_2, CH_4, CO, O_3, SO_2, NH_3, N_2O, NO, and NO_2 in air, O_2 and N_2 near STP, *Atmospheric Environment*, *32*(6), 1111–1127, doi:10.1016/S1352-2310(97)00391-9.

Matthews, E. (1997), Global litter production, pools, and turnover times: Estimates from measurement data and regression models, *Journal of Geophysical Research: Atmospheres*, *102*(D15), 18,771–18,800, doi:10.1029/97JD02956.

McManus, J. B., M. S. Zahniser, D. D. Nelson, J. H. Shorter, S. Herndon, E. Wood, and R. Wehr (2010), Application of quantum cascade lasers to high-precision atmospheric trace gas measurements, *Optical Engineering*, *49*(11), 111,124, doi:10.1117/1.3498782.

Mihalopoulos, N., B. C. Nguyen, J. P. Putaud, and S. Belviso (1992), The oceanic source of carbonyl sulfide (COS), *Atmospheric Environment*, *26*(8), 1383–1394, doi:10.1016/0960-1686(92)90123-3.

Miller, A. G., G. S. Espie, and D. T. Canvin (1989), Use of carbon oxysulfide, a structural analog of CO_2, to study active CO_2 transport in the cyanobacterium *Synechococcus* UTEX 625, *Plant Physiology*, *90*(3), 1221–1231, doi:10.1104/pp.90.3.1221.

Moldrup, P., T. Olesen, T. Komatsu, S. Yoshikawa, P. Schjønning, and D. Rolston (2003), Modeling diffusion and reaction in soils: X. A unifying model for solute and gas diffusivity in unsaturated soil, *Soil Science*, *168*(5), 321–337.

Montzka, S., P. Calvert, B. Hall, J. Elkins, T. Conway, P. Tans, and C. Sweeney (2007), On the global distribution, seasonality, and budget of atmospheric carbonyl sulfide (COS) and some similarities to CO_2, *Journal of Geophysical Research*, *112*, D09,302, doi:10.1029/2006JD007665.

Mörsdorf, G., K. Frunzke, D. Gadkari, and O. Meyer (1992), Microbial growth on carbon monoxide, *Biodegradation*, *3*(1), 61–82, doi:10.1007/BF00189635.

Moxley, J. M., and K. A. Smith (1998), Factors affecting utilisation of atmospheric CO by soils, *Soil Biology and Biochemistry*, *30*(1), 65–79, doi:10.1016/S0038-0717(97)00095-3.

Mu, Y., C. Geng, M. Wang, H. Wu, X. Zhang, and G. Jiang (2004), Photochemical production of carbonyl sulfide in precipitation, *Journal of Geophysical Research: Atmospheres*, *109*(D13), doi:10.1029/2003JD004206, d13301.

Muenter, J. S. (1968), Electric dipole moment of carbonyl sulfide, *The Journal of Chemical Physics*, *48*(10), 4544–4547, doi:10.1063/1.1668024.

Navarro-García, F., M. A. Casermeiro, and J. P. Schimel (2012), When structure means conservation: Effect of aggregate structure in controlling microbial responses to rewetting events, *Soil Biology and Biochemistry*, *44*, 1–8, doi:10.1016/j.soilbio.2011.09.019.

Notni, J., S. Schenk, G. Protoschill-Krebs, J. Kesselmeier, and E. Anders (2007), The missing link in COS metabolism: a model study on the reactivation of carbonic anhydrase from its hydrosulfide analogue, *ChemBioChem*, *8*(5), 530–536, doi:10.1002/cbic.200600436.

Ogawa, T., K. Noguchi, M. Saito, Y. Nagahata, H. Kato, A. Ohtaki, H. Nakayama, N. Dohmae, Y. Matsushita, M. Odaka, M. Yohda, H. Nyunoya, and Y. Katayama (2013), Carbonyl sulfide hydrolase from *Thiobacillus thioparus* strain THI115 is one of the β-carbonic anhydrase family enzymes, *Journal of the American Chemical Society*, *135*(10), 3818–3825, doi:10.1021/ja307735e.

Ogée, J., J. Sauze, J. Kesselmeier, B. Genty, H. Van Diest, T. Launois, and L. Wingate (2016), A new mechanistic framework to predict OCS fluxes from soils, *Biogeosciences*, *13*(8), 2221–2240, doi:10.5194/bg-13-2221-2016.

Oleson, K. W., D. M. Lawrence, G. B. Bonan, B. Drewniak, M. Huang, C. D. Koven, S. Levis, F. Li, W. J. Riley, Z. M. Subin, S. Swenson, P. E. Thornton, A. Bozbiyik, R. Fisher, C. L. Heald, E. Kluzek, J.-F. Lamarque, P. J. Lawrence, L. R. Leung, W. Lipscomb, S. P. Muszala, D. M. Ricciuto, W. J. Sacks, Y. Sun, J. Tang, , and Z.-L. Yang (2013), Technical description of version 4.5 of the Community Land Model (CLM), *NCAR Technical Report NCAR/TN-503+STR*, National Center for Atmospheric Research (NCAR), Boulder, CO, USA, doi:10.5065/D6RR1W7M.

Or, D., and J. M. Wraith (2002), Soil water content and water potential relationships, in *Soil Physics Companion*, edited by A. W. Warrick, pp. 49–84, CRC Press.

Peters-Lidard, C., E. Blackburn, X. Liang, and E. Wood (1998), The effect of soil thermal conductivity parameterization on surface energy fluxes and temperatures, *Journal of the Atmospheric Sciences*, *55*(7), 1209–1224.

Peterson, M. E., R. Eisenthal, M. J. Danson, A. Spence, and R. M. Daniel (2004), A new intrinsic thermal parameter for enzymes reveals true temperature optima, *Journal of Biological Chemistry*, *279*(20), 20,717–20,722, doi:10.1074/jbc.M309143200.

Pihlatie, M., J. Pumpanen, J. Rinne, H. Ilvesniemi, A. Simojoki, P. Hari, and T. Vesala (2007), Gas concentration driven fluxes of nitrous oxide and carbon dioxide in boreal forest soil, *Tellus B*, *59*(3), 458–469, doi:10.1111/j.1600-0889.2007.00278.x.

Pihlatie, M., Ü. Rannik, S. Haapanala, O. Peltola, N. Shurpali, P. J. Martikainen, S. Lind, N. Hyvönen, P. Virkajärvi, M. Zahniser, and I. Mammarella (2016), Seasonal and diurnal variation in CO fluxes from an agricultural bioenergy crop, *Biogeosciences*, *13*(19), 5471–5485, doi:10.5194/bg-13-5471-2016.

Pirinen, P., H. Simola, J. Aalto, J.-P. Kaukoranta, P. Karlsson, and R. Ruuhela (2012), Tilastoja Suomen Ilmastosta 1981–2010 (Statistics of the Climate of Finland 1981–2010), *Report 2012:1*, Finnish Meteorological Institute, Helsinki, Finland.

Placella, S. A., E. L. Brodie, and M. K. Firestone (2012), Rainfall-induced carbon dioxide pulses result from sequential resuscitation of phylogenetically clustered microbial groups, *Proceedings of the National Academy of Sciences*, *109*(27), 10,931–10,936, doi:10.1073/pnas.1204306109.

Prandtl, L. (1925), Bericht über Untersuchungen zur ausgebildeten Turbulenz, *Z. Angew. Math. Mech*, *5*(2), 136–139.

Protoschill-Krebs, G., and J. Kesselmeier (1992), Enzymatic pathways for the consumption of carbonyl sulphide (COS) by higher plants, *Botanica Acta*, *105*(206–212), doi:10.1111/j.1438-8677.1992.tb00288.x.

Protoschill-Krebs, G., C. Wilhelm, and J. Kesselmeier (1995), Consumption of carbonyl sulphide by *Chlamydomonas reinhardtii* with different activities of carbonic anhydrase (CA) induced by different CO_2 growing regimes, *Botanica Acta*, *108*, 445–448, doi:10.1111/j.1438-8677.1995.tb00519.x.

Protoschill-Krebs, G., C. Wilhelm, and J. Kesselmeier (1996), Consumption of carbonyl sulphide (COS) by higher plant carbonic anhydrase (CA), *Atmospheric Environment*, *30*(18), 3151–3156, doi: 10.1016/1352-2310(96)00026-X.

Pumpanen, J., and H. Ilvesniemi (2005), Calibration of time domain reflectometry for forest soil humus layers, *Boreal environment research*, *10*(6), 589.

Pumpanen, J., H. Ilvesniemi, L. Kulmala, E. Siivola, H. Laakso, P. Kolari, C. Helenelund, M. Laakso, M. Uusimaa, and P. Hari (2008), Respiration in boreal forest soil as determined from carbon dioxide concentration profile, *Soil Science Society of America Journal*, *72*(5), 1187–1196, doi: 10.2136/sssaj2007.0199.

Pumpanen, J. S., L.-M. Kulmala, A. S. Linden, P. P. Kolari, E. H. Nikinmaa, P. K. J. Hari, et al. (2015), Seasonal dynamics of autotrophic respiration in boreal forest soil estimated by continuous chamber measurements, *Boreal Environment Research*, *20*, 637–650.

Rasmussen, R. A., M. A. K. Khalil, and S. D. Hoyt (1982), The oceanic source of carbonyl sulfide (OCS), *Atmospheric Environment*, *16*(6), 1591–1594, doi:10.1016/0004-6981(82)90111-1.

Rennenberg, H. (1991), The significance of higher plants in the emission of sulfur compounds from terrestrial ecosystems, in *Trace Gas Emissions by Plants*, edited by T. D. Sharkey, E. A. Holland, and H. A. Mooney, pp. 217–260, Academic Press, San Diego, CA, USA.

Rutledge, S., D. I. Campbell, D. Baldocchi, and L. A. Schipper (2010), Photodegradation leads to increased carbon dioxide losses from terrestrial organic matter, *Global Change Biology*, *16*(11), 3065–3074, doi:10.1111/j.1365-2486.2009.02149.x.

Saito, M., T. Honna, T. Kanagawa, and Y. Katayama (2002), Microbial degradation of carbonyl sulfide in soils, *Microbes and Environments*, *17*(1), 32–38, doi:10.1264/jsme2.2002.32.

Sandoval-Soto, L., M. Stanimirov, M. v. Hobe, V. Schmitt, J. Valdes, A. Wild, and J. Kesselmeier (2005), Global uptake of carbonyl sulfide (COS) by terrestrial vegetation: Estimates corrected by deposition velocities normalized to the uptake of carbon dioxide (CO_2), *Biogeosciences*, *2*(2), 125–132, doi:10.5194/bg-2-125-2005.

Sanhueza, E., Y. Dong, D. Scharffe, J. M. Lobert, and P. J. Crutzen (1998), Carbon monoxide uptake by temperate forest soils: The effects of leaves and humus layers, *Tellus B*, *50*(1), 51–58, doi: 10.1034/j.1600-0889.1998.00004.x.

Schenk, S., J. Kesselmeier, and E. Anders (2004), How does the exchange of one oxygen atom with sulfur affect the catalytic cycle of carbonic anhydrase?, *Chemistry - A European Journal*, *10*(12), 3091–3105, doi:10.1002/chem.200305754.

Schlesinger, W. H., and E. S. Bernhardt (2013), *Biogeochemistry: an analysis of global change*, 3rd ed., Academic Press, Waltham, MA, USA.

Seefeldt, L. C., M. E. Rasche, and S. A. Ensign (1995), Carbonyl sulfide and carbon dioxide as new substrates, and carbon disulfide as a new inhibitor, of nitrogenase, *Biochemistry*, *34*(16), 5382–5389, doi:10.1021/bi00016a009.

Seibt, U., L. Wingate, J. Lloyd, and J. Berry (2006), Diurnally variable $\delta^{18}O$ signatures of soil CO_2 fluxes indicate carbonic anhydrase activity in a forest soil, *Journal of Geophysical Research*, *111*, G04,005, doi:10.1029/2006JG000177.

Seibt, U., J. Kesselmeier, L. Sandoval-Soto, U. Kuhn, and J. Berry (2010), A kinetic analysis of leaf uptake of COS and its relation to transpiration, photosynthesis and carbon isotope fractionation, *Biogeosciences*, *7*(1), 333–341, doi:10.5194/bg-7-333-2010.

Seinfeld, J. H., and S. N. Pandis (2006), *Atmospheric Chemistry and Physics: From Air Pollution to Climate Chang*, 2nd ed., John Wiley & Sons.

Simmons, J. S., L. Klemedtsson, H. Hultberg, and M. E. Hines (1999), Consumption of atmospheric carbonyl sulfide by coniferous boreal forest soils, *Journal of Geophysical Research*, *104*(D9), 11,569–11,576, doi:10.1029/1999JD900149.

Smeulders, M. J., T. R. M. Barends, A. Pol, A. Scherer, M. H. Zandvoort, A. Udvarhelyi, A. F. Khadem, A. Menzel, J. Hermans, R. L. Shoeman, H. J. C. T. Wessels, L. P. van den Heuvel, L. Russ, I. Schlichting, M. S. M. Jetten, and H. J. M. O. den Camp (2011), Evolution of a new enzyme for carbon disulphide conversion by an acidothermophilic archaeon, *Nature*, *478*, 412–416, doi: 10.1038/nature10464.

Steinbacher, M., H. G. Bingemer, and U. Schmidt (2004), Measurements of the exchange of carbonyl sulfide (OCS) and carbon disulfide (CS_2) between soil and atmosphere in a spruce forest in central Germany, *Atmospheric Environment*, *38*(35), 6043–6052, doi:10.1016/j.atmosenv.2004.06.022.

Stimler, K., S. A. Montzka, J. A. Berry, Y. Rudich, and D. Yakir (2010a), Relationships between carbonyl sulfide (COS) and CO_2 during leaf gas exchange, *New Phytologist*, *186*(4), 869–878, doi: 10.1111/j.1469-8137.2010.03218.x.

Stimler, K., D. Nelson, and D. Yakir (2010b), High precision measurements of atmospheric concentrations and plant exchange rates of carbonyl sulfide using mid-IR quantum cascade laser, *Global Change Biology*, *16*(9), 2496–2503, doi:10.1111/j.1365-2486.2009.02088.x.

Stimler, K., J. A. Berry, S. A. Montzka, and D. Yakir (2011), Association between carbonyl sulfide uptake and ^{18}O during gas exchange in C_3 and C_4 leaves, *Plant Physiology*, *157*(1), 509–517, doi: 10.1104/pp.111.176578.

Stull, R. B. (1988), *An Introduction to Boundary Layer Meteorology*, Kluwer Academic Publishers, Dordrecht, The Netherlands.

Sun, W., K. Maseyk, C. Lett, and U. Seibt (2015), A soil diffusion-reaction model for surface COS flux: COSSM v1, *Geoscientific Model Development*, *8*, 3055–3070, doi:10.5194/gmd-8-3055-2015.

Sun, W., K. Maseyk, C. Lett, and U. Seibt (2016), Litter dominates surface fluxes of carbonyl sulfide in a Californian oak woodland, *Journal of Geophysical Research: Biogeosciences*, *121*, 438–450, doi: 10.1002/2015JG003149.

Sun, W., L. M. J. Kooijmans, K. Maseyk, H. Chen, I. Mammarella, T. Vesala, J. Levula, H. Keskinen, , and U. Seibt (2017), Soil fluxes of carbonyl sulfide (COS), carbon monoxide, and carbon dioxide in a boreal forest in southern Finland, *Atmospheric Chemistry and Physics Discussions*, doi:10.5194/acp-2017-180, in review.

Suni, T., J. Rinne, A. Reissel, N. Altimir, P. Keronen, Ü. Rannik, M. Dal Maso, M. Kulmala, and T. Vesala (2003), Long-term measurements of surface fluxes above a Scots pine forest in Hyytiälä, southern Finland, 1996–2001, *Boreal Environment Research*, *4*, 287–301.

Suntharalingam, P., A. J. Kettle, S. M. Montzka, and D. J. Jacob (2008), Global 3-D model analysis of the seasonal cycle of atmospheric carbonyl sulfide: Implications for terrestrial vegetation uptake, *Geophysical Research Letters*, *35*(19), doi:10.1029/2008GL034332, l19801.

Sze, N. D., and M. K. W. Ko (1979), Is CS_2 a precursor for atmospheric COS?, *Nature*, *278*, 731–732, doi:10.1038/278731a0.

Tang, J., and W. Riley (2013), A new top boundary condition for modeling surface diffusive exchange of a generic volatile tracer: theoretical analysis and application to soil evaporation, *Hydrology and Earth System Sciences*, *17*(2), 873–893, doi:10.5194/hess-17-873-2013.

Tang, J., and W. Riley (2014), Technical Note: Simple formulations and solutions of the dual-phase diffusive transport for biogeochemical modeling, *Biogeosciences*, *11*(14), 3721–3728, doi:10.5194/bg-11-3721-2014.

Thompson, H. W., C. F. Kearton, and S. A. Lamb (1935), The kinetics of the reaction between carbonyl sulphide and water, *Journal of the Chemical Society*, pp. 1033–1037, doi:10.1039/JR9350001033.

Ulshöfer, V., and M. Andreae (1998), Carbonyl sulfide (COS) in the surface ocean and the atmospheric COS budget, *Aquatic Geochemistry*, *3*(4), 283–303, doi:10.1023/A:1009668400667.

Ulshöfer, V., O. Flock, G. Uher, and M. Andreae (1996), Photochemical production and air-sea exchange of carbonyl sulfide in the eastern mediterranean sea, *Marine Chemistry*, *53*(1), 25–39, doi:10.1016/0304-4203(96)00010-2.

USDA Natural Resources Conservation Service (2014), Web Soil Survey, Available online at http://websoilsurvey.nrcs.usda.gov/, accessed July 2014.

van Asperen, H., T. Warneke, S. Sabbatini, G. Nicolini, D. Papale, and J. Notholt (2015), The role of photo- and thermal degradation for CO_2 and CO fluxes in an arid ecosystem, *Biogeosciences*, *12*(13), 4161–4174, doi:10.5194/bg-12-4161-2015.

Van Diest, H., and J. Kesselmeier (2008), Soil atmosphere exchange of carbonyl sulfide (COS) regulated by diffusivity depending on water-filled pore space, *Biogeosciences*, *5*(2), 475–483, doi:10.5194/bg-5-475-2008.

Van Wijk, W. R., and D. A. de Vries (1963), Periodic temperature variations in a homogeneous soil, in *Physics of Plant Environment*, edited by W. R. Van Wijk, pp. 102–143, North Holland Publishing Company, Amsterdam, The Netherlands.

Vesala, T., T. Suni, Ü. Rannik, P. Keronen, T. Markkanen, S. Sevanto, T. Grönholm, S. Smolander, M. Kulmala, H. Ilvesniemi, et al. (2005), Effect of thinning on surface fluxes in a boreal forest, *Global Biogeochemical Cycles*, *19*(2), doi:10.1029/2004GB002316.

Vesala, T., S. Launiainen, P. Kolari, J. Pumpanen, S. Sevanto, P. Hari, E. Nikinmaa, P. Kaski, H. Mannila, E. Ukkonen, S. L. Piao, and P. Ciais (2010), Autumn temperature and carbon balance of a boreal Scots pine forest in Southern Finland, *Biogeosciences*, *7*(1), 163–176, doi:10.5194/bg-7-163-2010.

Von Hobe, M., A. Kettle, and M. Andreae (1999), Carbonyl sulphide in and over seawater: summer data from the northeast Atlantic Ocean, *Atmospheric Environment*, *33*(21), 3503–3514, doi:10.1016/S1352-2310(98)00236-2.

Von Hobe, M., G. A. Cutter, A. J. Kettle, and M. O. Andreae (2001), Dark production: A significant source of oceanic COS, *Journal of Geophysical Research: Oceans*, *106*(C12), 31,217–31,226, doi:10.1029/2000JC000567.

Walker, J. P. (1999), Estimating soil moisture profile dynamics from near-surface soil moisture

measurements and standard meteorological data, Ph.D. thesis, The University of Newcastle, New South Wales, Australia.

Wang, J., L. Liu, X. Wang, and Y. Chen (2015), The interaction between abiotic photodegradation and microbial decomposition under ultraviolet radiation, *Global Change Biology*, *21*(5), 2095–2104, doi:10.1111/gcb.12812.

Watts, S. F. (2000), The mass budgets of carbonyl sulfide, dimethyl sulfide, carbon disulfide and hydrogen sulfide, *Atmospheric Environment*, *34*(5), 761–779, doi:10.1016/S1352-2310(99)00342-8.

Wehr, R., R. Commane, J. W. Munger, J. B. McManus, D. D. Nelson, M. S. Zahniser, S. R. Saleska, and S. C. Wofsy (2017), Dynamics of canopy stomatal conductance, transpiration, and evaporation in a temperate deciduous forest, validated by carbonyl sulfide uptake, *Biogeosciences*, *14*(2), 389–401, doi:10.5194/bg-14-389-2017.

Weiss, R. F. (1974), Carbon dioxide in water and seawater: the solubility of a non-ideal gas, *Marine Chemistry*, *2*, 203–215, doi:10.1016/0304-4203(74)90015-2.

Whalen, S. C., and W. S. Reeburgh (2001), Carbon monoxide consumption in upland boreal forest soils, *Soil Biology and Biochemistry*, *33*(10), 1329–1338, doi:10.1016/S0038-0717(01)00038-4.

Whelan, M. E., and R. C. Rhew (2015), Carbonyl sulfide produced by abiotic thermal and photodegradation of soil organic matter from wheat field substrate, *Journal of Geophysical Research: Biogeosciences*, *120*, 54–62, doi:10.1002/2014JG002661.

Whelan, M. E., and R. C. Rhew (2016), Reduced sulfur trace gas exchange between a seasonally dry grassland and the atmosphere, *Biogeochemistry*, *online preview*, 1–14, doi:10.1007/s10533-016-0207-7.

Whelan, M. E., D.-H. Min, and R. C. Rhew (2013), Salt marsh vegetation as a carbonyl sulfide (COS) source to the atmosphere, *Atmospheric Environment*, *73*, 131–137, doi:10.1016/j.atmosenv.2013.02.048.

Whelan, M. E., T. W. Hilton, J. A. Berry, M. Berkelhammer, A. R. Desai, and J. E. Campbell (2016), Carbonyl sulfide exchange in soils for better estimates of ecosystem carbon uptake, *Atmospheric Chemistry and Physics*, *16*(6), 3711–3726, doi:10.5194/acp-16-3711-2016.

Wilhelm, E., R. Battino, and R. J. Wilcock (1977), Low-pressure solubility of gases in liquid water, *Chemical Reviews*, *77*(2), 219–262, doi:10.1021/cr60306a003.

Wingate, L., U. Seibt, K. Maseyk, J. Ogée, P. Almeida, D. Yakir, J. S. Pereira, and M. Mencuccini (2008), Evaporation and carbonic anhydrase activity recorded in oxygen isotope signatures of net CO_2 fluxes from a Mediterranean soil, *Global Change Biology*, *14*(9), 2178–2193, doi:10.1111/j.1365-2486.2008.01635.x.

Wingate, L., J. Ogée, M. Cuntz, B. Genty, I. Reiterd, U. Seibt, D. Yakir, K. Maseyk, E. G. Pendall, M. M. Barbour, B. Mortazavi, R. Burlett, P. Peylin, J. Miller, M. Mencuccini, J. H. Shim, J. Hunt, and J. Grace (2009), The impact of soil microorganisms on the global budget of $\delta^{18}O$ in atmospheric CO_2, *Proceedings of the National Academy of Sciences*, *106*(52), 22,411–22,415, doi:10.1073/pnas.0905210106.

Wohlfahrt, G., F. Brilli, L. Hörtnagl, X. Xu, H. Bingemer, A. Hansel, and F. Loreto (2012), Carbonyl sulfide (COS) as a tracer for canopy photosynthesis, transpiration and stomatal conductance: potential and limitations, *Plant, Cell & Environment*, *35*(4), 657–667, doi:10.1111/j.1365-3040.2011.02451.x.

Xu, L., M. D. Furtaw, R. A. Madsen, R. L. Garcia, D. J. Anderson, and D. K. McDermitt (2006), On maintaining pressure equilibrium between a soil CO_2 flux chamber and the ambient air, *Journal of Geophysical Research: Atmospheres*, *111*(D8), doi:10.1029/2005JD006435, D08S10.

Xu, X., H. G. Bingemer, H.-W. Georgii, U. Schmidt, and U. Bartell (2001), Measurements of carbonyl sulfide (COS) in surface seawater and marine air, and estimates of the air-sea flux from observations during two Atlantic cruises, *Journal of Geophysical Research: Atmospheres*, *106*(D4), 3491–3502, doi:10.1029/2000JD900571.

Yi, Z., X. Wang, G. Sheng, D. Zhang, G. Zhou, and J. Fu (2007), Soil uptake of carbonyl sulfide

in subtropical forests with different successional stages in south China, *Journal of Geophysical Research*, *112*, D08,302, doi:10.1029/2006JD008048.

Yi, Z., X. Wang, G. Sheng, and J. Fu (2008), Exchange of carbonyl sulfide (OCS) and dimethyl sulfide (DMS) between rice paddy fields and the atmosphere in subtropical China, *Agriculture, Ecosystems and Environment*, *123*, 116–124, doi:10.1016/j.agee.2007.05.011.

Yi, Z., L. Zheng, T. Wu, and X. Wang (2013), Contribution of aboveground plants, the rhizosphere and root-free-soils to total COS and DMS fluxes at three key growth stages in rice paddies, *Agriculture, Ecosystems and Environment*, *179*, 11–17, doi:10.1016/j.agee.2013.07.005.

Yonemura, S., S. Kawashima, and H. Tsuruta (2000a), Carbon monoxide, hydrogen, and methane uptake by soils in a temperate arable field and a forest, *Journal of Geophysical Research*, *105*(D11), 14,347–14,362, doi:10.1029/1999JD901156.

Yonemura, S., M. Yokozawa, S. Kawashima, and H. Tsuruta (2000b), Model analysis of the influence of gas diffusivity in soil on CO and H_2 uptake, *Tellus B*, *52*(3), 919–933, doi:10.1034/j.1600-0889.2000.d01-2.x.

Zepp, R. G., and M. O. Andreae (1994), Factors affecting the photochemical production of carbonyl sulfide in seawater, *Geophysical Research Letters*, *21*(25), 2813–2816, doi:10.1029/94GL03083.

Zepp, R. G., W. L. Miller, M. A. Tarr, R. A. Burke, and B. J. Stocks (1997), Soil–atmosphere fluxes of carbon monoxide during early stages of postfire succession in upland canadian boreal forests, *Journal of Geophysical Research: Atmospheres*, *102*(D24), 29,301–29,311, doi:10.1029/97JD01326.

Zhao, F. J., M. J. Hawkesford, and S. P. McGrath (1999), Sulphur assimilation and effects on yield and quality of wheat, *Journal of Cereal Science*, *30*(1), 1–17, doi:10.1006/jcrs.1998.0241.